SPERRY RAND

STRAPDOWN CALIBRATION AND ALIGNMENT STUDY

VOLUME 2

PROCEDURAL AND PARAMETRIC TRADE-OFF ANALYSES DOCUMENT

Prepared for

GUIDANCE LABORATORY
ELECTRONICS RESEARCH CENTER
NATIONAL AERONAUTICS AND SPACE ADMINISTRATION
CAMBRIDGE, MASSACHUSETTS

under Contract NAS 12-577

by
D.M. Garmer
E.J. Farrell
D.E. Jones

UNIVAC
FEDERAL SYSTEMS DIVISION

ACKNOWLEDGMENT

The authors would like to express their appreciation to Mr. J. A. Young, Mr. D. F. Hanf, Mr. R. L. Syverson, Mr. R. J. Ellingrod, and Mr. S. E. Gregory for their contributions to this document. Mr. Young computed the results of Section 2.2 and was the principal author of this section and Appendix A. Mr. Hanf and Mr. Syverson organized, programmed, and documented the simulation programming and also performed the evaluation of the error equations of Section 4.2. Mr. Gregory helped tabulate the results of Section 5.

ABSTRACT

This is Volume 2 of three volumes which report the results of a strapdown calibration and alignment study performed by the Univac Federal Systems Division for the Guidance Laboratory of NASA/ERC.

This study develops techniques to accomplish laboratory calibration and alignment of a strapdown inertial sensing unit (ISU) being configured by NASA/ERC. Calibration is accomplished by measuring specific input environments and using the relationship of known kinematic input to sensor outputs, to determine the constants of the sensor models. The environments used consist of inputs from the earth angular rate, the normal reaction force of gravity, and the angular rotation imposed by a test fixture in some cases. Techniques are also developed to accomplish alignment by three methods. First, Mirror Alignment employs autocollimators to measure the earth orientation of the normals to two mirrors mounted on the ISU. Second, Level Alignment uses an autocollimator to measure the azimuth of the normal to one ISU mirror and accelerometer measurements to determine the orientation of local vertical with respect to the body axes. Third, Gyrocompass Alignment determines earth alignment of the ISU by gyro and accelerometer measurement of the earth rate and gravity normal force vectors.

The three volumes of this study are composed as follows.

- Volume 1 – Development Document. This volume contains the detailed development of the calibration and alignment techniques. The development is presented as a rigorous systems engineering task and a step-by-step development of specific solutions is presented.
- Volume 2 – Procedural and Parametric Trade-off Analyses Document. This volume contains the detailed trade-off studies supporting the developments given in Volume 1.
- Volume 3 – Laboratory Procedures Manual. In Volume 3 the implementation of the selected procedures is presented. The laboratory procedures are presented by use of both detailed step-by-step check sheets and schematic representations of the laboratory depicting the entire process at each major step in the procedure. The equations to be programmed in the implementation of the procedures are contained in this volume.

TABLE OF CONTENTS

TABLE OF CONTENTS (Continued)

LIST OF ILLUSTRATIONS

LIST OF CHARTS

LIST OF CHARTS (Continued)

LIST OF TABLES

GLOSSARY

As an aid to understanding the symbolism, we present the following rules of notation.

- Wherever possible symbols will be used which suggest the name of the parameter involved.
- Lower case subscripts are used almost exclusively for indexing over several items of the same kind. Examples are the indexes used to identify the three gyros, the three accelerometers, the two pulse trains of each accelerometer, the two clock scale factors, etc.
- Lowercase superscripts are used to index over different positions.
- Uppercase superscripts and subscripts will be used to distinguish between parameters of the same kind. For example, T is used to identify a transformation matrix. Lettered superscripts such as BE in T^{BE} identify the particular transformation.
- An underline will identify a vector.
- Unit vectors are used to identify lines in space such as instrument axes and the axes of all frames of reference.
- Components of any vector along with any axis is indicated by a dot product of that vector with the unit vector along the axis of interest.
- The Greek sigma (Σ) will be used for summations. Where the limits of summation are clear from the context, they will not be indicated with the symbol.
- The Greek Δ is always used to indicate a difference.
- S ϕ and C ϕ are sometimes used to identify the sine and cosine of the angle ϕ.
- A triple line symbol ($\equiv$) will be used for definitions.
- A superior "$\sim$" denotes a prior estimate of the quantity.
- A superior "$\wedge$" denotes an estimate of the quantity from the estimation routine.

$\underline{a}$	Applied acceleration vector.
$(\underline{A}_i \cdot \underline{B}_j)$	Elements of $(Q^A)^{-1}$.
$\underline{A}_i$	Unit vector directed along the input axis of the ith accelerometer i = 1, 2, 3.
$\underline{b}$	A vector determined by the Alignment Parameter Evaluation Procedure and input to the Estimation Routine.
$\underline{B}_i$	Unit vector directed along the ith Body Axis i = 1, 2, 3.
B_I, B_O, B_S	Gyro unbalance coefficients.
C_{II},C_{SS},C_{IS},C_{IO},C_{OS}	Gyro Compliance Coefficients.
Counters	The six frequency counters used as data collection devices during calibration.
D_0	Accelerometer bias.
D_1	Accelerometer scale factor.
D_2	Accelerometer second order coefficient.
D_3	Accelerometer third order coefficient.
$\underline{E}$	Unit vector directed East ($\underline{E}_2$).
$\underline{E}_i$	Unit vector directed along the ith Earth Axis.
Eq	Quantization error.
f_1 , f_2	Frequencies of accelerometer strings 1 and 2, in zero crossings per second.
$\underline{F}_i$	A triad of orthogonal unit vectors attached to the base of the table.
$\underline{G}_i$	Unit vector directed along the ith input axis of the gyro.
$(\underline{G}_i \cdot \underline{B}_j)$	Elements of $(Q^G)^{-1}$.
$\underline{g}$	The vector directed up that represents the normal force to counteract gravity in a static orientation. Corresponding to popular convention, this is referred to as the "gravity vector".
I/O	Input/Output.

$\underline{I}_i$	Triad of orthogonal unit vectors attached to the inner axis of test table.
IEU	Interface Electronics Unit – system interface device for the laboratory computer.
ISU	Inertial Sensing Unit.
J	Gyro angular rate coefficient.
K	Number of samples of accelerometer and gyro data taken in Alignment.
m	Position index used in calibration (superscript).
M	Matrix generated by Alignment Parameter Evaluation and used by Alignment Estimation Routine.
$\underline{M}_1$	Unit normal to ith mirror.
$\underline{N}$	Unit vector directed North ($\underline{E}_3$).
N_1, N_2	Count of output pulses from strings 1 and 2 of accelerometer.
n_A	Instrument noise in accelerometer.
n_G	Instrument noise in gyro.
Σn^{ϕ}	Count of output pulses from strings 1 and 2 of accelerometer.
Σn_1^T	Count of timing pulses from master oscillator to frequency counters.
Σn_2^T	Count of timing pulses from master oscillator to IEU.
$\underline{O}$	Unit vector directed along the output axis of gyro.
$\underline{O}_1$	Triad of orthogonal unit vectors attached to the outer axis of the table.
$\underline{P}$	Unit vector in the direction of the projection of $\underline{M}_1$ in the plane formed by $\underline{E}$ and $\underline{N}$.
P_k^A	Defined on Chart 4-12 of the Development Document.
P_k^G	Defined on Chart 4-4 of the Development Document.
Q^A	The transformation from accelerometer input axes to body axes.
Q^G	The transformation from gyro input axes to body axes.

Q_{II}, Q_{IS}	Gyro dynamic coupling coefficients.
$\underline{r}$	Position vector.
R	Gyro bias.
$\underline{R}_1$	Triad of orthogonal unit vectors attached to rotary axis of table.
Resolver	Angular resolvers on each axis of the test table.
$\underline{S}_i$	Unit vector directed along the ith gyro spin axis.
$\underline{S}^{\phi}$	Scale factor associated with pulsed output from test table rotary axis.
S_1^T	Scale factor associated with timing pulses accumulated by the frequency counters.
S_2^T	Scale factor associated with timing pulses to the IEU.
t	Time.
T	In alignment, the determined alignment matrix to transform from body to earth axes. T is equivalent to T^{BE}.
T^{BI}	Transform from ISU body axes to inner axis frame.
T^{BRm}	Transform from ISU Body Frame Axes to Rotary Axis Frame in the mth orientation.
$\underline{T}_i$	Triad of orthogonal unit vectors attached to the trunnion axis of the test table.
$\underline{U}$	Unit vector directed up (E_1).
$\underline{V}$	Velocity vector.
$\underline{W}$	Unit vector directed along $\underline{\omega}^E$.
X-Y	Dual input on frequency counter that will difference two pulse trains for comparison with a third input (Z).
Z	Input on frequency counter for pulse train.
α_i	The azimuth angle of the normal to the ith mirror.
$(\Sigma\gamma)_{ij}$	Pulsed output from the jth string of the ith accelerometer.
$(\Sigma\delta)_i$	Pulsed output of the ith gyro.
$\Delta\Phi$	Gyro scale factor.

ϵ_C	The clock quantization error.
ϵ_T	In instantaneous alignment estimation techniques, this symbol represents the length of time after completion of the last measurement to the time at which the prediction is made.
θ_i	The zenith angle of the normal to the ith mirror.
λ	Local colatitude.
σ_g	The estimated rms error in the magnitude of $\underline{g}$.
σ_θ	The estimated rms error in the direction of "up".
ϕ_1^m	Angular displacement about the trunnion axis of the test table for calibration position m.
ϕ_2^m	Angular displacement about the rotary axis of the test table for calibration position m.
ϕ_3^m	Angular displacement about the outer axis of the test table for calibration position m.
ϕ_4^m	Angular displacement about the inner axis of the test table for calibration position m.
$\phi_n(t)$	Covariance function of accelerometer noise used in Alignment Parameter Evaluation.
$\phi_\alpha(t)$	Covariance function of translational acceleration noise used in Alignment Parameter Evaluation.
$\phi(t)$	Covariance function of rotational noise used in Alignment Parameter Evaluation.
$\underline{\omega}$	Angular velocity vector.
$\underline{\omega}^T$	Angular velocity of the test table rotary axis.
$\underline{\omega}^E$	Earth rotation vector.
$\underline{\omega}^E \cos \lambda$	Component of earth rotation vector along the vertical.
$\underline{\omega}^E \sin \lambda$	Component of earth rotation vector along north.

SECTION 1

SECTION 1
INTRODUCTION

This document, in conjunction with two other volumes, describes the achievements of a six month study conducted for the:

Guidance Laboratory
Electronics Research Center
National Aeronautics and Space Administration
Cambridge, Massachusetts

by the:

Aerospace Systems Analysis Department
Univac Federal Systems Division
Saint Paul, Minnesota
A Division of Sperry Rand Corporation

The purpose of the study is to develop techniques and outline procedures for the laboratory calibration and alignment of a strapdown inertial sensing unit. The Development Document, Volume 1, presents a detailed analysis of the calibration and alignment problem and develops a specific solution. This document, Volume 2, is a set of addenda which serve to justify the conclusions reached in the development of specific calibration and alignment techniques in Volume 1. Reference is made to the Development Document throughout the presentation of the procedural and parametric trade-off analyses. The Laboratory Procedures Manual, Volume 3, describes the procedures for an operational implementation of the solutions obtained in Volume 1. A statement of the study objectives is contained in Section 1 of the Development Document.

The trade-off analyses described herein assume a laboratory facility which includes a test table, a computer and interface unit, frequency counters, autocollimators, three gyroscopes and three accelerometers. This laboratory facility is described in detail in Section 3 of the Development Document. The instruments are described in detail in Section 2.2 of the Development Document. This laboratory definition was not considered an absolute constraint on the trade-off studies, however, for the effect of variations in laboratory equipment and instrument characteristics have been carefully considered. The intent of the trade-off analyses has been to provide sufficient data on the relationships between important trade-off parameters to assist the laboratory test program at ERC. This program is directed toward the larger problem of laboratory testing a strapdown inertial sensing unit for the purpose of evaluating many advanced guidance and navigation concepts.

It is beyond the scope of the study, however, to consider all of the parameters which would be important in the ISU application to any specific mission. Some of the interesting parameters could not reasonably be considered without a great deal of presently unavailable supporting data. For example, parameters such as instrument reliability, instrument cost, instrument location relative to the body and to each other, etc.

The parameters that have been considered in the trade-off analyses were agreed to by NASA/ERC and do provide a wealth of information on the variables one would like to control in designing an ISU for space application. These trade-off parameters have been organized into the trade-off analyses reported in this document.

Figure 1-1 (or 1-2) illustrates the dependence of calibration (or alignment) time and accuracy upon the selected parameters. Note that all of them are related to either accuracy or time for both calibration and alignment. Thus if either accuracy or time is constrained one would have a solvable optimization problem. Given a set of ISU accuracy requirements, one could select the instrument characteristics (in terms of calibration coefficient stability, internal noise, and readout quantization), environmental noise constraints required, alignment time, and calibration time which would satisfy the requirements in a "best" way. As used here, "best" implies minimization of instrument design and production complexity, calibration time, and alignment time.

The specific calibration and alignment procedural and parametric studies described in this document are listed by general category in Chart 1-1. The sections in which the studies are covered are listed in the margin of this chart.

The calibration trade-off analyses are the subject of Section 2. The alignment trade-off analyses are described in Sections 3, 4, 5, and 6. Section 3 serves as the introduction to alignment trade-offs. In Section 4, the general error equations relating errors in the estimate of $\underline{g}$ and $\underline{\omega}^E$ to a basic measure of alignment error are developed for all four orientations and for both level and gyrocompass alignment. The trade-offs leading to the selection of the $\underline{g}$ and $\underline{\omega}^E$ estimation techniques are the subject of Section 5. The expected alignment errors for these techniques as a function of instrument and environment noise, instrument readout quantization, sample time and number of samples, estimation iteration, and computer word length are also developed in Section 5 from a computer simulation. Section 6 develops alignment accuracy as a function of calibration accuracy. Both worst-case and one sigma errors are treated.

As a matter of easy reference, we list below a cross reference between the trade-off studies called for in the Statement of Work, and those covered in this document:

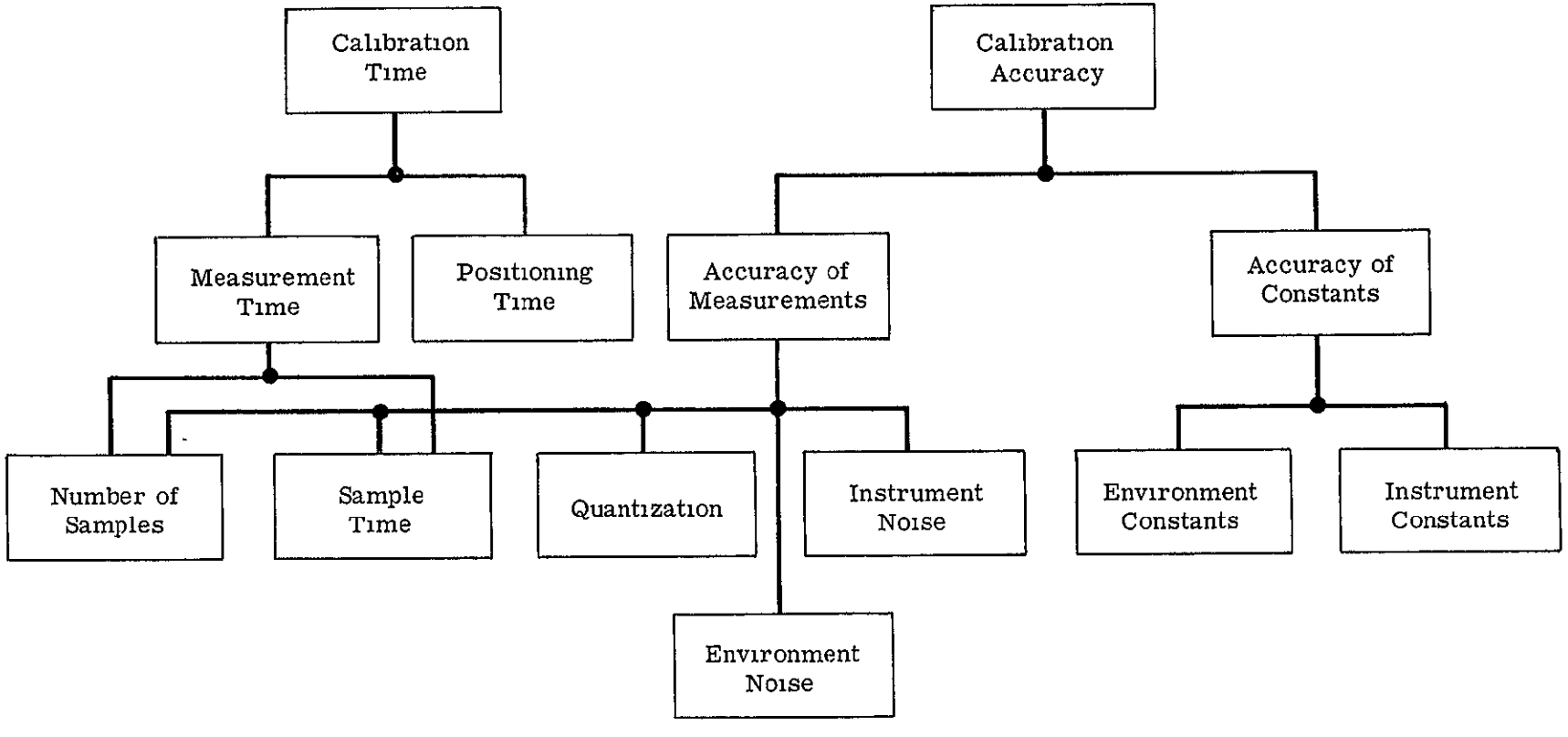

Figure 1-1. Calibration Trade-Off Parameters

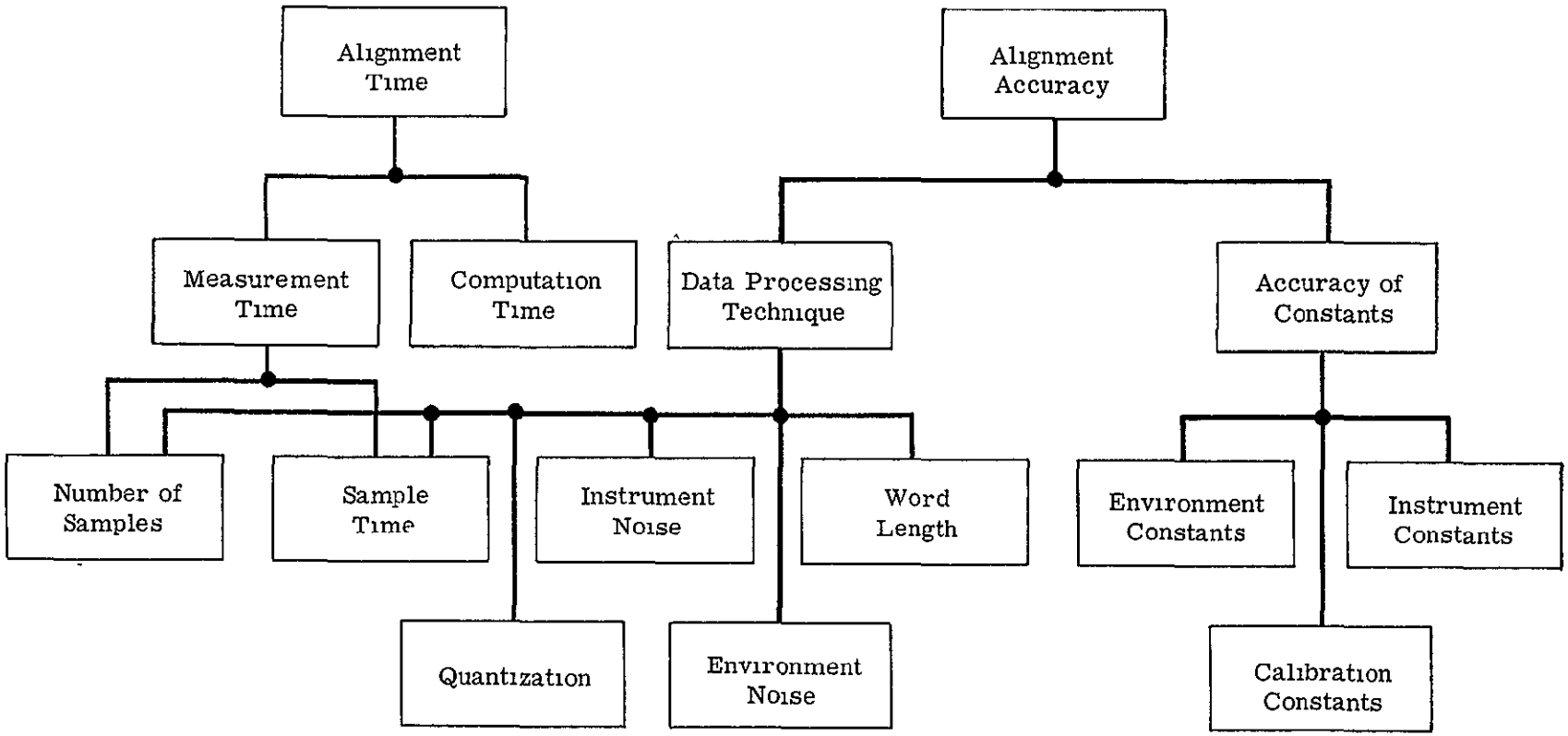

Figure 1-2. Alignment Trade-Off Parameters

CHART 1-1

Calibration and Alignment Trade-off Studies	
	Section Number
Calibration Trade-offs	2.0
• Procedural Trade-offs	
• Calibration Time vs Calibration Accuracy	
▲ Because of instrument quantization	
▲ Because of instrument and environment noise	
Alignment Trade-offs	
• Alignment Time vs Alignment Accuracy	3.3
▲ Because of instrument quantization	
• Alignment Matrix Accuracy vs Precision of the Estimation of Body Axes Components of Gravity and Earth Rate	4.0
• Estimation of Body Axes Components of Gravity and Earth Rate vs Estimation Technique	5.0
▲ Sampling rate considerations	
▲ Total sampling time considerations	
▲ Word length	
▲ Algorithm	
• Alignment Accuracy vs Calibration Accuracy	6.0

1. Alignment Time versus Alignment Accuracy
   Because of Worst-Case Quantization – Section 3.3
   Because of Simulated Noise and Quantization – Section 5

2. Alignment Time versus Sensor Quantization
   Worst-Case – Section 3.3
   Simulated Quantization – Section 5

3. Alignment Time versus Iterative Scheme – Section 5

4. Alignment Accuracy versus Word Length – Section 5

5. Alignment Accuracy versus Data Sampling Rate – Section 5

6. Alignment Accuracy versus Calibration Accuracy – Section 6

7. Calibration Time versus Calibration Accuracy – Section 2.2

8. Calibration Time versus Calibration Procedure – Section 2.1.

SECTION 2

SECTION 2
CALIBRATION TRADE-OFF STUDIES

Not all of the calibration trade-off analyses can be expressed analytically. Certain of the trade-offs are procedural in nature and deal with variables which cannot be measured quantitatively. Such variables were encountered as a choice to be made between a small number of alternatives before one could proceed in the calibration technique development. These procedural trade-offs are discussed in detail in the first subsection.

Calibration time is related to accuracy through the effects of instrument internal noise, instrument readout quantization, and environmental noise. The parametric analyses of calibration time and accuracy as a function of these parameters is the subject of the second subsection. Plots of calibration coefficient accuracy versus data collection time, as a function of worst-case quantization and statistical noise, are included at the end of that section. These plots are reproduced in Section II-6 of the Laboratory Procedures Manual.

2.1 PROCEDURAL TRADE-OFFS

Throughout the developments of the calibration techniques in Volume 1, procedures are chosen where alternatives could have been taken. In most instances explanations are given as to why the choices taken are better than the alternatives. In order to preserve the smoothness of presentation, the explanations are always rather brief in the Development Document. In this section of the trade-off document we present more detailed explanations for the more important decisions made in the Development Document. The presentation takes the form of a listing of explanations, where the order more or less indicates the relative importance.

2.1.1 Isolation of Calibration Constants

In the introduction to Section 4.2 of the Development Document it is mentioned that the calibration of the n constants in any instrument equation can be accomplished by the simultaneous solution of n calibration equations, where each equation corresponds to the input/output relationship for a particular environment. This technique involves, in general, the inversion of a n x n matrix, which would be a very cumbersome approach to calibration.

Our approach has been to choose environments such that a large number of the unknown parameters are not sensed by the instruments. This approach has several advantages over the more general inversion technique. The most important advantage is that a use of environments where the general calibration equations are considerably reduced allows for a satisfaction of the precision requirements on only those constants which are sensed. In environments where all terms are sensed, it is impossible to reduce the equations, and therefore it is impossible to control the precision on all constants independently. Another advantage of the use of reduced equations is that large matrices do not have to be inverted. Operational matrix inversion routines are always approximations when the matrices are large, as they would be for a general use of our equations. In the chosen techniques described in Section 4 of the Development Document, we never use more than two equations in the solution of any constants. Therefore, the inversions always involve 2 x 2 matrices, which can be accomplished with no approximations.

2.1.2 Use of Frequency Counters for Data Collection

In Section 4.3 of the Development Document it is mentioned that frequency counters (see Section 3.3) are to be used for all instrument data collections. For the defined ERC facility there is only one alternative to the use of frequency counters, that being a use of the laboratory computer interface. The frequency counters have one major advantage over the computer interface, that being the ability to cycle off of the instrument data train (that is, the ability to detect the leading edge of the instrument pulses), as opposed to cycling off of a clock. In reading the accelerometer outputs this is a distinct advantage, for the quantization error would be merely the uncertainty in reading the leading edge of the pulses, which was assumed to be one-tenth of a pulse for each of the accelerometer pulse trains. The computer interface, on the other hand, can only be cycled off of clock time, and the worst-case quantization error would be one pulse per pulse train. In reading the gyro outputs, the advantage of using the frequency counters is not so great as for the accelerometers. The gyro torquing is driven by a clock, resulting in the leading edges of the pulses not occurring simultaneously with increments of angular rotation. Such pulse trains have an implicit worst-case error of one quantum. Reading the leading edge does not reduce the error by any amount. A sampling of the gyro pulse trains asynchronously in time with the computer could result in a worst-case error of as much as the two quanta, so there is a small advantage in using the frequency counters. The principal reason for using the frequency counters for collecting the gyro data is not this small advantage. The principal reason is dictated by the necessity for keeping the computer out of the data collection process so that computer malfunctions would not disrupt the calibration.

2.1.3 Calibration of Gyro and Accelerometer Acceleration Sensitive Terms in Static Positions

Recall that we mention in the Development Document that the reason for not rotating the table during accelerometer calibration is so that no rotation-induced accelerations would be introduced to the accelerometers. All such induced acceleration environments would have to be measured independently for the purpose of calibration. Those rotation-induced accelerations would be functions of the distance from the axis of rotation, and it would be difficult to ascertain the radius which locates the sensitive point in the accelerometers. Additionally, the rotationally-induced accelerations would not be sufficiently large to be considered useful as inputs. There is, therefore, no reason to rotate the table during accelerometer calibration.

The reason for not rotating the gyros during the calibration of acceleration-sensitive terms is to minimize the influence of the scale factor and $(Q^G)^{-1}$ matrix imprecisions on the calibration of unbalance and compliance coefficients.

2.1.4 Use of Test Table Rather than Autocollimators for Measurement of Environment

In Section 4.2 of the Development Document the body-axis-components of $\underline{g}$, $\underline{\omega}^E$, and $\underline{\omega}^T$ are expressed in terms of test table parameters. In Section 3.2.1.3 of the same document it is stated that the transform of $\underline{g}$ and $\underline{\omega}^E$ from earth axes to body axes can be accomplished with the assistance of the autocollimators as well as the table resolvers. As a matter of fact the autocollimators might transform the vectors more accurately, for the resultant transformation would involve a smaller number of error sources. Unfortunately the transformation to body-axes-components must be accomplished for many different orientations of the ISU. To use the autocollimators for all positions would require a great deal of time. For each new position, the optical devices would have to be moved to a different location in the laboratory and resurveyed. Either that, or a large number of autocollimators would have to be purchased, two for each nominal position. A small compromise on precision must therefore be accepted, and the test table used for all transformations.

2.1.5 Whole Turn Data Taken During Calibration of Gyro Scale Factors and Misalignments

It is possible to calibrate the gyros in the presence of table motion without taking data from whole turns. The reason for using whole turn data only is that it is the simplest and most accurate technique. Taking data from fractions of whole turns would introduce the following undesirables:

- Fractions of whole turns of the test table cannot be measured as accurately as whole turns. That is, 360^{o} can be measured more accurately, with a resolver than, say, 20^{o} or any other fraction of a whole turn.
- The transient terms (integrals of sine and cosine of ϕ_2 or $2\phi_2$) in Chart 4-8 of the Development Document will always be evidenced in fractions of whole turns. The evaluation of those integrals would have to be accomplished digitally, which would introduce errors into the calibration.
- The whole turn equations allow for the nulling of linear acceleration inputs to the gyros (that is unbalance terms). Those terms can be nulled over whole turn integrations only.

It must be noted that the last two advantages would not be available if it were not for the fact that the table speed can be regulated sufficiently close to a constant.

2.1.6 Use of Maximum Speed of Table During Scale Factor and Misalignment Calibration

It was mentioned in Section 4.2.1 of the Development Document that the table will always be rotated at the maximum allowable speed (below the saturation of the gyros) during the data collection from the first six positions. The reasons are very simply stated:

- For a given precision requirement on the constants, the higher the speed the less the amount of time required for data collection. This is evidenced in the calibration equations found in Section 4.3.2 of the Development Document.
- During calibration of ω-sensitive coefficients it is advisable to make the angular velocity terms predominate. This is accomplished by using the highest possible speed.

Because the gyro scale factor is unknown at the beginning of calibration, the saturation level is not precisely known. Therefore, the speed will have to be regulated, experimentally, to be close to but be less than gyro saturation which introduces at least one pulse sign change over a finite period of time (say 10 seconds).

2.2 CALIBRATION TIME VERSUS CALIBRATION ACCURACY

In the development of the calibration equations (Section 4, Development Document), the effects of internal noise, environmental noise, and readout quantization on instrument output were neglected. Thus, the gyro output

$$P^{G} = \sum_{k} \delta_{k} - \frac{Eq}{\Delta\Phi} - \frac{\Delta n}{\Delta\Phi} - \frac{1}{\Delta\Phi}\int_{0}^{\Delta t} \Delta_{\underline{\omega}} \cdot \underline{G} dt$$

was approximated by

$$P^G = \sum_k \delta_k$$

so that we define

$$\Delta P^G = \frac{1}{\Delta\Phi}\left[Eq + \Delta n + \int_0^{\Delta t} \Delta\underline{\omega} \cdot \underline{G} dt\right] \tag{1}$$

In the same way, the accelerometer output (where internal noise is assumed negligible)

$$P^A = (N_2 - N_1) - Eq - D_1 \int_0^{\Delta t} \Delta\underline{a} \cdot \underline{A} dt$$

was approximated by

$$P^A = (N_2 - N_1)$$

so that we define

$$\Delta P^A = Eq + D_1 \int_0^{\Delta t} \Delta\underline{a} \cdot \underline{A} dt \tag{2}$$

where Δn is the internal noise of the gyro,
$\Delta\underline{\omega}$ and $\Delta\underline{a}$ are the environmental noise,
Eq is the quantization error.

These approximations produce errors in the calibration parameters which are functions of data collection time. In this subsection then, calibration accuracy will be studied as a function of calibration time.

The general calibration parameter error equation is developed in Section 2.2.1. The specific error equations for quantization and noise are developed in Sections 2.2.2 and 2.2.3, respectively. Finally, the calibration parameter errors are plotted as a function of data collection time, Δt, in Section 2.2.4.

It should be noted that while the errors plotted due to noise are statistical (standard deviation), the errors plotted due to quantization are worst case. The errors due to noise and quantization are treated as independent in the development which follows.

Thus, noise-free instruments and environment are assumed in the study of readout quantization, and conversely.

2.2.1 General Error Equation

The equations for calibration parameters, as a function of gyro or accelerometer data collected, are derived in Section 4.3.2 of the Development Document. All of these equations are linear and have the form

$$y = A \frac{P}{\Delta t} + B \tag{3}$$

where y is the parameter to be calibrated
A is some known constant
B is a function of previously computed quantities
Δt is the data collection time interval
P is the instrument readout summed over Δt.

Since equation (3) is linear, the error in y due to an error in P can be expressed by

$$\Delta y = \frac{A}{\Delta t} \Delta P \tag{4}$$

In the two subsections which follow, the ΔP due to noise, and the ΔP due to quantization of the instrument readout are discussed.

2.2.2 Quantization Errors

The magnitude of the error in the instrument readout due to quantization of the readout varies with the particular instants in time at which readout is commenced and ended. A worst-case error has been assumed to be

$$\Delta P^G = 1 \text{ pulse}$$

for the gyro, and

$$\Delta P^A = 0.1 \text{ pulse}$$

for the accelerometer.

Equation (4) can be rewritten in the form, with $\Delta y \equiv \beta_1$,

$$\beta_i \Delta t = A(\Delta P) \quad i = 1, 2, 3, 4 \tag{5}$$

The plot of the worst-case β_i against Δt is a family of hyperbolas. Chart 2-1 which follows, identifies the quantities β_i for the gyro. Chart 2-2 identifies the quantities β_1 for the accelerometer.

Figures 2-1 through 2-4 show plots of the β_1's for worst-case quantization.

2.2.3 Noise Errors

The analysis of noise-induced errors is based on equations (1) and (2) in the introduction to 2.2 after dropping the quantization terms. In equation (1) the integrand $\Delta\underline{\omega} \cdot \underline{G}$ includes a component of earth angular rate modulated by an angular displacement noise, $\Delta\theta$, in addition to the angular velocity from environment disturbances, which is sensed directly by the gyro. The development in Appendix A shows that the error input to the gyro is:

$$\Delta\underline{\omega} \cdot \underline{G} = (\omega^E \sin \theta_o) \Delta\theta + \omega^e$$

where ω^E is the earth rate (magnitude); $\theta = \theta_o + \Delta\theta$ is the angle between $\underline{\omega}^E$ and $\underline{N}$ (colatitude); and ω^e is the environment angular velocity noise, the time derivative of $\Delta\theta$. The environment angular displacement noise $\Delta\theta$ (and hence also its derivative, ω^e) is assumed zero about a vertical axis and isotropic in the horizontal plane. Therefore:

$$\begin{aligned} \Delta\underline{\omega} \cdot \underline{G} &= \omega^E(\Delta\theta/\sqrt{2}) + \omega^e, \text{ for gyro horizontal} \\ &= \omega^E \Delta\theta/\sqrt{2}, \text{ for gyro vertical} \end{aligned} \tag{6}$$

where θ_o has been assumed 45^o.

Similarly, for the accelerometer, the integrand in equation (2) $\Delta\underline{a} \cdot \underline{A}$ includes a component of gravity modulated by the angular displacement noise, $\Delta\theta$; in addition to $\underline{a}^e$, the acceleration from environment disturbances. As developed in Appendix A, the error input to the accelerometer is:

$$\Delta\underline{a} \cdot \underline{A} = a^e + (g \sin \theta_o) \Delta\theta$$

GYRO COEFFICIENT ERRORS FROM WORST CASE QUANTIZATION

1) $\beta_1 \Delta t = \frac{1}{300}$ (deg)

2) $\beta_2 \Delta t = \frac{2}{3600}$ (sec)

where

1) $\beta_1 = \frac{\Delta P}{(1/\Delta\Phi)\,\Delta t}$ (deg/hr)

$= \Delta R$, the gyro bias term

$= \Delta B a$, the gyro unbalance term

$= \Delta C a^2$, the gyro compliance term

2) $\beta_2 = \frac{\Delta P}{\omega^T (1/\Delta\Phi)\,\Delta t}$ (dimensionless)

$= \frac{\Delta(1/\Delta\Phi)}{(1/\Delta\Phi)}$, the gyro scale factor term

$= \Delta(\underline{G}_i \cdot \underline{B}_j)$, the gyro alignment term

$= \Delta Q\omega$, the gyro nonlinearity term

3) $a = g$

4) $\omega = \omega^T$

5) $\omega^T = 43200$ (deg/hr)

6) $\Delta\Phi = 12$ ($\widehat{\text{sec}}$/pulse)

7) $\Delta P = 1$ (pulse)

ACCELEROMETER COEFFICIENT ERRORS FROM WORST CASE QUANTIZATION

1) $\beta_3 \Delta t = \frac{1}{1270}$ (sec)

2) $\beta_4 \Delta t = \frac{1}{1270}$ (g-sec)

where

1) $\beta_3 = \frac{\Delta P}{(gD_1)\Delta t}$ (dimensionless)

$= \frac{\Delta D_1}{D_1}$, the accelerometer scale factor term

$= \Delta(\underline{A}_i \cdot \underline{B}_j)$, the accelerometer alignment term

$= \Delta D_2 a$, the accelerometer second order term

$= \Delta D_3 a^2$, the accelerometer third order term

2) $\beta_4 = \frac{\Delta P}{D_1 \Delta t}$ (g's)

$= \Delta D_0$, the accelerometer bias term

3) $a = g$

4) $D_1 = 254$ (pulse/sec/g)

5) $\Delta P = 0.2$ (pulse)

where a^e is the magnitude of the environment acceleration noise, g is the (constant) acceleration of gravity; and $\theta = \theta_o + \Delta\theta$ is the angle between $\underline{A}$ and the local vertical. Environment acceleration noise is assumed isotropic. Since θ_o is different in the horizontal and vertical orientations, we have:

$$\begin{aligned} \Delta\underline{a} \cdot \underline{A} &= a^e + g\,\Delta\theta, \text{ for accelerometer horizontal} \\ &= a^e, \text{ for accelerometer vertical} \end{aligned} \tag{7}$$

Thus for both gyro and accelerometer the effect of environmental noise is strongly dependent upon orientation of the instrument.

Substituting equations (6) into (1), and equations (7) into (2), and dropping the quantization terms, we get expressions for ΔP needed to implement equation (5) for the noise case. Since noise errors are indeterminate, a statistical approach is used, giving an rms value for the coefficient errors, β_i. The resulting equations are developed in Appendix A, and are listed in Charts 2-3 and 2-4. The functional relationships between noise-induced coefficient errors and calibration time are plotted in normalized form in Figures 2-1 through 2-4. The rest of this subsection outlines the approach and assumptions made:

- The variance (σ^2) of ΔP is calculated from the power spectral density of ΔP, which in turn is found from the power spectral densities of the input noises.
- Gyro internal noise* is introduced as an equivalent noise input.
- Accelerometer internal noise is negligible.
- Sensor dynamics are effectively neglected. That is, the sensor transfer function, T(s), is assumed flat out to a frequency where the noise falls off drastically.
- Intersample time is neglected; i. e., we assume continuous data instead of sampled data. This means replacing the summation of pulses with an integration.
- All noise sources are assumed stationary, independent, random processes of zero mean. In addition, angular displacement noise is assumed isotropic in the horizontal plane, and zero in the vertical. Acceleration noise is assumed isotropic.
- Environment noise is taken from Section 3. 2. 2 of the Development Document.** The acceleration environment noise spectrum, $P_a(f)$, is given in Figure 3-3 of that subsection, and the angular displacement noise spectrum (tilt), $P_\theta(f)$, is given in Figure 3-4. The angular velocity noise spectrum, $P_{\omega e}(f)$, is obtained from Figure 3-4; by multiplication by $(2\pi f)^2$.

*GG334 Gas Bearing Gyro, Technical Description ASD-3, Honeywell Aeronautical Division, Minneapolis, 28 November 1966.

**Also from H. Weinstock, Limitations on Inertial Sensor Testing Produced by Test Platform Vibrations, NASA TN D-3683, Washington, D. C., November 1966.

GYRO COEFFICIENT ERRORS FROM STATISTICAL NOISE

1) $$(\beta_1)_{rms} = \left[\sigma^2\left\{\frac{1}{\Delta t}\int_0^{\Delta t}(\Delta n + \Delta\underline{\omega}\cdot\underline{G})dt\right\}\right]^{1/2}$$

$$= \frac{1}{\Delta t}\left[\int_0^{\infty} P_P(f)\,df\right]^{1/2}$$

2) $$(\beta_2)_{rms} = \frac{1}{\omega^T}(\beta_1)_{rms}$$

where

1) $$\beta_1 = \frac{\Delta P}{(1/\Delta\Phi)\Delta t} \quad (\text{deg/hr})$$

$= \Delta R$, the gyro bias term

$= \Delta B a$, the gyro unbalance term

$= \Delta C a^2$, the gyro compliance term

2) $$\beta_2 = \frac{\Delta P}{\omega^T(1/\Delta\Phi)\,\Delta t} \quad (\text{dimensionless})$$

$$= \frac{\Delta(1/\Delta\Phi)}{(1/\Delta\Phi)}, \text{ the gyro scale factor term}$$

$= \Delta(\underline{G}_i \cdot \underline{B}_j)$, the gyro alignment term

$= \Delta Q\omega$, the gyro nonlinearity term

3) $a = g$

$\Delta\Phi = 12$ ($\widehat{\text{sec}}$/pulse)

$\omega^T = 43200$ (deg/hr)

$\omega^E = 15$ (deg/hr)

4) $$P_P(f) = \left|T_s(j\omega)\right|^2 \frac{2(1-\cos 2\pi f\,\Delta t)}{(2\pi f\,\Delta t)^2}\left\{P_n(f) + \cos^2\phi_o P_{\omega^e}(f) + (\omega^E \sin\theta_o)^2 P_\theta(f)\right\}$$

$=$ power spectral density of ΔP $((\text{deg/hr})^2/\text{cps})$

5) $$\left|T_s(j\omega)\right|^2 = 1$$

6) $\cos\phi_o = 0$, gyro horizontal

$= 1$, gyro vertical

$\sin\theta_o = 1/\sqrt{2}$, gyro horizontal or vertical

ACCELEROMETER COEFFICIENT ERRORS FROM STATISTICAL NOISE

1) $$(\beta_3)_{rms} = \left[\sigma^2\left\{\frac{1}{g\Delta t}\int_0^{\Delta t} \underline{\Delta a}\cdot\underline{A}dt\right\}\right]^{1/2}$$

$$= \frac{1}{g\Delta t}\left[\int_0^{\infty} P_P(f)\, df\right]^{1/2}$$

2) $$(\beta_4)_{rms} = g(\beta_3)_{rms}$$

where

1) $$\beta_3 = \frac{\Delta P}{(gD_1)\Delta t} \quad \text{(dimensionless)}$$

$$= \frac{\Delta D_1}{D_1}\text{, the accelerometer scale factor term}$$

$$= \Delta(\underline{A}_i\cdot\underline{B}_j)\text{, the accelerometer alignment term}$$

$$= \Delta D_2 a\text{, the accelerometer second order term}$$

$$= \Delta D_3 a^2\text{, the accelerometer third order term}$$

2) $$\beta_4 = \frac{\Delta P}{D_1\Delta t} \quad \text{(g's)}$$

$$= \Delta D_0\text{, the accelerometer bias term}$$

3) $$a = g$$

$$D_1 = 254 \text{ ((pulses/sec)/g)}$$

4) $$P_P(f) = \left|T_s(j\omega)\right|^2 \frac{2(1-\cos 2\pi f\Delta t)}{(2\pi f\Delta t)^2}\left\{P_{ae}(f) + (g\sin\theta_0)^2 P_\theta(f)\right\}$$

$$= \text{power spectral density of } \Delta P \quad (g^2/\text{cps})$$

5) $$\left|T_s(j\omega)\right|^2 = 1$$

6) $$\sin\theta_0 = 1\text{, for accelerometer horizontal}$$

$$= 0\text{, for accelerometer vertical}$$

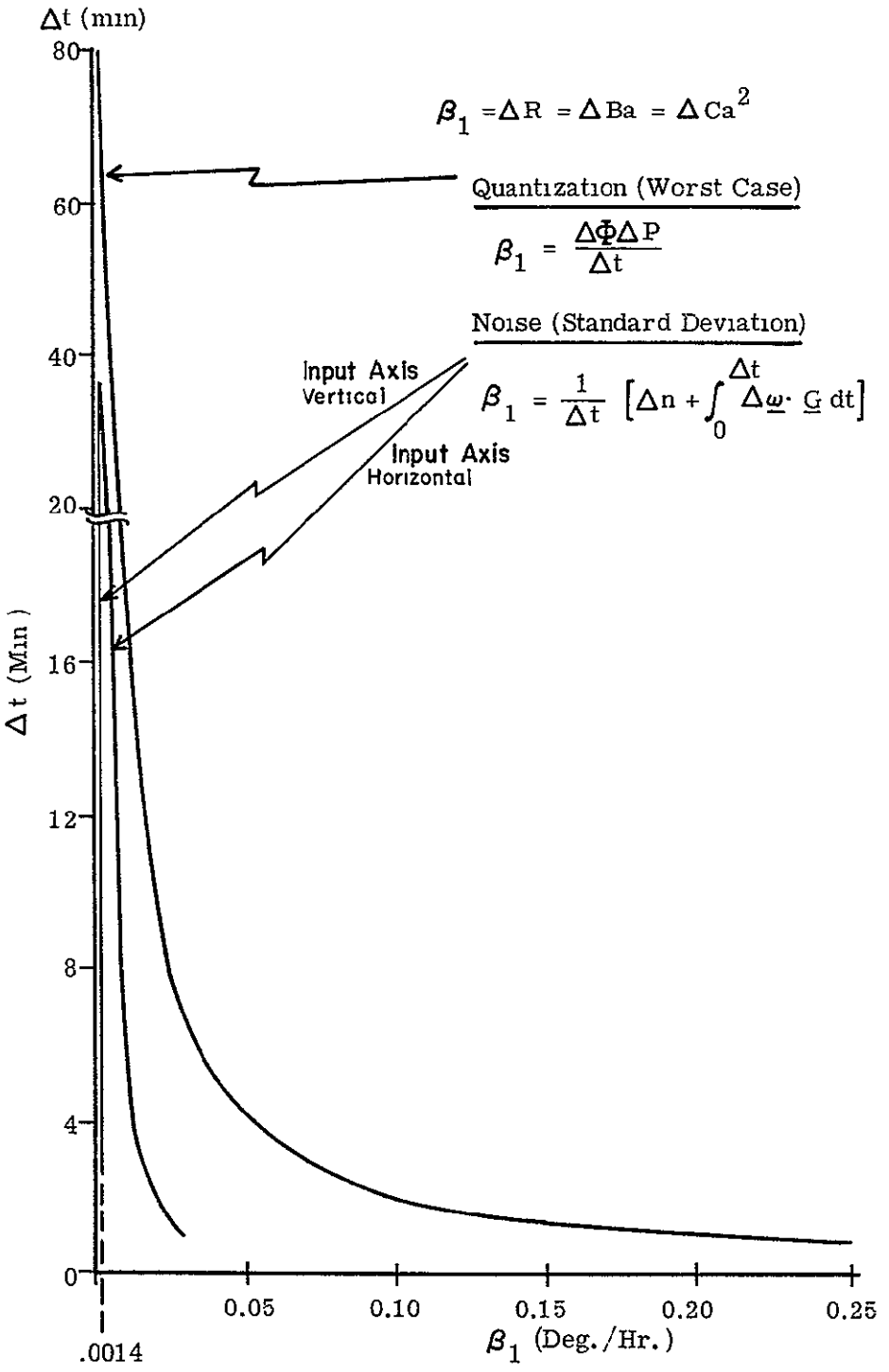

Figure 2-1. Gyro Bias Error vs Time

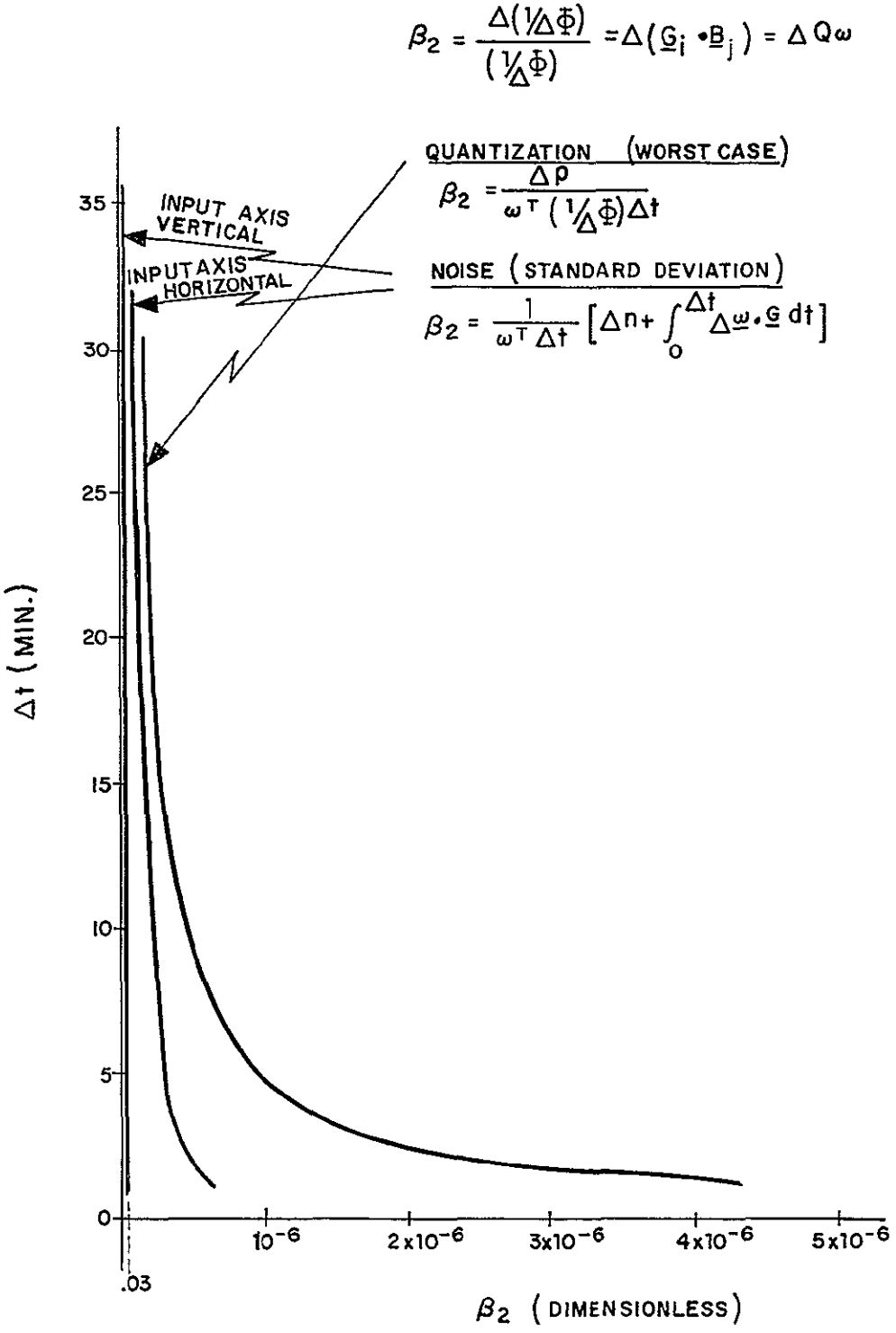

Figure 2-2. Gyro Scale Factor Error vs Time

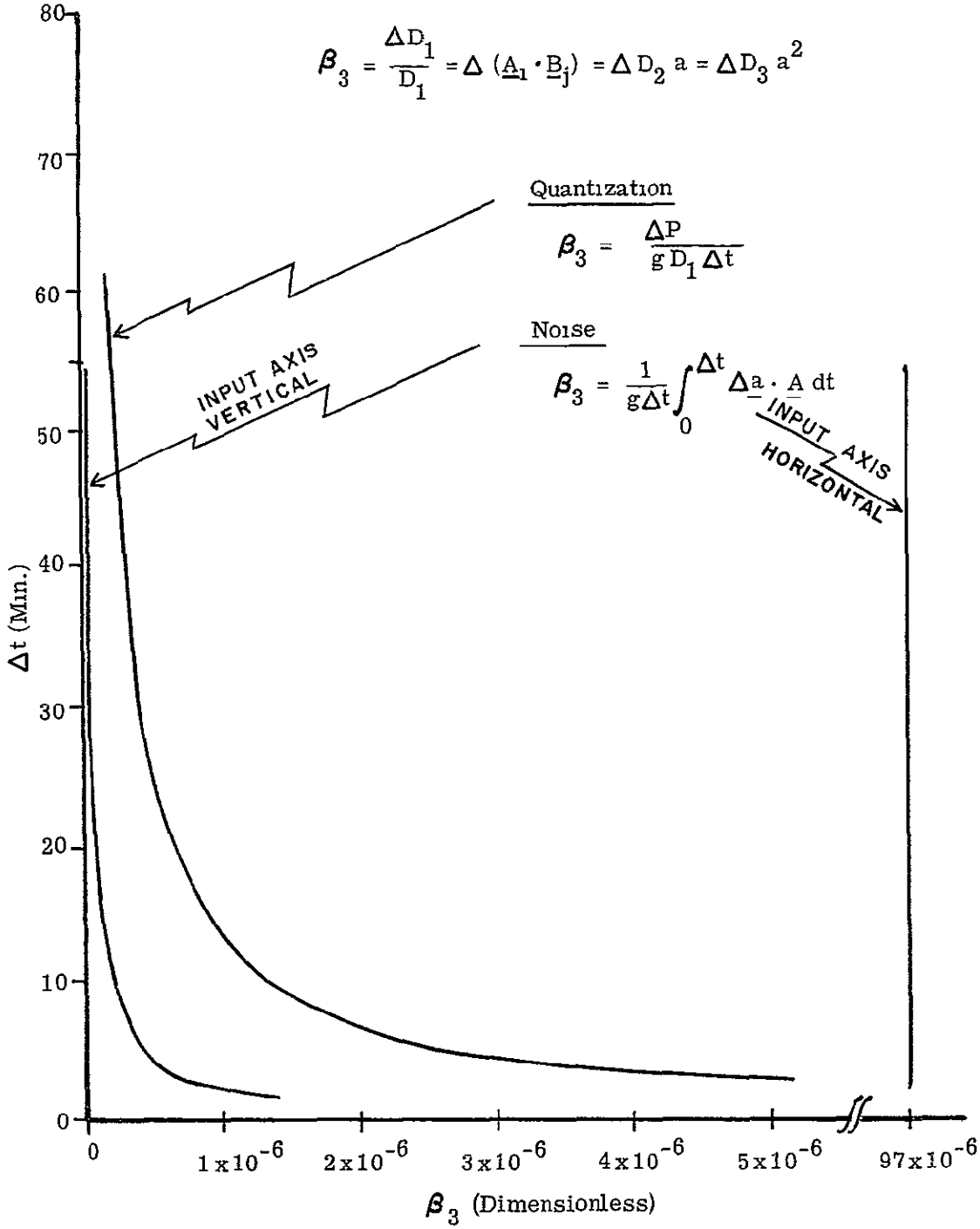

Figure 2-3. Accelerometer Scale Factor Error vs Time

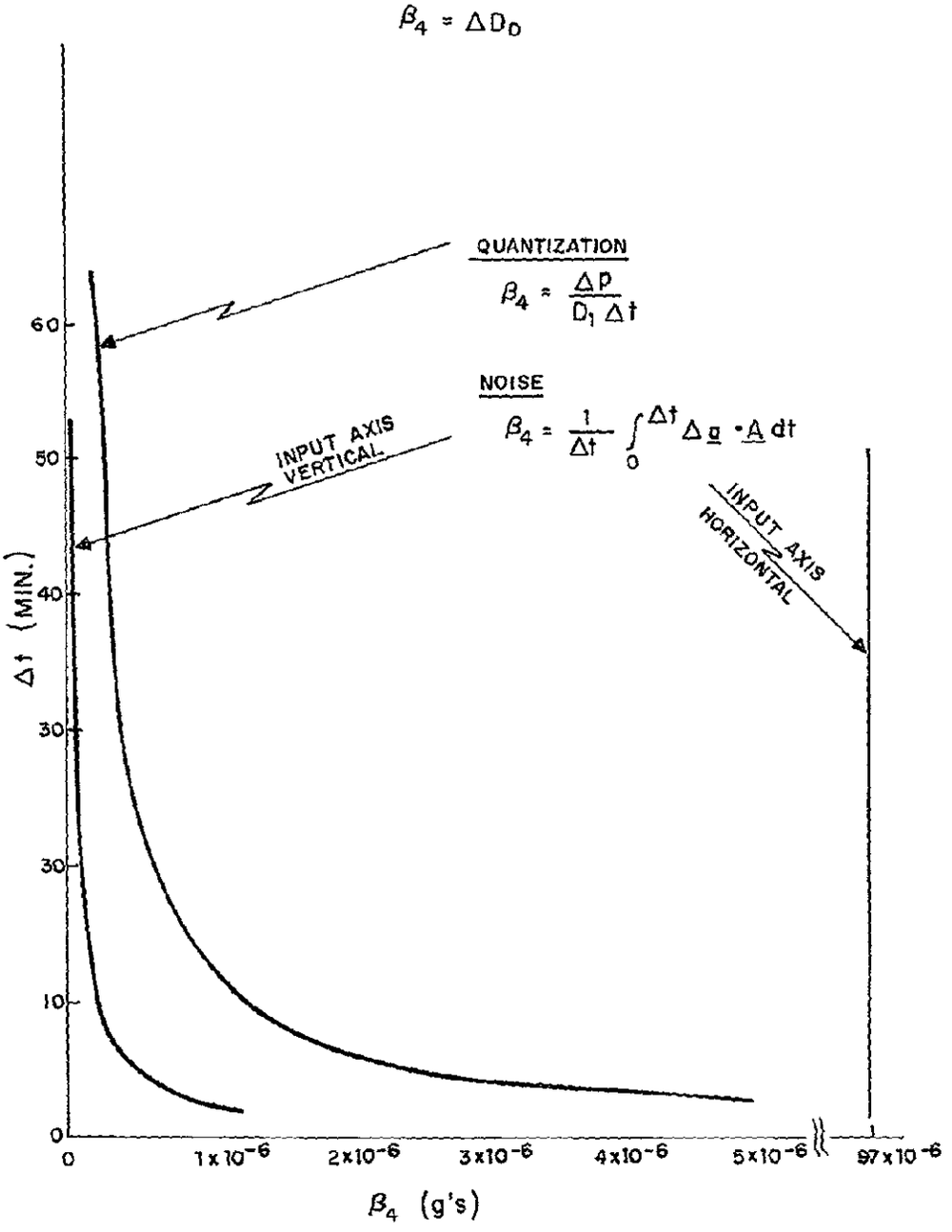

Figure 2-4. Accelerometer Bias Error vs Time

- Geometrical assumptions: $\underline{g}$ defines the vertical and earth rate $\underline{\omega}^E$ is a constant vector in inertial space, at an angle of 45^0 to the vertical.
- The gyro is fixed relative to the turntable, which rotates at a constant angular velocity $\underline{\omega}^T$ relative to the laboratory.

2.2.4 Bubble Level Compensation

In the course of the computations required for Figures 2-3 and 2-4, it was noticed that, for the horizontal position of the accelerometer, the dominant term was the pickup of a variable component of $\underline{g}$ due to rotational environment noise. This effect could be reduced if a bubble level were used periodically to measure the low frequency rotational motion during the calibration. Correcting for this motion, either mechanically or mathematically, would reduce the low frequency part of the rotational noise spectrum. Two models were tried:

1) The rotational noise spectrum, $P_\theta(f)$, was reduced to zero below a frequency corresponding to a 50-minute period. This result is tagged by the following symbol in graphs of accelerometer coefficient errors β_3 and β_4 in Figures 2-5 and 2-6:

2) The rotational noise spectrum, $P_\theta(f)$, was assumed to be the squared modulus of a first order transfer function having an rms noise in $\Delta\theta$ of 4.5 seconds of arc and a half-power frequency of 10^{-2} cps. This result is tagged by the following symbol in the figures:

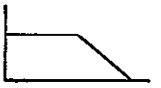

The results under these assumptions are plotted in Figures 2-5 and 2-6.

2.2.5 Concluding Remarks

Care should be exercised in drawing quantitative conclusions from the curves of noise-induced calibration errors. The noise data on which these curves are based are too scarce and too scattered geographically to be considered as the noise environment during a real calibration test. However, the curves can be used to support qualitative or comparative inferences such as the following:

- A longer averaging time will reduce the calibration errors due to environment noise.
- Calibration accuracy is strongly dependent on sensor orientation for both gyros and accelerometers.

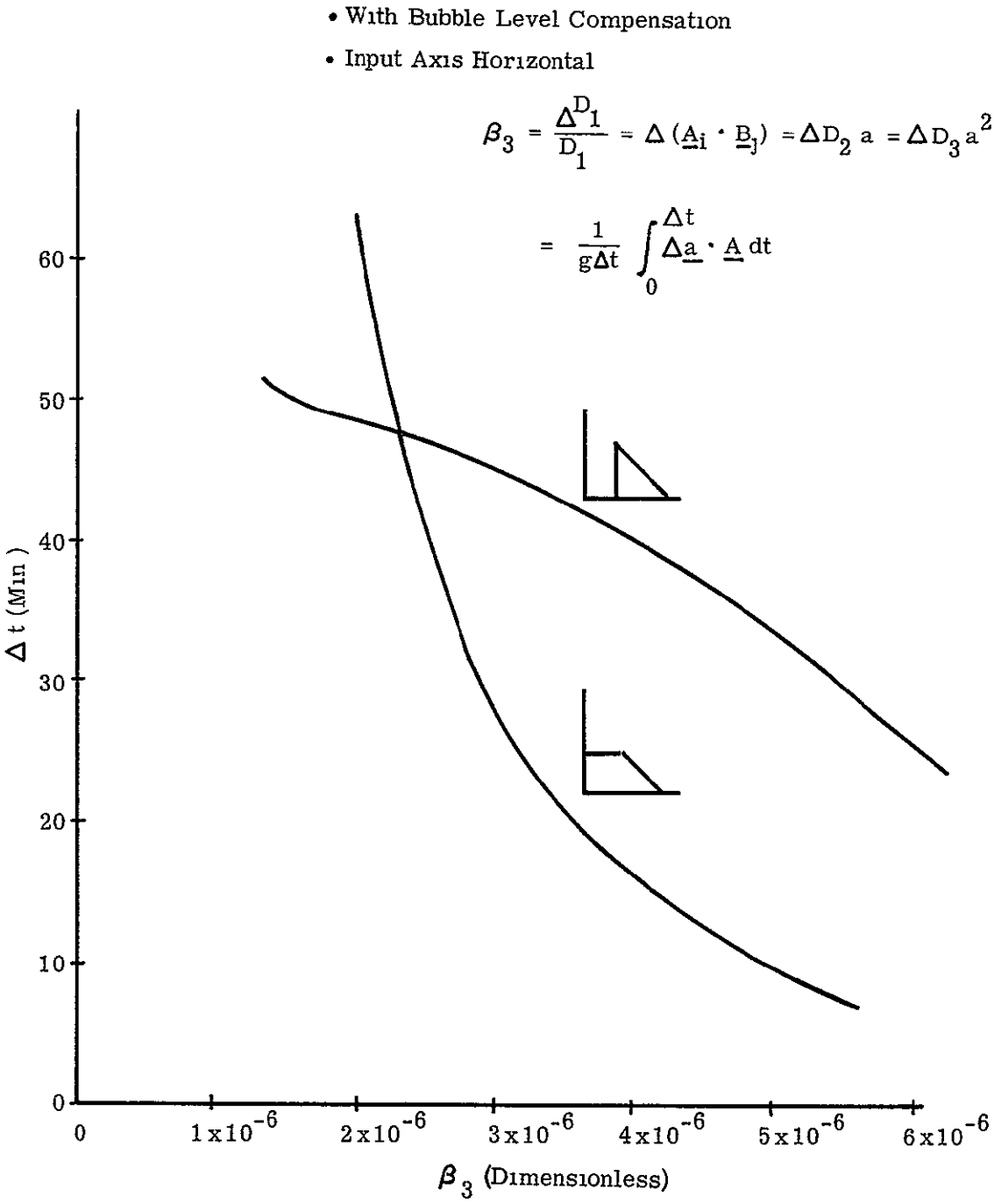

Figure 2-5. Accelerometer Scale Factor Error vs Time

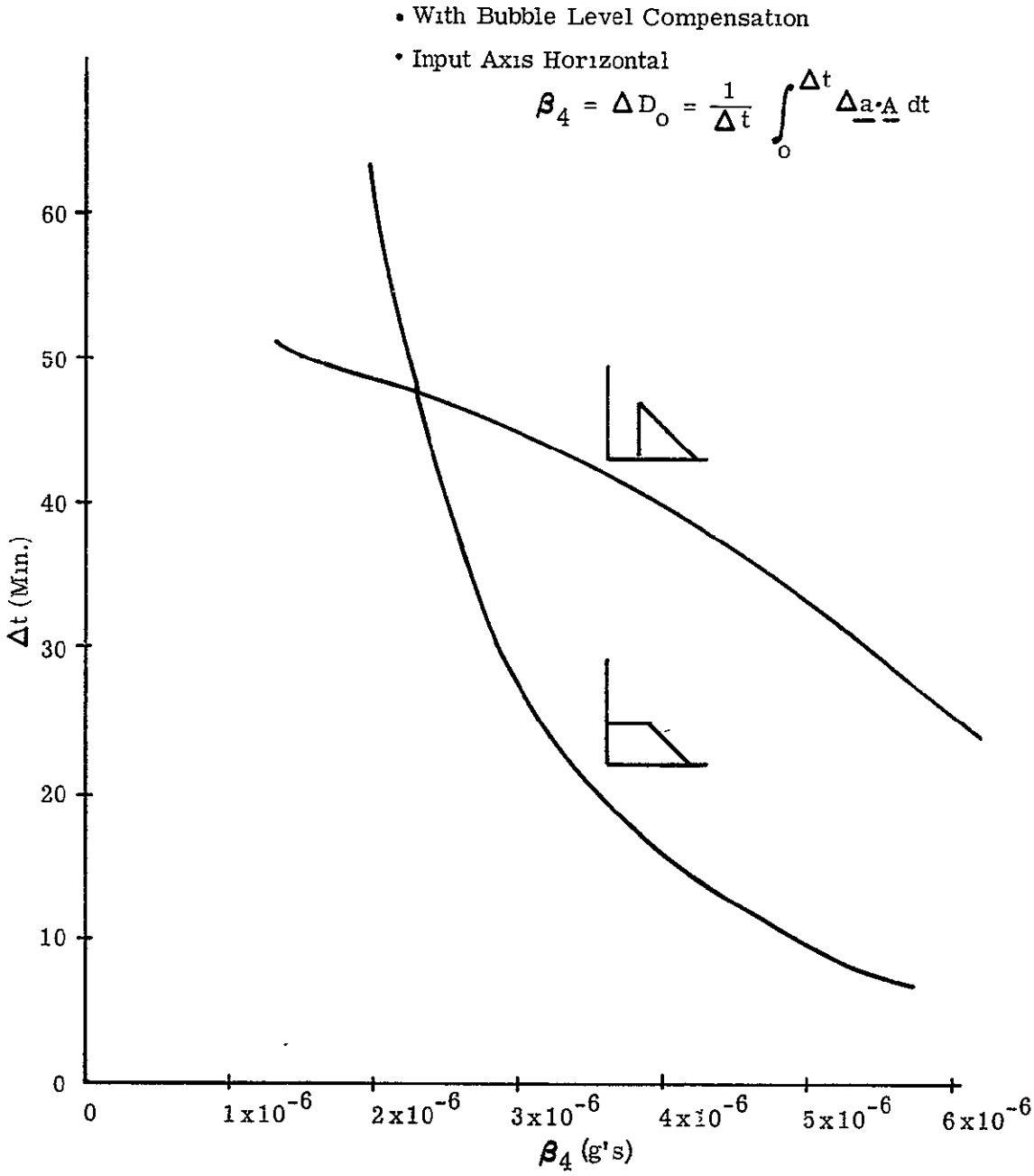

Figure 2-6. Accelerometer Bias Error vs Time

- The large errors found for the horizontal accelerometer calibration can be reduced considerably with bubble level corrections before and during the test.

- To the extent that the assumed power spectra represent the actual test environment, these results support Weinstock's conclusion* that the test bed should be isolated from the rotational (tilt) noise environment if a relative accuracy of the order of 10^{-6} is desired in the calibration of the sensor coefficients.

- Subject to how realistic these power spectra are, it may be concluded that, for the gyro coefficients, and for the vertical accelerometer, the quantization error predominates.

*H. Weinstock, loc. cit., p. 45.

SECTION 3

SECTION 3
INTRODUCTION TO ALIGNMENT TRADE-OFF STUDIES

This section serves as an introduction to the alignment trade-offs described in subsequent sections. In the first subsection, the trade-off analyses are partitioned into three parts, each part corresponding to the contents of one of the Sections 4, 5, and 6. In the second subsection the four nominal ISU orientations which are used in all alignment analyses are introduced. The last subsection describes the worst-case alignment errors due to instrument quantization.

3.1 ALIGNMENT TRADE-OFFS DEFINED

The introduction to this document (Section 1) describes the alignment trade-offs which are accomplished in this study. The tabulation of the trade-off categories in the introduction is dictated by the listing as it exists in the contract statement of work. In accomplishing these trade-offs, it is very convenient to partition the presentation into three parts. The partitioning is dictated by the functional descriptions of alignment as shown in Chart 3-1.

The contents of Chart 3-1 are described in detail in Section 3 of the Development Document. For the purpose of this section, a brief description of the three separate routines is repeated. The three diagrams correspond to the three alignment techniques under study. Each diagram contains a routine entitled "Alignment Matrix Computations". This routine corresponds to the mathematics which evaluates the elements of the alignment matrix as a function of the indicated inputs. The "Preprocessing Computations" transform the inertial instrument outputs into integrals of the measured values of applied acceleration or both applied acceleration and angular velocity components. The "Estimation Routine" produces estimates of $\underline{g}$ and $\underline{\omega}^E$ from the outputs of the preprocessing routine. The coefficients of the "Estimation Routine" are set by the "Estimation Matrix Computations" to provide optimum estimation of $\underline{g}$ and $\underline{\omega}^E$ from inputs corrupted by both environmental and quantization noise.

The alignment trade-off problem is basically a question of determining alignment accuracy and time as functions of certain sources of error in the alignment technique. Thus there will in general be three cases corresponding to the three alignment techniques indicated in Chart 3-1. Moreover, since each technique can be considered as a collection of separate routines, a further breakdown of the alignment trade-off study by consideration of the several separate routines will be convenient. Each of the error sources to be considered is

CHART 3-1

ALIGNMENT FUNCTIONAL DIAGRAMS

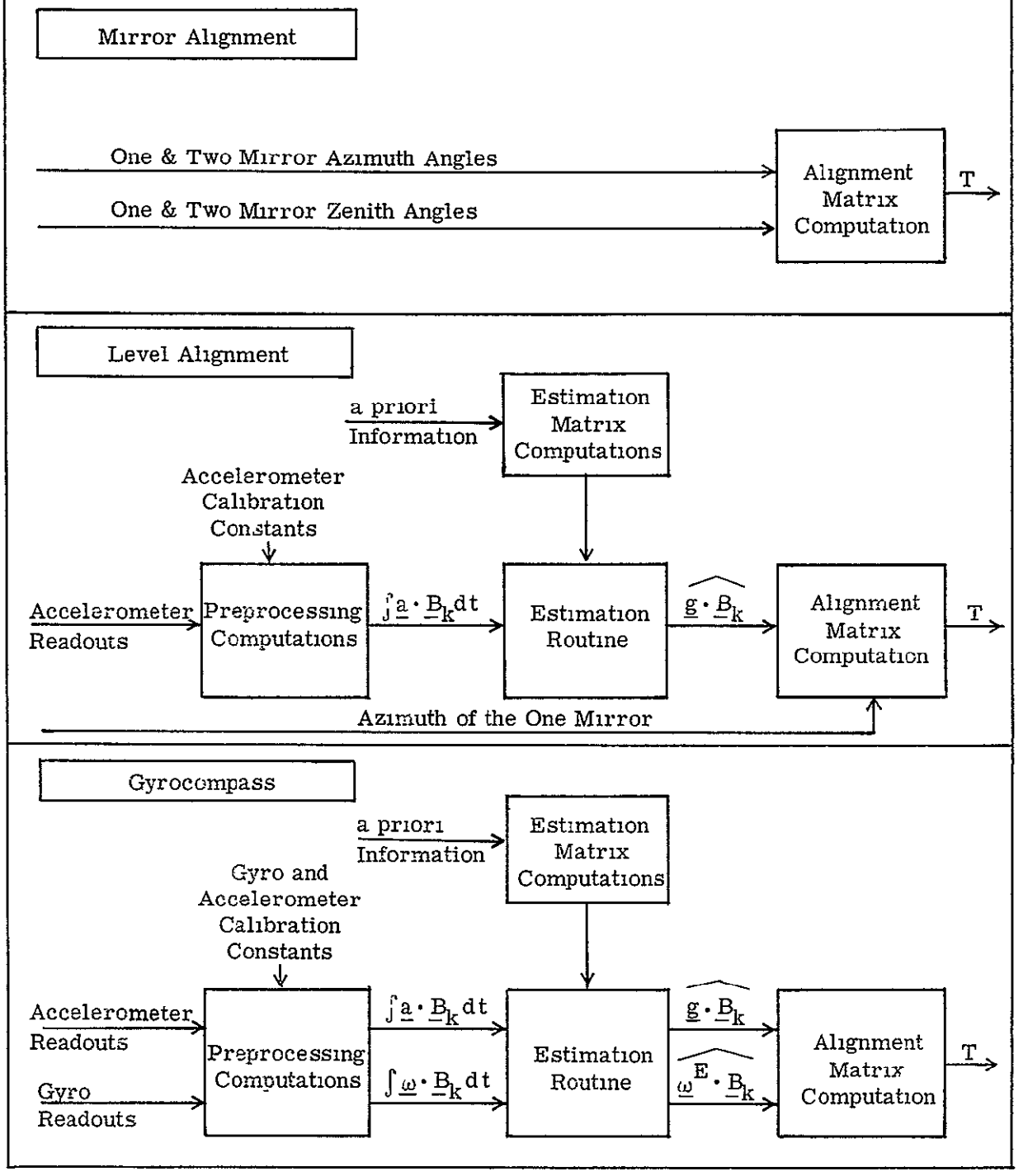

either an error in the input to one of the routines or an approximation in the arithmetic employed in a routine. More explicitly, Mirror Alignment accuracy is a function of:

1. Autocollimator readout errors.

In Level Alignment both accuracy and time are functions of 1. plus:

2. Environment (acceleration) noise
3. Accelerometer readout quantization
4. Accelerometer calibration accuracy
5. Estimation Technique
6. Estimation Computation (word length).

In Gyrocompass Alignment both accuracy and time are functions of 2. through 6. above, plus.

7. Environment (rotational) noise
8. Gyro internal noise
9. Gyro readout quantization
10. Gyro calibration accuracy.

The trade-off analysis in this study is thus directed toward discerning the effect of these error sources on the accuracy of the alignment matrix obtained. However, autocollimator errors are not covered in this study because of unavailability of laboratory autocollimator data; and therefore Mirror Alignment will not be discussed in the succeeding sections.

We see from Chart 3-1 that in the last two cases T is explicitly a function of $\underline{g}$, and in the last case, $\underline{\omega}^E$. The trade-off study begins in Section 4 by relating errors in T to errors in estimating $\underline{g}$ and $\underline{\omega}^E$. Sections 5 and 6 then relate the errors in the estimates of $\underline{g}$ and $\underline{\omega}^E$ to the alignment error sources 2. through 10. listed above as they apply. Section 5 considers all of the error sources except inaccuracies in calibration constants, which are considered in Section 6. By combining the results of Section 4 with the results of Section 5 and 6 a complete picture of alignment accuracy and time, as a function of the error sources 2. through 10., is obtained.

3.2 ALIGNMENT ORIENTATION (CASES 1 TO 4)

As will be seen in the general error equations of Charts 4-5 and 4-6 (Section 4), the appearance of terms such as $(\underline{U} \cdot \underline{B}_k)$, $(\underline{W} \cdot \underline{B}_k)$ etc. illustrates the dependence of alignment accuracy on the nominal orientation of the body axes relative to the earth.

Experience has shown that four specific orientations bracket the extremes of this dependence. These four orientations are defined in Charts 3-2 through 3-5 which follow. All alignment accuracy analyses are developed for all four of these orientations.

3.3 ALIGNMENT TIME VERSUS ALIGNMENT ACCURACY FOR WORST-CASE QUANTIZATION

In Chart 3-6 we develop the relationship between worst-case quantization errors and errors in the estimate of $\underline{g}$ and $\underline{\omega}^E$ as a function of sample time. Alignment errors in terms of errors in the T matrix, ΔT, are obtained by substitution of these worst-case quantization error expressions into the error matrices of Section 4.2. Alignment errors in terms of total rotation angle or cone angles are obtained by substitution of the elements of the $\Delta T T^T$ of Section 4.2 into the expressions developed in Chart 4-3.

Application of these results show that the gyrocompass azimuth error, due to a worst-case, one pulse, "east gyro" quantization error ($\Delta\Phi = 12$ seconds of arc per pulse) is on the order of $3700/\Delta t$ seconds of arc (Δt is in minutes). On the other hand, the level error due to worse-case, one pulse, accelerometer quantization error ($D_1 = 254$ pulses per g) is on the order of $37/\Delta t$ seconds of arch (Δt in minutes). Thus the gyrocompass alignment error is dominated by "east gyro" quantization. An alignment time on the order of two hours is therefore required to reduce the azimuth error to the order of the level error.

Because of this gyro quantization effect, the alignment studies of Section 5 are devoted principally to an investigation of noise filtering techniques for level alignment.

NOMINAL ALIGNMENT ORIENTATION

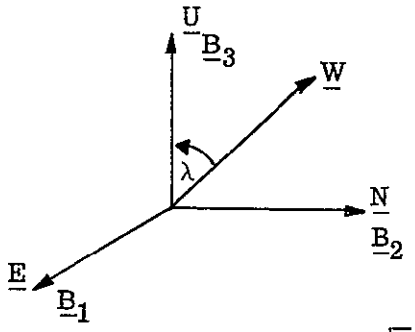

Case 1

$\underline{B}_1$ is pointing east

$\underline{B}_2$ is pointing north

$\underline{B}_3$ is pointing up

$$[T] = \begin{bmatrix} 0 & 0 & 1 \\ 1 & 0 & 0 \\ 0 & 1 & 0 \end{bmatrix}$$

$$\underline{\omega}^E \cdot \underline{B}_1 = 0 \qquad \underline{g} \cdot \underline{B}_1 = 0$$

$$\underline{\omega}^E \cdot \underline{B}_2 = \omega^E \sin \lambda \qquad \underline{g} \cdot \underline{B}_2 = 0$$

$$\underline{\omega}^E \cdot \underline{B}_3 = \omega^E \cos \lambda \qquad \underline{g} \cdot \underline{B}_3 = g$$

when $\lambda = 45^o$

$$\underline{\omega}^E \cdot \underline{B}_1 = 0$$

$$\underline{\omega}^E \cdot \underline{B}_2 = 0.707\ \omega^E$$

$$\underline{\omega}^E \cdot \underline{B}_3 = 0.707\ \omega^E$$

$$\underline{g} \cdot \underline{B}_1 = 0$$

$$\underline{g} \cdot \underline{B}_2 = 0$$

$$\underline{g} \cdot \underline{B}_3 = g$$

NOMINAL ALIGNMENT ORIENTATION

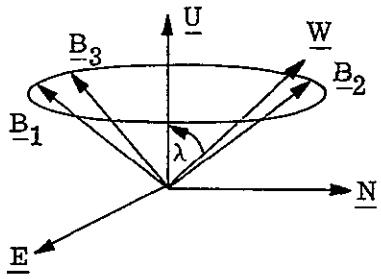

Case 2

$\underline{B}_1$, $\underline{B}_2$ and $\underline{B}_3$ are equal angles from up

$\underline{B}_1$ is in the up-east plane

$$[T] = \begin{bmatrix} 0.577 & 0.577 & 0.577 \\ 0.815 & -0.407 & -0.407 \\ 0 & 0.707 & -0.707 \end{bmatrix}$$

$$\underline{\omega}^E \cdot \underline{B}_1 = (\sqrt{1/3}\cos\lambda)\,\omega^E \qquad \underline{g} \cdot \underline{B}_1 = \sqrt{1/3}\,g$$

$$\underline{\omega}^E \cdot \underline{B}_2 = (\sqrt{1/3}\cos\lambda + \sqrt{1/2}\sin\lambda)\,\omega^E \qquad \underline{g} \cdot \underline{B}_2 = \sqrt{1/3}\,g$$

$$\underline{\omega}^E \cdot \underline{B}_3 = (\sqrt{1/3}\cos\lambda - \sqrt{1/2}\sin\lambda)\,\omega^E \qquad \underline{g} \cdot \underline{B}_3 = \sqrt{1/3}\,g$$

when $\lambda = 45^o$

$$\underline{\omega}^E \cdot \underline{B}_1 = 0.407\,\omega^E$$

$$\underline{\omega}^E \cdot \underline{B}_2 = 0.907\,\omega^E$$

$$\underline{\omega}^E \cdot \underline{B}_3 = -0.093\,\omega^E$$

$$\underline{g} \cdot \underline{B}_1 = 0.577\,g$$

$$\underline{g} \cdot \underline{B}_2 = 0.577\,g$$

$$\underline{g} \cdot \underline{B}_3 = 0.577\,g$$

NOMINAL ALIGNMENT ORIENTATION

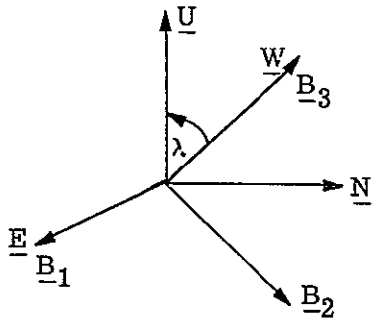

Case 3

$\underline{B}_1$ is pointing east

$\underline{B}_3$ is pointing along earth rate

$$[T] = \begin{bmatrix} 0 & -\sin\lambda & \cos\lambda \\ 1 & 0 & 0 \\ 0 & \cos\lambda & \sin\lambda \end{bmatrix}$$

$$\underline{\omega}^E \cdot \underline{B}_1 = 0 \qquad \underline{g} \cdot \underline{B}_1 = 0$$

$$\underline{\omega}^E \cdot \underline{B}_2 = 0 \qquad \underline{g} \cdot \underline{B}_2 = -g \sin\lambda$$

$$\underline{\omega}^E \cdot \underline{B}_3 = \omega^E \qquad \underline{g} \cdot \underline{B}_3 = g \cos\lambda$$

when $\lambda = 45^o$

$$[T] = \begin{bmatrix} 0 & -0.707 & 0.707 \\ 1 & 0 & 0 \\ 0 & 0.707 & 0.707 \end{bmatrix}$$

$$\underline{\omega}^E \cdot \underline{B}_1 = 0$$

$$\underline{\omega}^E \cdot \underline{B}_2 = 0$$

$$\underline{\omega}^E \cdot \underline{B}_3 = 0$$

$$\underline{g} \cdot \underline{B}_1 = 0$$

$$\underline{g} \cdot \underline{B}_2 = -0.707\,g$$

$$\underline{g} \cdot \underline{B}_3 = 0.707\,g$$

NOMINAL ALIGNMENT ORIENTATION

Case 4

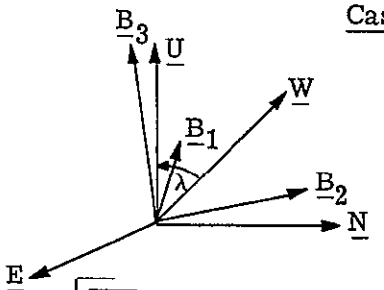

$\underline{B}_1$, $\underline{B}_2$ and $\underline{B}_3$ are equal angles from earth rate

$\underline{B}_1$ is in the earth rate-east plane

$$[T] = \begin{bmatrix} \sqrt{1/3}\cos\lambda & \sqrt{1/3}\cos\lambda - \sqrt{1/2}\sin\lambda & \sqrt{1/3}\cos\lambda - \sqrt{1/2}\sin\lambda \\ \sqrt{2/3} & -\sqrt{1/6} & -\sqrt{1/6} \\ \sqrt{1/3}\sin\lambda & \sqrt{1/3}\sin\lambda + \sqrt{1/2}\cos\lambda & \sqrt{1/3}\sin\lambda - \sqrt{1/2}\cos\lambda \end{bmatrix}$$

$$\underline{\omega}^E \cdot \underline{B}_1 = \sqrt{1/3}\,\omega^E \qquad \underline{g} \cdot \underline{B}_1 = (\sqrt{1/2}\cos\lambda)\,g$$

$$\underline{\omega}^E \cdot \underline{B}_2 = \sqrt{1/3}\,\omega^E \qquad \underline{g} \cdot \underline{B}_2 = (\sqrt{1/3}\cos\lambda - \sqrt{1/2}\sin\lambda)\,g$$

$$\underline{\omega}^E \cdot \underline{B}_3 = \sqrt{1/3}\,\omega^E \qquad \underline{g} \cdot \underline{B}_3 = (\sqrt{1/3}\cos\lambda + \sqrt{1/2}\sin\lambda)\,g$$

when $\lambda = 45^o$

$$[T] = \begin{bmatrix} \sqrt{1/6} & (\sqrt{1/6} - 1/2) & (\sqrt{1/6} + 1/2) \\ \sqrt{2/3} & -\sqrt{1/6} & -\sqrt{1/6} \\ \sqrt{1/6} & (\sqrt{1/6} + 1/2) & (\sqrt{1/6} - 1/2) \end{bmatrix} = \begin{bmatrix} 0.407 & -0.093 & 0.907 \\ 0.815 & -0.407 & -0.407 \\ 0.417 & 0.907 & -0.093 \end{bmatrix}$$

$$\underline{\omega}^E \cdot \underline{B}_1 = 0.577\,\omega^E$$

$$\underline{\omega}^E \cdot \underline{B}_2 = 0.577\,\omega^E$$

$$\underline{\omega}^E \cdot \underline{B}_3 = 0.577\,\omega^E$$

$$\underline{g} \cdot \underline{B}_1 = 0.407\,g$$

$$\underline{g} \cdot \underline{B}_2 = -0.093\,g$$

$$\underline{g} \cdot \underline{B}_3 = 0.907\,g$$

QUANTIZATION ERROR

Assumptions

- Linear instruments
- No noise
- Perfect calibration
- Constant gravity and earth rate inputs
- Instrument and body axes are perfectly aligned

These assumptions say that

$$\underline{\omega}^E \cdot \underline{B}_k = (\Delta\Phi)P_k^G/\Delta t$$

$$\underline{g} \cdot \underline{B}_k = (1/D_1)(P_k^A/\Delta t)$$

Assuming a n^G quantum error in P_k^G and a n^A quantum error in P_k^A we have

$$\frac{\Delta(\underline{\omega}^E \cdot \underline{B}_k)}{\omega^E} = \frac{(\Delta\Phi)n^G}{\omega^E \Delta t}$$

$$\frac{\Delta(\underline{g} \cdot \underline{B}_k)}{g} = \frac{n^A}{D_1 g \Delta t}$$

Substituting the nominal scale factors and

$$n^G = 1 \text{ pulse} \qquad n^A = 2 \text{ pulses}$$

we have

$$\frac{\Delta(\underline{\omega}^E \cdot \underline{B}_k)}{\omega^E} = \frac{133 \times 10^{-4}}{\Delta t(\text{in minutes})}$$

$$\frac{\Delta(\underline{g} \cdot \underline{B}_k)}{g} = \frac{131 \times 10^{-6}}{\Delta t(\text{in minutes})}$$

SECTION 4

SECTION 4
ALIGNMENT ACCURACY VERSUS $\underline{g}$, $\underline{\omega}^E$ PRECISION

We begin this section by defining a basic measure of alignment errors (the elements of the ΔTT^T matrix). We then relate this basic measure, through the T matrix, to errors in estimates $\underline{g}$ and $\underline{\omega}^E$ for each of the four orientation cases and for both level and gyrocompass alignment. Finally, we develop the statistics of the basic measure of the alignment errors in terms of the statistics of the errors in the estimates of $\underline{g}$ and $\underline{\omega}^E$.

The results of this section will be used in Section 5 and 6 to transform errors in $\underline{g}$ and $\underline{\omega}^E$ to equivalent errors in the defined basic measure.

4.1 GENERALIZED ERROR EQUATIONS

In the Development Document, alignment was defined as the initialization of the T matrix which transforms from an ISU fixed set of axes to an earth-fixed, local level set. Three types of alignment techniques were presented: Mirror Alignment, Level Alignment and Gyrocompass Alignment. Errors in Mirror Alignment are directly a function of the autocollimator survey and not a function of the outputs of the inertial instruments or computations. For this reason, the following generalized error equations are developed for Level and Gyrocompass Alignment only.

The T matrices for level alignment and gyrocompass alignment are reproduced for reference in Charts 4-1 and 4-2, respectively. It should be noted that the computed matrix is always orthonormal irrespective of the errors in $\underline{U}$ and $\underline{W}$. Thus, the alignment error can be expressed as the difference between two sets of orthogonal axes – the true and computed sets. This difference can be expressed by a single rotation which aligns the two sets. This rotation will be called the "total rotation angle" in the discussions which follow. The difference can also be expressed by the three angles between pairs of corresponding axes in the two sets. These angles will be called "cone angles".

Referring to Chart 4-3, the cone angles are approximated by the magnitude of the cross product between corresponding axes in the true and computed sets. The equations for the squares of the cone angles given in Chart 4-3 are developed in Chart 4-4.

Both the cone angles and the total rotational angle are developed as functions of ΔTT^T. As the errors in $\underline{g}$ and $\underline{\omega}$ will be small, the ΔT matrix is obtained by taking the first difference of the T matrix in terms of $\underline{g}$ and $\underline{\omega}$. The ΔT matrices for level alignment and gyrocompass alignment are presented in Chart 4-5 and 4-6, respectively.

LEVEL ALIGNMENT MATRIX

Inputs $(\underline{g}\cdot\underline{B}_1)$, $(\underline{g}\cdot\underline{B}_2)$, $(\underline{g}\cdot\underline{B}_3)$ and α_1

From these quantities the alignment matrix is given by:

$$\begin{bmatrix} \\ T \\ \\ \end{bmatrix} = \begin{bmatrix} 1 & 0 & 0 \\ 0 & \sin\alpha_1 & \cos\alpha_1 \\ 0 & -\cos\alpha_1 & \sin\alpha_1 \end{bmatrix} \begin{bmatrix} 0 & 1 & 0 \\ 0 & 0 & \dfrac{1}{|\underline{M}_1\times\underline{U}|} \\ \dfrac{1}{|\underline{M}_1\times\underline{U}|} & \dfrac{(\underline{M}_1\cdot\underline{U})}{|\underline{M}_1\times\underline{U}|} & 0 \end{bmatrix} \begin{bmatrix} 1 & 0 & 0 \\ (\underline{U}\cdot\underline{B}_1) & (\underline{U}\cdot\underline{B}_2) & (\underline{U}\cdot\underline{B}_3) \\ 0 & -(\underline{U}\cdot\underline{B}_3) & (\underline{U}\cdot\underline{B}_2) \end{bmatrix}$$

where

- $(\underline{M}_1\cdot\underline{U}) = (\underline{U}\cdot\underline{B}_1)$
- $|\underline{M}_1\times\underline{U}| = [1 - (\underline{M}_1\cdot\underline{U}^2]^{1/2}$
- $(\underline{U}\cdot\underline{B}_k) = (\underline{g}\cdot\underline{B}_k)/g$
- $g = [(\underline{g}\cdot\underline{B}_1)^2 + (\underline{g}\cdot\underline{B}_2)^2 + (\underline{g}\cdot\underline{B}_3)^2]^{1/2}$

An optional technique might utilize any of the following additional inputs:

- The zenith angle (θ_1) of mirror one might be utilized to find $(\underline{M}_1\cdot\underline{U})$ from
$$(\underline{M}_1\cdot\underline{U}) = \cos\theta_1$$
- The magnitude of gravity (g) might be supplied from a local survey. This piece of information can be utilized to reduce the number of required accelerometers to two.

GYROCOMPASS MATRIX

Inputs $(\underline{g}\cdot\underline{B}_1)$, $(\underline{g}\cdot\underline{B}_2)$, $(\underline{g}\cdot\underline{B}_3)$, $(\underline{\omega}^E\cdot\underline{B}_1)$, $(\underline{\omega}^E\cdot\underline{B}_2)$, and $(\underline{\omega}^E\cdot\underline{B}_3)$

From these quantities the alignment matrix is given by:

$$\begin{bmatrix} \\ T \\ \\ \end{bmatrix} = \begin{bmatrix} 0 & 1 & 0 \\ 0 & 0 & \dfrac{1}{|\underline{W}\times\underline{U}|} \\ \dfrac{1}{|\underline{W}\times\underline{U}|} & -\dfrac{(\underline{W}\cdot\underline{U})}{|\underline{W}\times\underline{U}|} & 0 \end{bmatrix} \begin{bmatrix} (\underline{W}\cdot\underline{B}_1) & (\underline{W}\cdot\underline{B}_2) & (\underline{W}\cdot\underline{B}_3) \\ (\underline{U}\cdot\underline{B}_1) & (\underline{U}\cdot\underline{B}_2) & (\underline{U}\cdot\underline{B}_3) \\ (\underline{W}\times\underline{U})\cdot(\underline{B}_2\times\underline{B}_3) & (\underline{W}\times\underline{U})\cdot(\underline{B}_3\times\underline{B}_1) & (\underline{W}\times\underline{U})\cdot(\underline{B}_1\times\underline{B}_2) \end{bmatrix}$$

where

- $(\underline{W}\cdot\underline{U}) = (\underline{W}\cdot\underline{B}_1)(\underline{U}\cdot\underline{B}_1) + (\underline{W}\cdot\underline{B}_2)(\underline{U}\cdot\underline{B}_2) + (\underline{W}\cdot\underline{B}_3)(\underline{U}\cdot\underline{B}_3)$
- $|\underline{W}\times\underline{U}| = [1 - (\underline{W}\cdot\underline{U})^2]^{1/2}$
- $(\underline{W}\cdot\underline{B}_k) = (\underline{\omega}^E\cdot\underline{B}_k)/\omega^E$
- $(\underline{U}\cdot\underline{B}_k) = (\underline{g}\cdot\underline{B}_k)/g$
- $\omega^E = [(\underline{\omega}^E\cdot\underline{B}_1)^2 + (\underline{\omega}^E\cdot\underline{B}_2)^2 + (\underline{\omega}^E\cdot\underline{B}_3)^2]^{1/2}$
- $g = [(\underline{g}\cdot\underline{B}_1)^2 + (\underline{g}\cdot\underline{B}_2)^2 + (\underline{g}\cdot\underline{B}_3)^2]^{1/2}$

An optional technique might utilize any of the following additional inputs:

- The local latitude (λ) might be utilized to find $(\underline{W}\cdot\underline{U})$ from
$$(\underline{W}\cdot\underline{U}) = \cos\lambda$$
- The magnitude of gravity (g) might be supplied from a local survey.
- The magnitude of earth rate (ω^E) might be supplied from a local survey.

A use of all additional inputs could reduce the number of necessary instruments to three (either two accelerometers and one gyro, or one accelerometer and two gyros).

ALIGNMENT PRECISION

The alignment matrix has been defined as a transformation from body to earth axes. That is

$$\begin{bmatrix} \underline{E}_1 \\ \underline{E}_2 \\ \underline{E}_3 \end{bmatrix} = \begin{bmatrix} \underline{U} \\ \underline{E} \\ \underline{N} \end{bmatrix} = \begin{bmatrix} \\ T \\ \\ \end{bmatrix} \begin{bmatrix} \underline{B}_1 \\ \underline{B}_2 \\ \underline{B}_3 \end{bmatrix}$$

If the elements of T are in error, an erroneous earth frame will be defined, or

$$\begin{bmatrix} \underline{E}'_1 \\ \underline{E}'_2 \\ \underline{E}'_3 \end{bmatrix} = \begin{bmatrix} \\ T + \Delta T \\ \\ \end{bmatrix} \begin{bmatrix} \underline{B}_1 \\ \underline{B}_2 \\ \underline{B}_3 \end{bmatrix}$$

A multiplication of this matrix by T^T will yield a transformation from the real earth axes to the erroneous axes.

$$\begin{bmatrix} \underline{E}'_1 \\ \underline{E}'_2 \\ \underline{E}'_3 \end{bmatrix} = \begin{bmatrix} \\ T + \Delta T \\ \\ \end{bmatrix} \begin{bmatrix} \\ T^T \\ \\ \end{bmatrix} \begin{bmatrix} \underline{E}_1 \\ \underline{E}_2 \\ \underline{E}_3 \end{bmatrix} = \begin{bmatrix} \\ I + \Delta T T^T \\ \\ \end{bmatrix} \begin{bmatrix} \underline{E}_1 \\ \underline{E}_2 \\ \underline{E}_3 \end{bmatrix}$$

From Chart 4-4, which follows, the cone angle errors of up, east, and north are given by

$$\begin{aligned} \left| \underline{U} \times \underline{U}' \right|^2 &= \left[\Delta T T^T \right]^2_{12} + \left[\Delta T T^T \right]^2_{13} \\ \left| \underline{E}' \times \underline{E} \right|^2 &= \left[\Delta T T^T \right]^2_{21} + \left[\Delta T T^T \right]^2_{23} \\ \left| \underline{N}' \times \underline{N} \right|^2 &= \left[\Delta T T^T \right]^2_{31} + \left[\Delta T T^T \right]^2_{32} \end{aligned}$$

In all error analyses in this document we have constrained the computed ($\underline{E}'_k$) frame to always be orthonormal. The real ($\underline{E}_k$) frame is by definition orthonormal. Therefore, the $\Delta T T^T$ matrix (to first order) will always be an antisymmetric rotation matrix. The three independent quantities in that matrix will therefore represent the up, east and north components of the small angle rotation vector. A representation of the rigid body rotation between the computed and real frame will therefore be

$$(\text{total rotation angle})^2 = (\Delta T T^T)^2_{12} + (\Delta T T^T)^2_{13} + (\Delta T T^T)^2_{23}$$

CONE ANGLES FROM ΔTT^T MATRIX

$$\left|\underline{U} \times \underline{U}'\right|^2 = (\underline{U} \times \underline{U}') \cdot (\underline{U} \times \underline{U}')$$

$$= (\underline{U}' \cdot \underline{U}') - (\underline{U} \cdot \underline{U}')^2$$

From Chart 4-3,

$$\begin{bmatrix} \underline{U}' \\ \underline{E}' \\ \underline{N}' \end{bmatrix} = \begin{bmatrix} I + \Delta TT^T \end{bmatrix} \begin{bmatrix} \underline{U} \\ \underline{E} \\ \underline{N} \end{bmatrix}$$

From which it follows that

$$\underline{U}' - \underline{U} = (\Delta TT^T)_{11}\underline{U} + (\Delta TT^T)_{12}\underline{E} + (\Delta TT^T)_{13}\underline{N}$$

$$(\underline{U}' - \underline{U}) \cdot (\underline{U}' - \underline{U}) = (\underline{U}' \cdot \underline{U}') - 2(\underline{U}' \cdot \underline{U}) + 1$$

$$= \left[(\Delta TT^T)_{11}\right]^2 + \left[(\Delta TT^T)_{12}\right]^2 + \left[(\Delta TT^T)_{13}\right]^2$$

Also

$$\left[(\underline{U}' - \underline{U}) \cdot \underline{U}\right]^2 = (\underline{U}' \cdot \underline{U})^2 - 2(\underline{U}' \cdot \underline{U}) + 1$$

$$= \left[(\Delta TT^T)_{11}\right]^2$$

From which it follows after substitution

$$\left|\underline{U} \times \underline{U}'\right|^2 = \left[(\Delta TT^T)_{12}\right]^2 + \left[(\Delta TT^T)_{13}\right]^2$$

In the same way,

$$\left|\underline{E} \times \underline{E}'\right|^2 = \left[(\Delta TT^T)_{21}\right]^2 + \left[(\Delta TT^T)_{23}\right]^2$$

$$\left|\underline{N} \times \underline{N}'\right|^2 = \left[(\Delta TT^T)_{31}\right]^2 + \left[(\Delta TT^T)_{32}\right]^2$$

LEVEL ALIGNMENT ERROR EQUATIONS

Assuming
- $(\underline{g}\cdot\underline{B}_1)$, $(\underline{g}\cdot\underline{B}_2)$, and $(\underline{g}\cdot\underline{B}_3)$ are in error
- No constraints, such as the magnitude of gravity, are used in the solution of T

Then, the first order error in the alignment matrix is given by

$$[\Delta T] = \begin{bmatrix} 1 & 0 & 0 \\ 0 & \sin\alpha_1 & \cos\alpha_1 \\ 0 & -\cos\alpha_1 & \sin\alpha_1 \end{bmatrix} \begin{bmatrix} \Delta(\underline{U}\cdot\underline{B}_1) & \Delta(\underline{U}\cdot\underline{B}_2) & \Delta(\underline{U}\cdot\underline{B}_3) \\ 0 & -\left[\dfrac{(\underline{U}\cdot\underline{B}_1)(\underline{U}\cdot\underline{B}_3)}{|\underline{U}\times\underline{B}_1|^3}\Delta(\underline{U}\cdot\underline{B}_1) + \dfrac{\Delta(\underline{U}\cdot\underline{B}_3)}{|\underline{U}\times\underline{B}_1|}\right] & \left[\dfrac{(\underline{U}\cdot\underline{B}_1)(\underline{U}\cdot\underline{B}_2)}{|\underline{U}\times\underline{B}_1|^3}\Delta(\underline{U}\cdot\underline{B}_1) + \dfrac{\Delta(\underline{U}\cdot\underline{B}_2)}{|\underline{U}\times\underline{B}_1|}\right] \\ -\dfrac{(\underline{U}\cdot\underline{B}_1)}{|\underline{U}\times\underline{B}_1|}\Delta(\underline{U}\cdot\underline{B}_1) & -\left[\dfrac{(\underline{U}\cdot\underline{B}_2)}{|\underline{U}\times\underline{B}_1|^3}\Delta(\underline{U}\cdot\underline{B}_1) + \dfrac{(\underline{U}\cdot\underline{B}_1)}{|\underline{U}\times\underline{B}_1|}\Delta(\underline{U}\cdot\underline{B}_2)\right] & -\left[\dfrac{(\underline{U}\cdot\underline{B}_3)}{|\underline{U}\times\underline{B}_1|^3}\Delta(\underline{U}\cdot\underline{B}_1) + \dfrac{(\underline{U}\cdot\underline{B}_1)}{|\underline{U}\times\underline{B}_1|}\Delta(\underline{U}\cdot\underline{B}_3)\right] \end{bmatrix}$$

where $$\Delta(\underline{U}\cdot\underline{B}_k) = \sum_{\ell}\left[\delta_{k\ell} - (\underline{U}\cdot\underline{B}_k)(\underline{U}\cdot\underline{B}_\ell)\right]\left[\frac{\Delta(\underline{g}\cdot\underline{B}_\ell)}{g}\right], \quad k = 1, 2, 3$$

and $(\underline{U}\cdot\underline{B}_k)$ for $(k=1, 2, 3)$ are the zenith angles of the body axes.

The rotation matrix is given by $\left[\Delta T T^T\right] = \left[\Delta T\right]\left[T^T\right]$

GYROCOMPASS ERROR EQUATIONS

ASSUMING

- $(\underline{g}\cdot\underline{B}_1)$, $(\underline{g}\cdot\underline{B}_2)$, $(\underline{g}\cdot\underline{B}_3)$, $(\underline{\omega}^E\ \underline{B}_1)$, $(\underline{\omega}^E\cdot\underline{B}_2)$, and $(\underline{\omega}^E\cdot\underline{B}_3)$ are in error
- No constraints have been used in the solution of T
- The nominal latitude has been chosen to be 45^o

Then the first order error in the alignment matrix is given by.

$$[\Delta T] = \begin{bmatrix} [\Delta(\underline{U}\cdot\underline{B}_1)] & [\Delta(\underline{U}\cdot\underline{B}_2)] & [\Delta(\underline{U}\cdot\underline{B}_3)] \\ [\sqrt{2\Delta}(\underline{W}\cdot\underline{U})\underline{E}\cdot\underline{B}_1+\sqrt{2\Delta}(\underline{W}\times\underline{U}\cdot\underline{B}_2\times\underline{B}_3)] & [\sqrt{2\Delta}(\underline{W}\cdot\underline{U})\underline{E}\cdot\underline{B}_2+\sqrt{2\Delta}(\underline{W}\times\underline{U}\cdot\underline{B}_3\times\underline{B}_1)] & [\sqrt{2\Delta}(\underline{W}\cdot\underline{U})\underline{E}\cdot\underline{B}_3+\sqrt{2\Delta}(\underline{W}\times\underline{U}\cdot\underline{B}_1\times\underline{B}_2)] \\ [2\Delta(\underline{W}\cdot\underline{U})(\underline{W}\cdot\underline{B}_1-\sqrt{2\underline{U}}\cdot\underline{B}_1)+\sqrt{2\Delta}(\underline{W}\cdot\underline{B}_1)-\Delta(\underline{U}\cdot\underline{B}_1)] & [2\Delta(\underline{W}\cdot\underline{U})(\underline{W}\cdot\underline{B}_2-\sqrt{2\underline{U}}\cdot\underline{B}_2)+\sqrt{2\Delta}(\underline{W}\cdot\underline{B}_2)-\Delta(\underline{U}\cdot\underline{B}_2)] & [2\Delta(\underline{W}\cdot\underline{U})(\underline{W}\cdot\underline{B}_3-\sqrt{2\underline{U}}\cdot\underline{B}_3)+\sqrt{2\Delta}(\underline{W}\cdot\underline{B}_3)-\Delta(\underline{U}\cdot\underline{B}_3)] \end{bmatrix}$$

where

- $\Delta(\underline{W}\times\underline{U}\cdot\underline{B}_k\times\underline{B}_\ell) = (\underline{W}\cdot\underline{B}_k)\Delta(\underline{U}\cdot\underline{B}_\ell)+(\underline{U}\cdot\underline{B}_\ell)\Delta(\underline{W}\cdot\underline{B}_k)-(\underline{U}\cdot\underline{B}_k)\Delta(\underline{W}\cdot\underline{B}_\ell)-(\underline{W}\cdot\underline{B}_\ell)\Delta(\underline{U}\cdot\underline{B}_k)$
- $\Delta(\underline{W}\cdot\underline{U}) = \sum_k(\underline{W}\cdot\underline{B}_k)\Delta(\underline{U}\cdot\underline{B}_k)+\sum_k(\underline{U}\cdot\underline{B}_k)\Delta(\underline{W}\cdot\underline{B}_k)$
- $\Delta(\underline{U}\cdot\underline{B}_k) = \sum_\ell[\delta_{k\ell}-(\underline{U}\cdot\underline{B}_k)(\underline{U}\cdot\underline{B}_\ell)]\left[\dfrac{\Delta(\underline{g}\cdot\underline{B}_\ell)}{g}\right]$
- $\Delta(\underline{W}\cdot\underline{B}_k) = \sum_\ell[\delta_{k\ell}-(\underline{W}\cdot\underline{B}_k)(\underline{W}\cdot\underline{B}_\ell)]\left[\dfrac{\Delta(\underline{\omega}^E\cdot\underline{B}_\ell)}{\omega^E}\right]$

where $\delta_{k\ell}$ is the "Kronecker delta" and $(\underline{U}\cdot\underline{B}_k)$ $(\underline{W}\cdot\underline{B}_k)$ and $(\underline{E}\cdot\underline{B}_k)$ are the nominal orientations of $\underline{U}$,$\underline{W}$ and $\underline{E}$ in the body frame.

The rotation matrix is given by

$$[\Delta TT^T] = [\Delta T][T^T]$$

4.2 ERROR EQUATIONS FOR CASES 1 TO 4

In this subsection the error equations are evaluated for each of the four selected orientations. In the eight charts (4-7 through 4-14) which follow, the ΔT and ΔTT^T matrices are listed for the four orientations for both level and gyrocompass alignment.

4.3 STATISTICS OF T FROM THE STATISTICS OF g AND ω^E

The one-sigma of the elements of T and ΔTT^T are derived from the statistics of $\underline{g}$ and $\underline{\omega}^E$ as follows.

An element of either ΔT or ΔTT^T can be expressed in the form

$$\sum_k \left(\frac{C_k \Delta(\underline{g} \cdot \underline{B}_k)}{g} + \frac{C_{k+3} \Delta(\underline{\omega}^E \cdot \underline{B}_k)}{\omega^E} \right)$$

where C_k and C_{k+3} are constants. The one-sigma value of this expression is

$$\sigma = \left\{ E\left[\left(\sum_k \left(\frac{C_k \Delta(\underline{g} \cdot \underline{B}_k)}{g} - \mu_k + \frac{C_{k+3} \Delta(\underline{\omega}^E \cdot \underline{B}_k)}{\omega^E} - \mu_{k+3} \right) \right)^2 \right] \right\}^{1/2}$$

where $E[A]$ is the expected value of A,

$$\mu_k = E\left[\frac{C_k \Delta(\underline{g} \cdot \underline{B}_k)}{g} \right]$$

$$\mu_{k+3} = E\left[\frac{C_{k+3} \Delta(\underline{\omega}^E \cdot \underline{B}_k)}{\omega^E} \right]$$

As before, we assume that the functions

$$\frac{\Delta(\underline{g} \cdot \underline{B}_k)}{g} \quad \text{and} \quad \frac{\Delta(\underline{\omega}^E \cdot \underline{B}_k)}{\omega^E}$$

LEVEL ALIGNMENT

CASE 1

$$\Delta T = \begin{bmatrix} 1.000\,\dfrac{\Delta(\underline{g}\cdot\underline{B}_1)}{g} & 1.000\,\dfrac{\Delta(\underline{g}\cdot\underline{B}_2)}{g} & 0.000 \\ 0.000 & 0.000 & -1.000\,\dfrac{\Delta(\underline{g}\cdot\underline{B}_1)}{g} \\ 0.000 & 0.000 & -1.000\,\dfrac{\Delta(\underline{g}\cdot\underline{B}_2)}{g} \end{bmatrix}$$

$$\Delta TT^T = \begin{bmatrix} 0.000 & 1.000\,\dfrac{\Delta(\underline{g}\cdot\underline{B}_1)}{g} & 1.000\,\dfrac{\Delta(\underline{g}\cdot\underline{B}_2)}{g} \\ -1.000\,\dfrac{\Delta(\underline{g}\cdot\underline{B}_1)}{g} & 0.000 & 0.000 \\ -1.000\,\dfrac{\Delta(\underline{g}\cdot\underline{B}_2)}{g} & 0.000 & 0.000 \end{bmatrix}$$

CHART 4-7

CHART 4-8

LEVEL ALIGNMENT

CASE 2

$$\Delta T = \begin{bmatrix} 0.667\frac{\Delta(g\cdot B_1)}{g} - 0.333\frac{\Delta(g\cdot B_2)}{g} - 0.333\frac{\Delta(g\cdot B_3)}{g} & -0.333\frac{\Delta(g\cdot B_1)}{g} + 0.667\frac{\Delta(g\cdot B_2)}{g} - 0.333\frac{\Delta(g\cdot B_3)}{g} & -0.333\frac{\Delta(g\cdot B_1)}{g} - 0.333\frac{\Delta(g\cdot B_2)}{g} + 0.667\frac{\Delta(g\cdot B_3)}{g} \\ -0.471\frac{\Delta(g\cdot B_1)}{g} + 0.236\frac{\Delta(g\cdot B_2)}{g} + 0.236\frac{\Delta(g\cdot B_3)}{g} & -0.471\frac{\Delta(g\cdot B_1)}{g} - 0.118\frac{\Delta(g\cdot B_2)}{g} + 0.589\frac{\Delta(g\cdot B_3)}{g} & -0.471\frac{\Delta(g\cdot B_1)}{g} + 0.589\frac{\Delta(g\cdot B_2)}{g} - 0.118\frac{\Delta(g\cdot B_3)}{g} \\ 0.000 & -0.612\frac{\Delta(g\cdot B_2)}{g} + 0.612\frac{\Delta(g\cdot B_3)}{g} & -0.612\frac{\Delta(g\cdot B_2)}{g} + 0.612\frac{\Delta(g\cdot B_3)}{g} \end{bmatrix}$$

$$\Delta TT^T = \begin{bmatrix} 0.000 & 0.816\frac{\Delta(g\cdot B_1)}{g} - 0.408\frac{\Delta(g\cdot B_2)}{g} - 0.408\frac{\Delta(g\cdot B_3)}{g} & 0.707\frac{\Delta(g\cdot B_2)}{g} - 0.707\frac{\Delta(g\cdot B_3)}{g} \\ -0.816\frac{\Delta(g\cdot B_1)}{g} + 0.408\frac{\Delta(g\cdot B_2)}{g} + 0.408\frac{\Delta(g\cdot B_3)}{g} & 0\ 000 & -0.500\frac{\Delta(g\cdot B_2)}{g} + 0.500\frac{\Delta(g\cdot B_3)}{g} \\ -0.707\frac{\Delta(g\cdot B_2)}{g} + 0.707\frac{\Delta(g\cdot B_3)}{g} & 0.500\frac{\Delta(g\cdot B_2)}{g} - 0.500\frac{\Delta(g\cdot B_3)}{g} & 0.000 \end{bmatrix}$$

LEVEL ALIGNMENT

CASE 3

$$\Delta T = \begin{bmatrix} 1.000\,\frac{\Delta(\underline{g}\cdot\underline{B}_1)}{g} & 0.500\,\frac{\Delta(\underline{g}\cdot\underline{B}_2)}{g} + 0.500\,\frac{\Delta(\underline{g}\cdot\underline{B}_3)}{g} & 0.500\,\frac{\Delta(\underline{g}\cdot\underline{B}_2)}{g} + 0.500\,\frac{\Delta(\underline{g}\cdot\underline{B}_3)}{g} \\ 0.000 & 0.707\,\frac{\Delta(\underline{g}\cdot\underline{B}_1)}{g} & -0.707\,\frac{\Delta(\underline{g}\cdot\underline{B}_1)}{g} \\ 0.000 & 0.500\,\frac{\Delta(\underline{g}\cdot\underline{B}_2)}{g} + 0.500\,\frac{\Delta(\underline{g}\cdot\underline{B}_3)}{g} & -0.500\,\frac{\Delta(\underline{g}\cdot\underline{B}_2)}{g} - 0.500\,\frac{\Delta(\underline{g}\cdot\underline{B}_3)}{g} \end{bmatrix}$$

$$\Delta TT^T = \begin{bmatrix} 0.000 & 1.000\,\frac{\Delta(\underline{g}\cdot\underline{B}_1)}{g} & 0.707\,\frac{\Delta(\underline{g}\cdot\underline{B}_2)}{g} + 0.707\,\frac{\Delta(\underline{g}\cdot\underline{B}_3)}{g} \\ -1.000\,\frac{\Delta(\underline{g}\cdot\underline{B}_1)}{g} & 0.000 & 0.000 \\ -0.707\,\frac{\Delta(\underline{g}\cdot\underline{B}_2)}{g} - 0.707\,\frac{\Delta(\underline{g}\cdot\underline{B}_3)}{g} & 0.000 & 0.000 \end{bmatrix}$$

CHART 4-9

CHART 4-10

LEVEL ALIGNMENT

CASE 4

$$\Delta T = \begin{bmatrix} 0.833\frac{\Delta(\underline{g}\cdot\underline{B}_1)}{g} + 0.037\frac{\Delta(\underline{g}\cdot\underline{B}_2)}{g} - 0.371\frac{\Delta(\underline{g}\cdot\underline{B}_3)}{g} & 0.037\frac{\Delta(\underline{g}\cdot\underline{B}_1)}{g} + 0.992\frac{\Delta(\underline{g}\cdot\underline{B}_2)}{g} + 0.083\frac{\Delta(\underline{g}\cdot\underline{B}_3)}{g} & -0.371\frac{\Delta(\underline{g}\cdot\underline{B}_1)}{g} + 0.083\frac{\Delta(\underline{g}\cdot\underline{B}_2)}{g} + 0.175\frac{\Delta(\underline{g}\cdot\underline{B}_3)}{g} \\ -0.333\frac{\Delta(\underline{g}\cdot\underline{B}_1)}{g} - 0.015\frac{\Delta(\underline{g}\cdot\underline{B}_2)}{g} + 0.148\frac{\Delta(\underline{g}\cdot\underline{B}_3)}{g} & 0.075\frac{\Delta(\underline{g}\cdot\underline{B}_1)}{g} - 0.442\frac{\Delta(\underline{g}\cdot\underline{B}_2)}{g} - 0.078\frac{\Delta(\underline{g}\cdot\underline{B}_3)}{g} & -0.742\frac{\Delta(\underline{g}\cdot\underline{B}_1)}{g} + 0.412\frac{\Delta(\underline{g}\cdot\underline{B}_2)}{g} + 0.375\frac{\Delta(\underline{g}\cdot\underline{B}_3)}{g} \\ -0.167\frac{\Delta(\underline{g}\cdot\underline{B}_1)}{g} - 0.007\frac{\Delta(\underline{g}\cdot\underline{B}_2)}{g} + 0.074\frac{\Delta(\underline{g}\cdot\underline{B}_3)}{g} & 0.037\frac{\Delta(\underline{g}\cdot\underline{B}_1)}{g} - 0.098\frac{\Delta(\underline{g}\cdot\underline{B}_2)}{g} - 0.027\frac{\Delta(\underline{g}\cdot\underline{B}_3)}{g} & -0.371\frac{\Delta(\underline{g}\cdot\underline{B}_1)}{g} - 1.007\frac{\Delta(\underline{g}\cdot\underline{B}_2)}{g} + 0.065\frac{\Delta(\underline{g}\cdot\underline{B}_3)}{g} \end{bmatrix}$$

$$\Delta TT^T = \begin{bmatrix} 0.000 & 0.816\frac{\Delta(\underline{g}\cdot\underline{B}_1)}{g} - 0.408\frac{\Delta(\underline{g}\cdot\underline{B}_2)}{g} - 0.408\frac{\Delta(\underline{g}\cdot\underline{B}_3)}{g} & 0.408\frac{\Delta(\underline{g}\cdot\underline{B}_1)}{g} + 0.908\frac{\Delta(\underline{g}\cdot\underline{B}_2)}{g} - 0.092\frac{\Delta(\underline{g}\cdot\underline{B}_3)}{g} \\ -0.816\frac{\Delta(\underline{g}\cdot\underline{B}_1)}{g} + 0.408\frac{\Delta(\underline{g}\cdot\underline{B}_2)}{g} + 0.408\frac{\Delta(\underline{g}\cdot\underline{B}_3)}{g} & 0.000 & -0.445\frac{\Delta(\underline{g}\cdot\underline{B}_2)}{g} - 0.045\frac{\Delta(\underline{g}\cdot\underline{B}_3)}{g} \\ -0.408\frac{\Delta(\underline{g}\cdot\underline{B}_1)}{g} - 0.908\frac{\Delta(\underline{g}\cdot\underline{B}_2)}{g} + 0.092\frac{\Delta(\underline{g}\cdot\underline{B}_3)}{g} & 0.445\frac{\Delta(\underline{g}\cdot\underline{B}_2)}{g} + 0.045\frac{\Delta(\underline{g}\cdot\underline{B}_3)}{g} & 0.000 \end{bmatrix}$$

GYRO COMPASS

CASE 1

$$\Delta T = \begin{bmatrix} 1.000\,\frac{\Delta(\underline{g}\cdot\underline{B}_1)}{g} & 1.000\,\frac{\Delta(\underline{g}\cdot\underline{B}_2)}{g} & 0.000 \\ 0.000 & 1.000\,\frac{\Delta(\underline{g}\cdot\underline{B}_1)}{g} - 1.414\,\frac{\Delta(\underline{\omega}^E\cdot\underline{B}_1)}{\omega^E} & -1.000\,\frac{\Delta(\underline{g}\cdot\underline{B}_1)}{g} \\ -1.000\,\frac{\Delta(\underline{g}\cdot\underline{B}_1)}{g} + 1.414\,\frac{\Delta(\underline{\omega}^E\cdot\underline{B}_1)}{\omega^E} & 0.000 & -1.000\,\frac{\Delta(\underline{g}\cdot\underline{B}_2)}{g} \end{bmatrix}$$

$$\Delta TT^T = \begin{bmatrix} 0.000 & 1.000\,\frac{\Delta(\underline{g}\cdot\underline{B}_1)}{g} & 1.000\,\frac{\Delta(\underline{g}\cdot\underline{B}_2)}{g} \\ -1.000\,\frac{\Delta(\underline{g}\cdot\underline{B}_1)}{g} & 0.000 & 1.000\,\frac{\Delta(\underline{g}\cdot\underline{B}_1)}{g} - 1.414\,\frac{\Delta(\underline{\omega}^E\cdot\underline{B}_1)}{\omega^E} \\ -1.000\,\frac{\Delta(\underline{g}\cdot\underline{B}_2)}{g} & -1.000\,\frac{\Delta(\underline{g}\cdot\underline{B}_1)}{g} + 1.414\,\frac{\Delta(\underline{\omega}^E\cdot\underline{B}_1)}{\omega^E} & 0.000 \end{bmatrix}$$

CHART 4-11

GYRO COMPASS

CASE 2

$$\Delta T =$$

$$\begin{bmatrix}
0.667\frac{\Delta(g\,B_1)}{g} - 0.333\frac{\Delta(g\,B_2)}{g} - 0.333\frac{\Delta(g\,B_3)}{g} & -0.333\frac{\Delta(g\,B_1)}{g} + 0.667\frac{\Delta(g\,B_2)}{b} - 0.333\frac{\Delta(g\,B_3)}{b} & -0.333\frac{\Delta(b\,B_1)}{b} - 0.333\frac{\Delta(g\,B_2)}{g} - 0.667\frac{\Delta(b\,B_3)}{g} \\
-0.471\frac{\Delta(g\,B_1)}{g} + 0.236\frac{\Delta(g\,B_2)}{g} + 0.236\frac{\Delta(g\,B_3)}{g} & 0.106\frac{\Delta(g\,B_1)}{g} - 0.053\frac{\Delta(g\,B_2)}{g} - 0.053\frac{\Delta(g\,B_3)}{g} & -1.049\frac{\Delta(b\,B_1)}{b} + 0.524\frac{\Delta(g\,B_2)}{g} + 0.524\frac{\Delta(g\,B_3)}{g} \\
 & -0.816\frac{\Delta(\omega^E B_1)}{\omega^E} + 0.408\frac{\Delta(\omega^E B_2)}{\omega^E} + 0.408\frac{\Delta(\omega^E B_3)}{\omega^E} & +0.816\frac{\Delta(\omega^E B_1)}{\omega^E} - 0.408\frac{\Delta(\omega^E B_2)}{\omega^E} - 0.408\frac{\Delta(\omega^E B_3)}{\omega^E} \\
-0.667\frac{\Delta(g\,B_1)}{g} - 0.075\frac{\Delta(g\,B_2)}{g} + 0.742\frac{\Delta(g\,B_3)}{g} & 0.333\frac{\Delta(g\,B_1)}{g} - 0.575\frac{\Delta(g\,B_2)}{g} + 0.242\frac{\Delta(g\,B_3)}{g} & 0.333\frac{\Delta(g\,B_1)}{g} - 0.575\frac{\Delta(b\,B_2)}{b} + 0.242\frac{\Delta(g\,B_3)}{g} \\
+0.943\frac{\Delta(\omega^E B_1)}{\omega^E} - 0.471\frac{\Delta(\omega^E B_2)}{\omega^E} - 0.471\frac{\Delta(\omega^E B_3)}{\omega^E} & -0.471\frac{\Delta(\omega^E B_1)}{\omega^E} + 0.236\frac{\Delta(\omega^E B_2)}{\omega^E} + 0.236\frac{\Delta(\omega^E B_3)}{\omega^E} & -0.471\frac{\Delta(\omega^E B_1)}{\omega^E} + 0.236\frac{\Delta(\omega^E B_2)}{\omega^E} + 0.236\frac{\Delta(\omega^E B_3)}{\omega^E}
\end{bmatrix}$$

$$\Delta TT^T =$$

$$\begin{bmatrix}
0.000 & 0.816\frac{\Delta(g\,B_1)}{g} - 0.408\frac{\Delta(g\,B_2)}{g} - 0.408\frac{\Delta(g\,B_3)}{g} & 0.707\frac{\Delta(g\,B_2)}{g} - 0.707\frac{\Delta(b\,B_3)}{b} \\
-0.816\frac{\Delta(g\,B_1)}{g} + 0.408\frac{\Delta(g\,B_2)}{g} + 0.408\frac{\Delta(g\,B_3)}{g} & 0.000 & 0.816\frac{\Delta(b\,B_1)}{b} - 0.408\frac{\Delta(g\,B_2)}{g} - 0.408\frac{\Delta(g\,B_3)}{g} \\
 & & -1.154\frac{\Delta(\omega^E B_1)}{\omega^E} - 0.577\frac{\Delta(\omega^E B_2)}{\omega^E} - 0.577\frac{\Delta(\omega^E B_3)}{\omega^E} \\
-0.707\frac{\Delta(g\,B_2)}{g} + 0.707\frac{\Delta(g\,B_3)}{g} & -0.816\frac{\Delta(g\,B_1)}{b} - 0.408\frac{\Delta(g\,B_2)}{g} - 0.408\frac{\Delta(g\,B_3)}{b} & 0.000 \\
 & -1.155\frac{\Delta(\omega^E B_1)}{\omega^E} - 0.577\frac{\Delta(\omega^E B_2)}{\omega^E} - 0.577\frac{\Delta(\omega^E B_3)}{\omega^E} &
\end{bmatrix}$$

GYRO COMPASS

CASE 3

$$\Delta T = \begin{bmatrix} 1.000\,\dfrac{\Delta(\underline{g}\cdot\underline{B}_1)}{g} & 0.500\,\dfrac{\Delta(\underline{g}\cdot\underline{B}_2)}{g} + 0.500\,\dfrac{\Delta(\underline{g}\cdot\underline{B}_3)}{g} & 0.500\,\dfrac{\Delta(\underline{g}\cdot\underline{B}_2)}{g} + 0.500\,\dfrac{\Delta(\underline{g}\cdot\underline{B}_3)}{g} \\ 0.000 & 1.414\,\dfrac{\Delta(\underline{g}\cdot\underline{B}_1)}{g} - 1.000\,\dfrac{\Delta(\underline{\omega}^E\cdot\underline{B}_1)}{\omega^E} & -1.000\,\dfrac{\Delta(\underline{\omega}^E\cdot\underline{B}_1)}{\omega^E} \\ -1.000\,\dfrac{\Delta(\underline{g}\cdot\underline{B}_1)}{g} + 1.414\,\dfrac{\Delta(\underline{\omega}^E\cdot\underline{B}_1)}{\omega^E} & 0.500\,\dfrac{\Delta(\underline{g}\cdot\underline{B}_2)}{g} + 0.500\,\dfrac{\Delta(\underline{g}\cdot\underline{B}_3)}{g} & -0.500\,\dfrac{\Delta(\underline{g}\cdot\underline{B}_2)}{g} - 0.500\,\dfrac{\Delta(\underline{g}\cdot\underline{B}_3)}{g} \end{bmatrix}$$

$$\Delta TT^T = \begin{bmatrix} 0.000 & 1.000\,\dfrac{\Delta(\underline{g}\cdot\underline{B}_1)}{g} & 0.707\,\dfrac{\Delta(\underline{g}\cdot\underline{B}_2)}{g} + 0.707\,\dfrac{\Delta(\underline{g}\cdot\underline{B}_3)}{g} \\ -1.000\,\dfrac{\Delta(\underline{g}\cdot\underline{B}_1)}{g} & 0.000 & 1.000\,\dfrac{\Delta(\underline{g}\cdot\underline{B}_1)}{g} - 1.414\,\dfrac{\Delta(\underline{\omega}^E\cdot\underline{B}_1)}{\omega^E} \\ -0.707\,\dfrac{\Delta(\underline{g}\cdot\underline{B}_2)}{g} - 0.707\,\dfrac{\Delta(\underline{g}\cdot\underline{B}_3)}{g} & -1.000\,\dfrac{\Delta(\underline{g}\cdot\underline{B}_1)}{g} + 1.414\,\dfrac{\Delta(\underline{\omega}^E\cdot\underline{B}_1)}{\omega^E} & 0.000 \end{bmatrix}$$

CHART 4-13

GYRO COMPASS

CASE 4

$$\Delta T = \begin{bmatrix} 0.833\frac{\Delta(g\,B_1)}{g} + 0.037\frac{\Delta(g\,B_2)}{g} - 0.371\frac{\Delta(g\,B_3)}{g} & 0.037\frac{\Delta(g\,B_1)}{g} + 0.992\frac{\Delta(h\,B_2)}{g} + 0.083\frac{\Delta(g\,B_3)}{g} & -0.371\frac{\Delta(g\,B_1)}{g} + 0.083\frac{\Delta(h\,B_2)}{g} - 0.175\frac{\Delta(g\,B_3)}{g} \\ -0.471\frac{\Delta(\omega^E B_1)}{\omega^E} + 0.236\frac{\Delta(\omega^E B_2)}{\omega^E} + 0.236\frac{\Delta(\omega^E B_3)}{\omega^E} & \begin{matrix} 0.816\frac{\Delta(g\,B_1)}{g} - 0.408\frac{\Delta(g\,B_2)}{g} - 0.408\frac{\Delta(h\,B_3)}{h} \\ -1.049\frac{\Delta(\omega^E B_1)}{\omega^E} + 0.524\frac{\Delta(\omega^E B_2)}{\omega^E} + 0.524\frac{\Delta(\omega^E B_3)}{\omega^E} \end{matrix} & \begin{matrix} -0.816\frac{\Delta(g\cdot B_1)}{g} + 0.408\frac{\Delta(g\,B_2)}{g} - 0.408\frac{\Delta(g\,B_3)}{h} \\ +0.106\frac{\Delta(\omega^E B_1)}{\omega^E} - 0.053\frac{\Delta(\omega^E B_2)}{\omega^E} - 0.053\frac{\Delta(\omega^E B_3)}{\omega^E} \end{matrix} \\ -0.833\frac{\Delta(g\,B_1)}{g} - 0.037\frac{\Delta(g\cdot B_2)}{g} + 0.371\frac{\Delta(g\cdot B_3)}{g} & 0.371\frac{\Delta(g\cdot B_1)}{g} - 0.083\frac{\Delta(g\cdot B_2)}{g} - 0.175\frac{\Delta(g\,B_3)}{g} & -0.037\frac{\Delta(g\cdot B_1)}{g} - 0.992\frac{\Delta(g\cdot B_2)}{g} - 0.083\frac{\Delta(g\cdot B_3)}{g} \\ +0.943\frac{\Delta(\omega^E B_1)}{\omega^E} - 0.471\frac{\Delta(\omega^E B_2)}{\omega^E} - 0.471\frac{\Delta(\omega^E B_3)}{\omega^E} & -0.471\frac{\Delta(\omega^E B_1)}{\omega^E} + 0.236\frac{\Delta(\omega^E B_2)}{\omega^E} + 0.236\frac{\Delta(\omega^E B_3)}{\omega^E} & -0.471\frac{\Delta(\omega^E B_1)}{\omega^E} + 0.236\frac{\Delta(\omega^E B_2)}{\omega^E} - 0.236\frac{\Delta(\omega^E B_3)}{\omega^E} \end{bmatrix}$$

$$\Delta TT^T = \begin{bmatrix} 0.000 & 0.816\frac{\Delta(g\,B_1)}{g} - 0.408\frac{\Delta(g\,B_2)}{g} - 0.408\frac{\Delta(g\,B_3)}{g} & 0.408\frac{\Delta(h\,B_1)}{h} - 0.908\frac{\Delta(g\,B_2)}{g} - 0.092\frac{\Delta(h\,B_3)}{g} \\ -0.816\frac{\Delta(g\cdot B_1)}{g} + 0.408\frac{\Delta(g\,B_2)}{h} - 0.408\frac{\Delta(g\cdot B_3)}{g} & 0.000 & \begin{matrix} 0.816\frac{\Delta(h\,B_1)}{h} - 0.408\frac{\Delta(g\,B_2)}{g} - 0.408\frac{\Delta(g\,B_3)}{g} \\ -1.155\frac{\Delta(\omega^E B_1)}{\omega^E} - 0.577\frac{\Delta(\omega^E B_2)}{\omega^E} - 0.577\frac{\Delta(\omega^E B_3)}{\omega^E} \end{matrix} \\ -0.408\frac{\Delta(g\cdot B_1)}{g} - 0.908\frac{\Delta(g\,B_2)}{g} + 0.092\frac{\Delta(g\cdot B_3)}{g} & \begin{matrix} -0.816\frac{\Delta(g\cdot B_1)}{g} - 0.408\frac{\Delta(g\cdot B_2)}{g} - 0.408\frac{\Delta(g\,B_3)}{h} \\ -1.155\frac{\Delta(\omega^E B_1)}{\omega^E} - 0.577\frac{\Delta(\omega^E B_2)}{\omega^E} - 0.577\frac{\Delta(\omega^E B_3)}{\omega^E} \end{matrix} & 0.000 \end{bmatrix}$$

have a zero mean and are uncorrelated so that,

finally: $$\mu_k = \mu_{k+3} = 0$$

$$\sigma = \left\{ \sum_k \left(C_k E \left[\left\{ \frac{\Delta(\underline{g} \cdot \underline{B}_k)}{g} \right\}^2 \right] + C_{k+3} E \left[\left\{ \frac{\Delta(\underline{\omega}^E \cdot \underline{B}_k)}{\omega^E} \right\}^2 \right] \right) \right\}^{1/2}$$

SECTION 5

SECTION 5
ALIGNMENT PROCESSING TECHNIQUES

In this section we investigate the effects of noise, quantization and computer word length upon alignment accuracy. The analysis is based on a Monte Carlo simulation which is described in Section 5.1. In Section 5.2 the general properties of several estimation techniques are developed and a "recommended technique" is selected. These techniques are investigated in detail in Sections 5.3 and 5.4. In particular, we investigate the following relationships:

1) Alignment accuracy and alignment time versus sample rate
2) Alignment accuracy versus number of iterative steps
3) Alignment accuracy versus sensor quantization
4) Alignment accuracy versus computer word length.

We briefly summarize the results of these investigations in the following paragraphs.

The recommended technique for level alignment is the posterior-mean estimate of the instantaneous components. An alternate technique is the simple average. These recommendations are based on the results presented in Tables 5-1 and 5-2. The posterior-mean estimate is not sensitive to the distribution of the environment noise, i.e., gaussian or nongaussian.

Rotational motion from the environment is the dominant source of level alignment error for long integration intervals of the order of one minute or greater. Quantization and sensor noise are dominant for short integration intervals, less than one-fourth minute. The posterior-mean estimate of the instantaneous gravity components is more accurate than the simple average in most cases of interest. For very short intervals (on the order of 15 seconds) these methods have comparable accuracy. The posterior-mean estimate is less accurate than the simple average for large quantization and small integration intervals, the order to 30 seconds.

For Gyrocompass, the simulation results confirm the conclusions of Section 3.3 – that the alignment error is dominated by gyro readout quantization. For this reason, only qualitative relationships between alignment accuracy, alignment time, sample rate, sensor quantization and computer word length are developed.

These results employ the environment data given by Weinstock.* It is recommended that the motions of a proposed test laboratory be studied, since deviations from the nominal environment described by Weinstock will change the characteristics of the recommended techniques. Deviations from the nominal environment will be most likely in magnitude of the spectrum and not in the shape. In other words, low frequency motion is larger than the high frequency motion. The magnitude of the low frequency motion depends on the location of the test bed, the time of day, local human activities, etc, it may change by an order of magnitude.

5.1 DESCRIPTION OF SIMULATION PROGRAM

The function of the computer simulation is to generate data similar to that which is obtained from the accelerometers and gyros, to process the data with various estimation techniques, and to compare the true alignment matrix with the estimated alignment matrix. A functional description of the simulation appears in Figure 5-1. A detailed description of the simulation appears in the report describing the LABSIM Program.**

A functional description of the simulation is presented in Figure 5-1. The components of gravity, $\underline{g}$, and earth rate, $\underline{\omega}^E$, in the earth frame are transformed to components in the level frame, i.e., a frame nominally aligned with the earth frame but moving with the laboratory. This transformation depends on the low frequency (LF) rotational motion of the laboratory (10^{-4} to 10^{-2} cps). The high frequency (HF) motion (10^{-2} to 10 cps) does not significantly change the orientation of the level frame, because the amplitude is smaller (see Figure 5-2). The resultant components, $\underline{g} \cdot \underline{L}_i(t)$ and $\underline{\omega}^E \cdot \underline{L}_i(t)$, are integrated to simulate the integral readout of the sensors. (In the simulation program, the integration is done analytically. The integrals serve as the input to the program.) The integral of the HF rotational noise is added to these components, and the sum is transformed to the body frame. In the simulation we assume that the sensor input axes are parallel to the body axes. Gyro noise is added to the gyro components. No accelerometer noise is added. The resultant signal and noise is quantized. (Quantization is accomplished by dividing by the appropriate scale factor, rounding and then multiplying by the same factor.) The outputs of the quantization routine simulates the actual sensor outputs.

The estimation routine computes the estimates of gravity and earth rate in the body frame, $\underline{g} \cdot \underline{B}_i$ and $\underline{\omega}^E \cdot \underline{B}_i$. The estimation routine uses certain estimation matrices

---

*H. Weinstock, "Limitations of Inertial Sensor Testing Produced by Test Platform Vibrations", NASA Electronics Research Center, Cambridge, NASA TN D-3683, 1966.

**The LABSIM program is described in "Simulation Program of Inertial Sensing Unit for Evaluation of Alignment Techniques", a technical report prepared by Univac, Aerospace Analysis Department, St. Paul, Minnesota, January 1968.

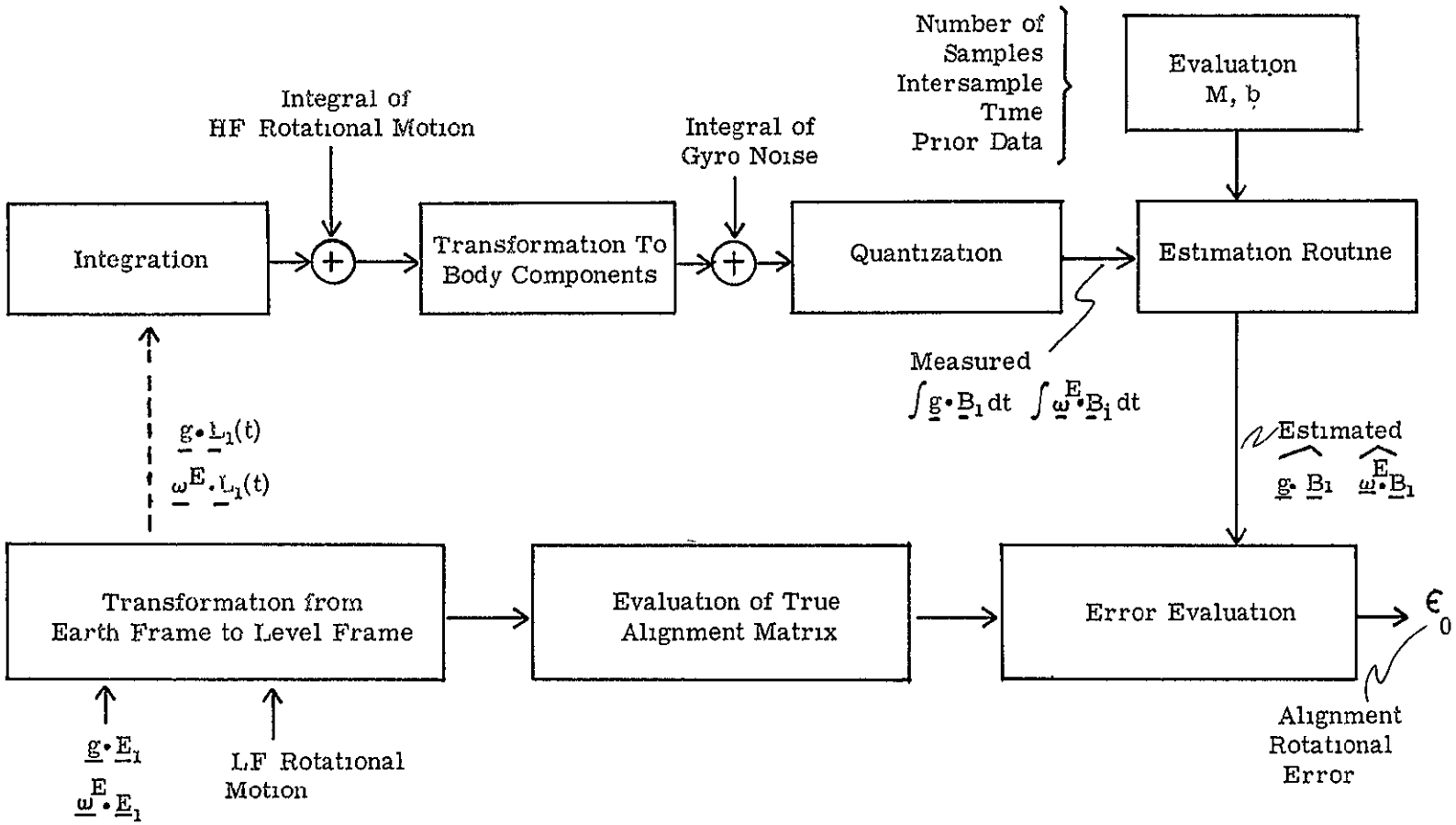

Figure 5-1. Functional Description of Simulation

M and $\underline{b}$. The matrices are computed as part of the simulation, but in a laboratory system M and $\underline{b}$ will be computed before the alignment. The quality of the estimate is measured by the alignment total rotational error. This error is defined in Section 4 as the magnitude of the single rotation required to bring the estimated earth frame into coincidence with the true earth frame.

In the following subsections, various routines in the simulations are discussed: test inputs (5.1.1), estimation routine (5.1.2), estimation-matrix routine(5.1.3), rotational alignment error (5.1.4).

5.1.1 Test Inputs

The laboratory environment introduces two types of "noise" – rotational and translational motion. The acceleration introduced by the translational motion was not simulated, since it is much smaller than the accelration modulation due to rotational motion.

The rotational motion was divided into two components – high frequency and low frequency. The high frequency component was formed with a random-number generator which had a gaussian distribution. The power spectrum was shaped with a recursive filter to give the spectrum illustrated in Figure 5-2. Independent HF motions were applied to the N-S axis and the E-W axis. The rms amplitudes were 0.8 second of arc. A nongaussian high frequency rotational noise was also simulated. A bimodal density function was used for this purpose with the second peak containing one tenth of the total probability. The nongaussian random-number sequence was formed from the original gaussian sequence by replacing every tenth number on the average with a gaussian variate whose mean is 1.6 seconds of arc and variance is 0.8 second of arc. The variance of the nongaussian noise was greater than the variance of the gaussian noise.

The low frequency rotational components were simulated with a harmonic motion. Two motions were used: 1) one hour period and one minute of arc amplitude, and 2) one-half hour period and 30 seconds of arc amplitude (see Figure 5-2). The axis of rotation was chosen in the horizontal plane, 45° north and east. The experimental data in Figure 5-2 was obtained from Weinstock.*

The rms noise level of the gyro is 0.005°/hr. It was formed with a random-number generator which had a gaussian distribution. The power spectrum was shaped with a recursive filter to give a half-power frequency of 2×10^{-5} cps and a roll-off of 6 db/Oct. The noise applied to each axis was independent of that on the other two axes.

*H. Weinstock, "Limitations on Inertial Sensor Testing Produced by Test Platform Vibrations", NASA Electronics Research Center, Cambridge, NASA TN D-3683, 1966.

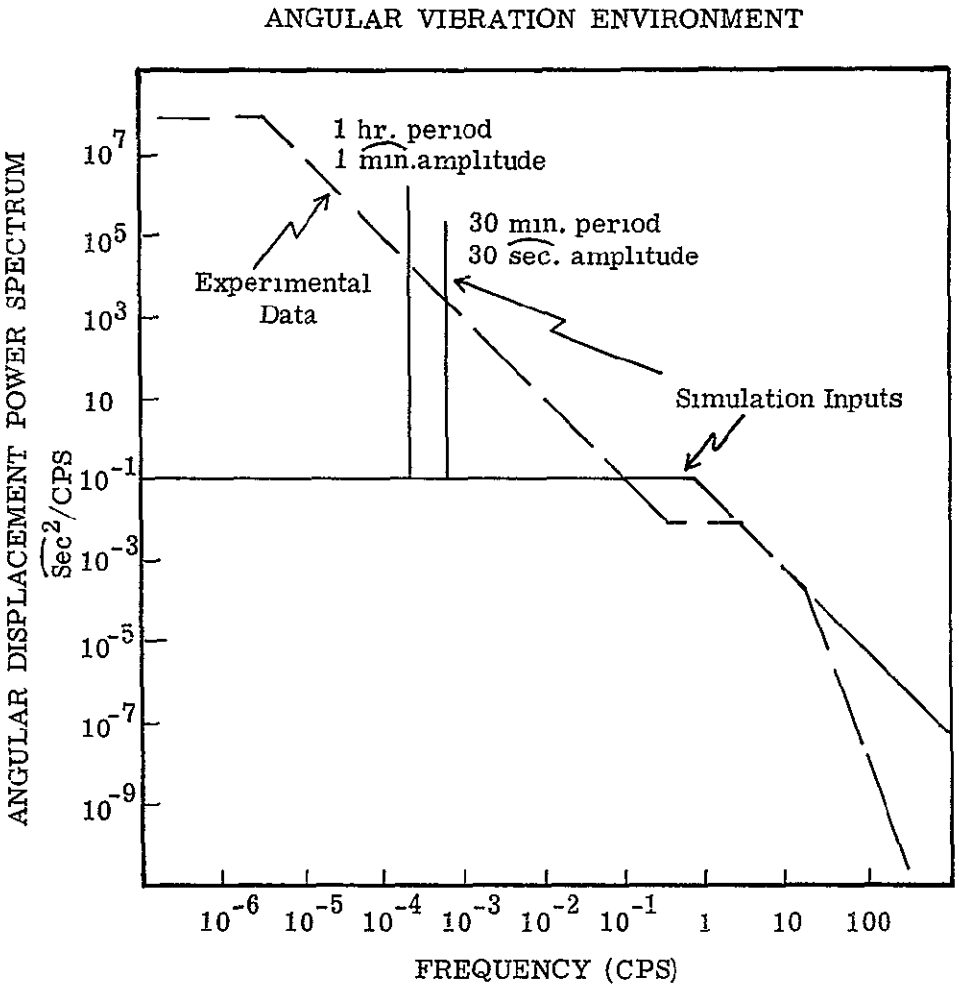

Figure 5-2. Simulation Rotational Inputs

5.1.2 Estimation Routine

The estimation routine implements the basic equation for the estimated components, e.g., in level alignment

$$\begin{bmatrix} \underline{g} \cdot \underline{\hat{B}}_1 \\ \underline{g} \cdot \underline{\hat{B}}_2 \\ \underline{g} \cdot \underline{\hat{B}}_3 \end{bmatrix} = M\underline{X} + \underline{b} \qquad (5\text{-}1)$$

where $\underline{X}$ is the preprocessed measurements

$$\int_0^{\Delta t} (\underline{a} \cdot \underline{B}_i)dt, \cdots, \int_{(K-1)\Delta t}^{K\Delta t} (\underline{a} \cdot \underline{B}_i)dt \; ; \quad i = 1,2,3$$

The matrices M and $\underline{b}$ are evaluated in the M and $\underline{b}$ Evaluation Routine. The computer word length restriction is introduced in the evaluation of (5-1). Word lengths of 27, 24 and 15 bits were used. A detailed discussion of the estimation routine is presented in the report on LABSIM.

5.1.3 M and $\underline{b}$ Evaluation Routine

The elements of M and $\underline{b}$ of equation (5-1) are computed in the M and $\underline{b}$ Evaluation Routine. These matrices are in most cases functions of the number of samples K, the intersample time Δt, prior measurement of the noise power spectra, initial estimate of the alignment matrix, and prior measurements of gravity and earth rate. The equations for M and $\underline{b}$ depend on the alignment technique being used. The simple average estimation techniques do not require all of the above quantities to evaluate M and $\underline{b}$. The basic estimation equations are developed in Section 5 of the Development Document.

5.1.4 Error Evaluation Routine

The Error Evaluation Routine computes the rotational alignment error defined in Chart 4-3. This angular error is the rotation required to bring the estimated earth frame into coincidence with the true earth frame. The absolute magnitude of this rotational error will be used to compare various techniques. Note that the earth frame is moving relative to the body frame. The alignment error is based on the predicted orientation of the earth frame one second after the last measurement. This is a

worst-case delay for initializing the navigation program. The errors presented in the following subsections are the rms rotational errors based on 10 independent Monte Carlo trials.

5.2 SELECTION OF RECOMMENDED TECHNIQUES

In Section 5 of the Development Document, several alignment estimation techniques were derived. We will select a "recommended" estimation technique in this subsection, for both Level and Gyrocompass Alignment, from among those derived in the Development Document. The selection is based upon three criteria:

- The sensitivity of alignment accuracy to the noise distribution, gaussian and nongaussian. Only techniques which are not sensitive to the noise distribution will be considered further.
- The relative accuracy of the techniques for different integration times, Δt; orientations, T^{EB}; and number of samples, K.
- The general computational requirements which include complexity, accuracy (double precision, etc.) and setup procedures for laboratory test.

The selected techniques can be considered "recommended" only to the extent that the actual laboratory environment noise approximates the simulated noise. (The noise simulation was based upon the environment data given by Weinstock, loc. cit.) Deviation from this nominal environment could change the characteristics of the estimation techniques enough to change our choice for recommended technique. Specifically, if the low-frequency motion were small (on the order to five seconds of arc), then our choice would be different.

The following parameters were used in the test simulations. Nominal quantization was introduced: 1.27×10^{-2} ft/sec and 1.22×10^{-4} rad. No word-length restriction was used in the estimation routine. The low-frequency rotational motion was one minute of arc with a one hour period. Inputs to the Estimation Routine were taken symmetrically about the zero phase of the LF motion, i.e., maximum angular velocity. A nongaussian, high-frequency, rotational noise was also introduced. It had a bimodal density function with the second peak containing one tenth of the "total probability" (see subsection 5.1.1). Two orientation cases are considered — 1 and 2 (see orientation cases in Section 3).

5.2.1 Level Alignment

In the Development Document four estimation techniques for Level Alignment were presented: simple average, least-squares and posterior-mean estimate of average components, and posterior-mean estimate of instantaneous components. The least-squares

estimate has not been investigated in detail, because it is a special case of the posterior-mean estimate, from a functional viewpoint (see Section 5 of the Development Document).

The simulation results are presented in Tables 5-1 and 5-2 for gaussian and nongaussian HF noise, respectively. The table entries are the rms rotational alignment errors expressed in seconds of arc for 10 trials. In all cases the instantaneous estimates are superior to the estimates of the average components. The accuracy of the instantaneous estimate is not sensitive to the HF noise distribution.

The posterior-mean estimate of the instantaneous components is selected as the recommended estimation technique for level alignment. The simple average is an alternate technique because of its computational simplicity. The posterior-mean estimate can be used iteratively. The characteristics of this technique are presented in Section 5.3.2.

5.2.2 Gyrocompass Alignment

In the Development Document three estimation techniques for Gyrocompass were presented: simple average, least-squares estimate of average components, and posterior-mean estimate of average components. The least-squares estimate is not investigated in detail, because it is a special case of the posterior-mean estimate, from a functional viewpoint.

The simulation results are presented in Table 5-1 and 5-2 for gaussian and nongaussian noise, respectively. The table entries are the rms rotational alignment errors expressed in seconds of arc. The posterior-mean estimate is not significantly better than the simple-average estimate. Since the dominant source of error in Gyrocompass Alignment is gyro quantization (see Section 3.3), this result is expected. The simple average is therefore selected as the recommended technique. Note that if the gyro quantization effect could be made small, the recommended technique could be improved upon by using the instantaneous estimate of gravity (given in Section 5.2.1) and the average estimate of earth rate.

5.3 CHARACTERISTICS OF RECOMMENDED TECHNIQUES

In the preceding subsection, the posterior-mean estimate of instantaneous components was selected for level alignment. In this subsection, we investigate the characteristics of this technique and the simple-average technique.

For gyrocompass alignment, the simple-average estimation technique was selected; its characteristics are also investigated. Specifically, the relationships are developed between:

TABLE 5-1

SELECTION OF RECOMMENDED TECHNIQUES

Rotational Alignment Error ($\widehat{sec}$)

Gaussian Noise Distribution

A - Simple Average
B - Posterior-Mean Estimate of Average Components
C - Posterior-Mean Estimate of Instantaneous Components
D - Simple Average
E - Posterior-Mean Estimate of Average Components

K = 1
Δt = 10 min

ORIENTATION	LEVEL			GYRO	
	A	B	C	D	E
I	31.1	31.1	31.1	260	320
II	36.4	47.8	34.6	297	324

K = 5
Δt = 2 min

ORIENTATION	LEVEL			GYRO	
	A	B	C	D	E
I	31.0	31.0	18.4	31	574
II	34.7	32.2	21.8	300	647

K = 5
Δt = 5 min

ORIENTATION	LEVEL			GYRO	
	A	B	C	D	E
I	60.0	60.1	34.0	120	392
II	66.8	45.4	39.8	220	520

TABLE 5-2

SELECTION OF RECOMMENDED TECHNIQUES

Rotational Alignment Error (sec)

Non-Gaussian Noise Distribution

A - Simple Average
B - Posterior-Mean Estimate of Average Components
C - Posterior-Mean Estimate of Instantaneous Components
D - Simple Average
E - Posterior-Mean Estimate of Average Components

K = 1 Δt = 10 min					
ORIENTATION	LEVEL			GYRO	
	A	B	C	D	E
I	30.8	30.8	30.8	260	320
II	34.4	48.9	34.4	410	332

K = 5 Δt = 5 min					
ORIENTATION	LEVEL			GYRO	
	A	B	C	D	E
I	60	60	34	60	364
II	68	45	40	207	495

- Alignment accuracy, alignment time, and sample rate
- Alignment accuracy and sensor quantization
- Alignment accuracy and computer word length
- Alignment accuracy and number of iterative steps (level alignment only).

These are the topics of the following subsections. Since gyro quantization is the dominate source of error, we obtain only qualitative relationships for gyrocompass alignment.

5.3.1 Alignment Accuracy

Alignment accuracy is measured by the rms rotational alignment error. The alignment time is the total measurement interval $K\Delta t$. Note that the computation time is small relative to $K\Delta t$. The object is to relate alignment error, alignment time, and the intersample time Δt.

Several tests were performed with the following parameters. Nominal quantization was introduced, 1.27×10^{-2} ft/sec and 1.22×10^{-4} rad. No word length restriction was used in the estimation routine. The low-frequency motion was one minute of arc with a one-hour period. The inputs to the Estimation Routine were taken symmetrically about the zero phase of the LF motion, i.e., maximum angular velocity. A gaussian high-frequency noise was introduced. Orientation cases 1 and 2 were considered. In the following subsections a noniterative and an iterative level alignment techniques are discussed. Subsequently, gyrocompass alignment accuracy is described.

5.3.1.1 Noniterative Level Alignment

The alignment error for the posterior-mean estimate of the instantaneous components is given in Figure 5-3 as a function of alignment time $K\Delta t$ for K = 1, 2, 5, 10. For K = 1, the error is the same as that for the simple average. The error peaks at 30 minutes since the low-frequency rotational noise has a one-hour period and data is taken symmetrically about vertical. The rotational alignment error is based on the instantaneous orientation at the end of the measurement interval. For K = 1 and Δt equal to one hour, the rotational motion would be eliminated completely. Note that there is a significant error reduction in using K = 5 instead of K = 1. The reduction in going from K = 5 to K = 10 is not significant. In the following discussions we will use K = 5. Since data was taken symmetrically about zero phase, the error appears to approach zero as $K\Delta t$ approaches zero. The sampling and quantization are "in phase". A detailed investigation is required for small $K\Delta t$.

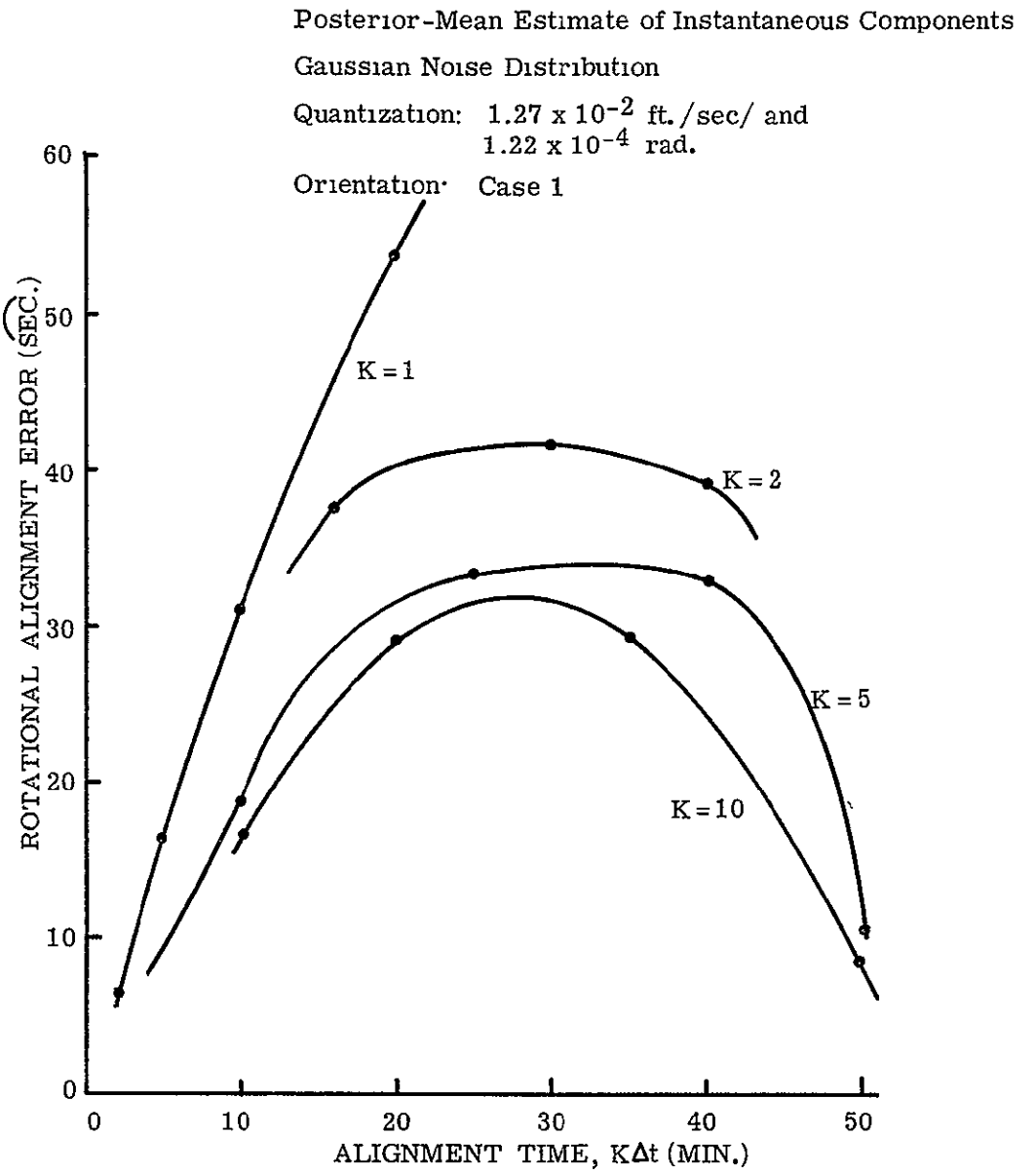

Figure 5-3. Level Alignment Error vs Alignment Time

There are two basic types of errors: prediction error and noise error. The first type of error occurs since we attempt to predict the position of the gravity vector at the end of the measurement interval. When the measurement interval $K\Delta t$ is decreased, the prediction error is decreased. The noise error results from the HF rotational motion and accelerometer quantization. When the measurement interval $K\Delta t$ is decreased, the noise error is increased. The optimum interval is one for which these two errors are equal. In the following subsection, we find that the optimum Δt is of the order of thirty seconds for $K = 5$ and for the noise spectra given at the beginning of this subsection. Since the choice of Δt is strongly dependent upon the noise spectra, the final selection must be based upon measurements of the actual noise spectra in the laboratory.

The alignment error for the simple average is presented in Figure 5-4. For simple average, only one sample is taken, i.e., $K = 1$. Note that alignment accuracy is not strongly dependent on orientation.

5.3.1.2 Iterative Level Alignment

The posterior-mean estimate of the instantaneous gravity components can be used in an iterative alignment technique. Initially we have a prior estimate of the gravity components and the associated covariance matrix (see Section 5.4.1.3 of the Development Document). These are inputs to the first step of the iteration. Using the posterior-mean estimate, we obtain refined values for the gravity components and covariance matrix. These refined values are inputs to the second iteration step. The procedure continues in this way.

This procedure was tested with different intersample times Δt and different noise inputs. Specifically, $K = 5$ and $\Delta t = 0.25, 0.5, 1.0, 2.0$ minutes. The quantization levels used were 1.27×10^{-2} ft/sec and 1.22×10^{-4} rad. The word length was not restricted in the estimation routine. The high-frequency rotational noise was gaussian. The low-frequency noise had a period of 58 minutes and amplitude of one arc minute, and in a second case, a period of 29 minutes and an amplitude of 0.5 arc minutes. The initial input to the Estimation Routine was taken when the body frame was level. Orientation Case I was used for all tests.

The simulation results are presented in Figure 5-5, 5-6, 5-7, and 5-8 for the 58-minute period. The simple average is also plotted for comparison. Note that the simple average is not iterative. The ordinate is the rotational alignment error in seconds of arc.*

*These errors are the result of a single trial and not the rms error of ten trials as used above.

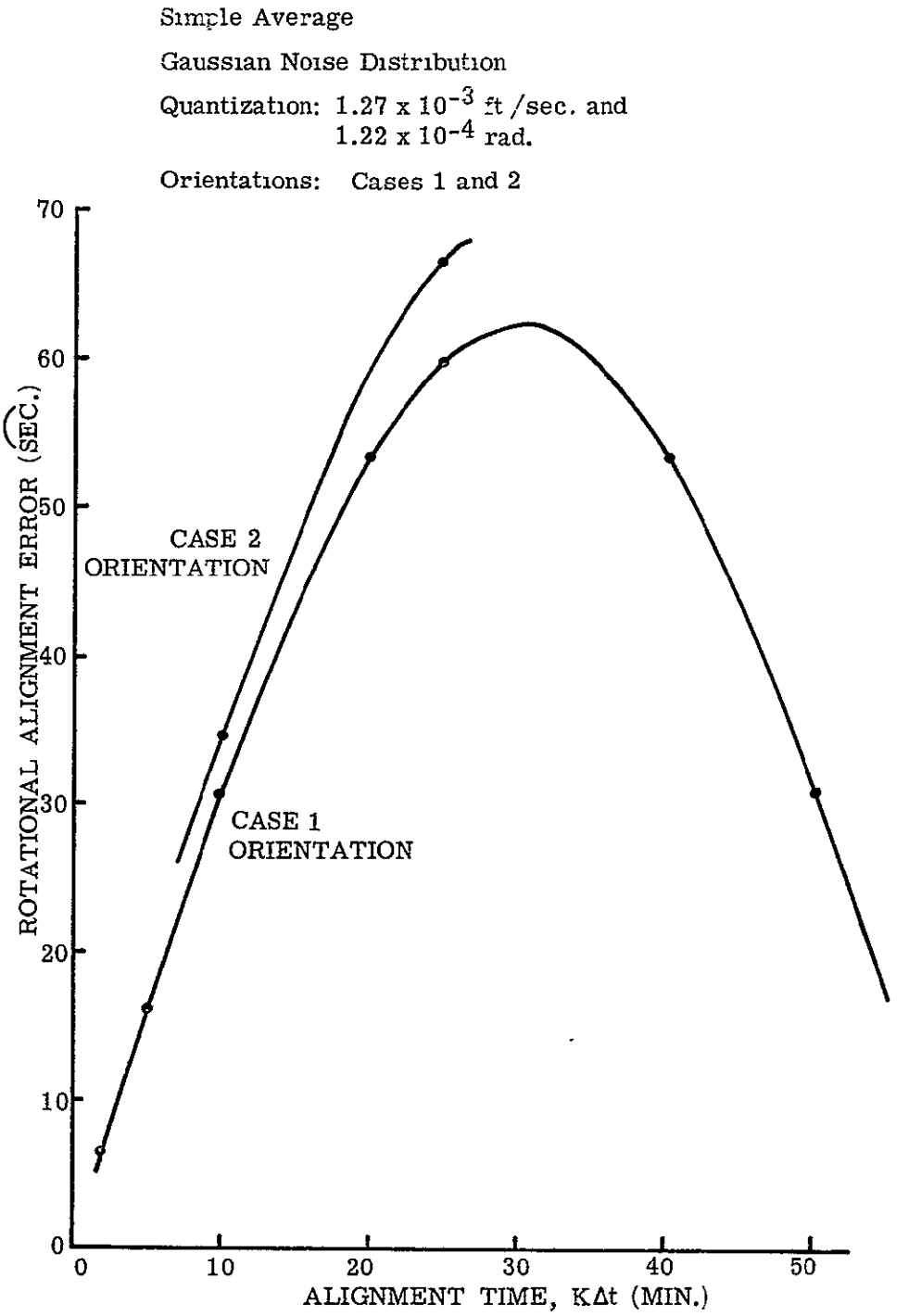

Figure 5-4. Level Alignment Error vs Alignment Time For Simple Average

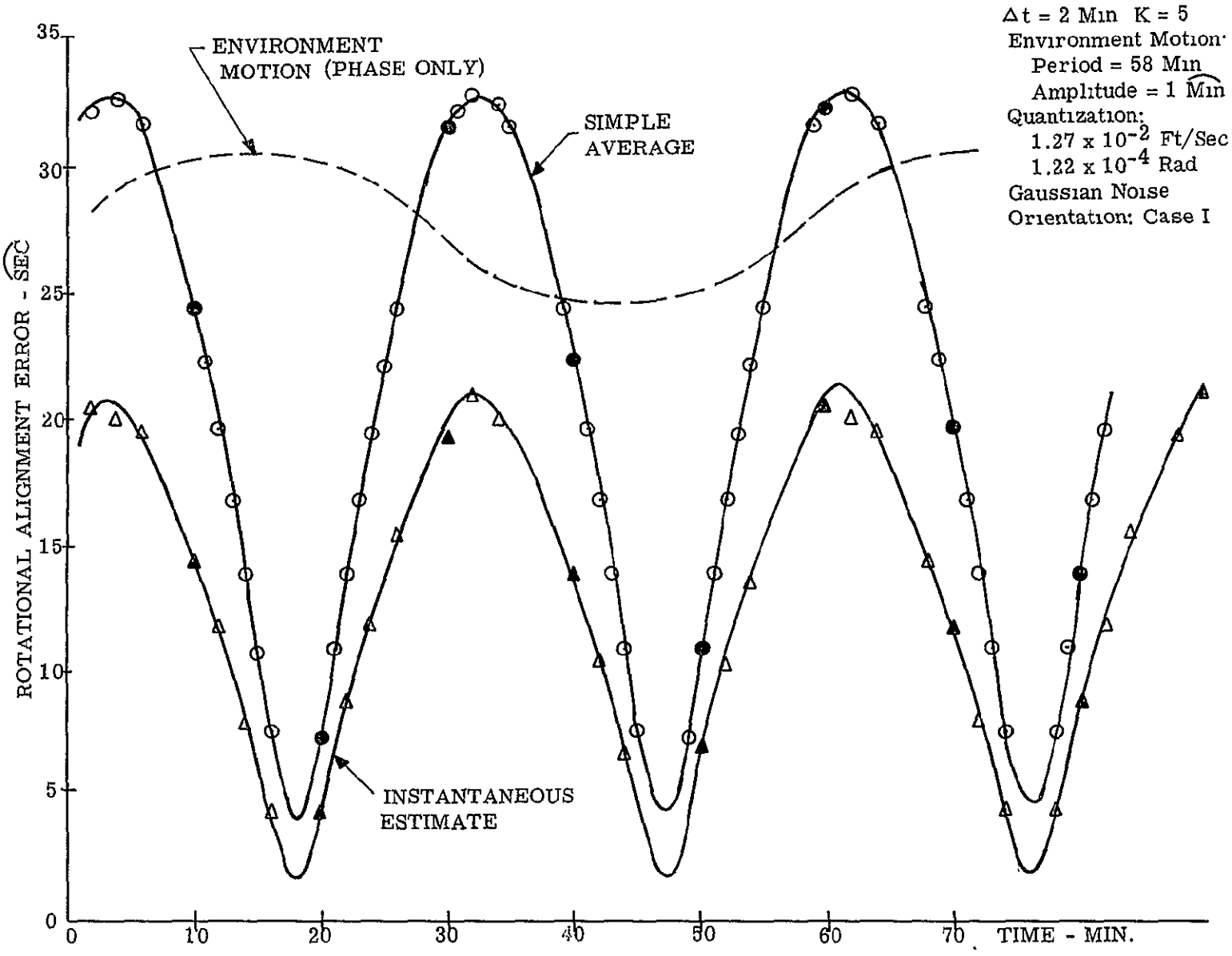

Figure 5-5. Alignment Error – Iterative Technique

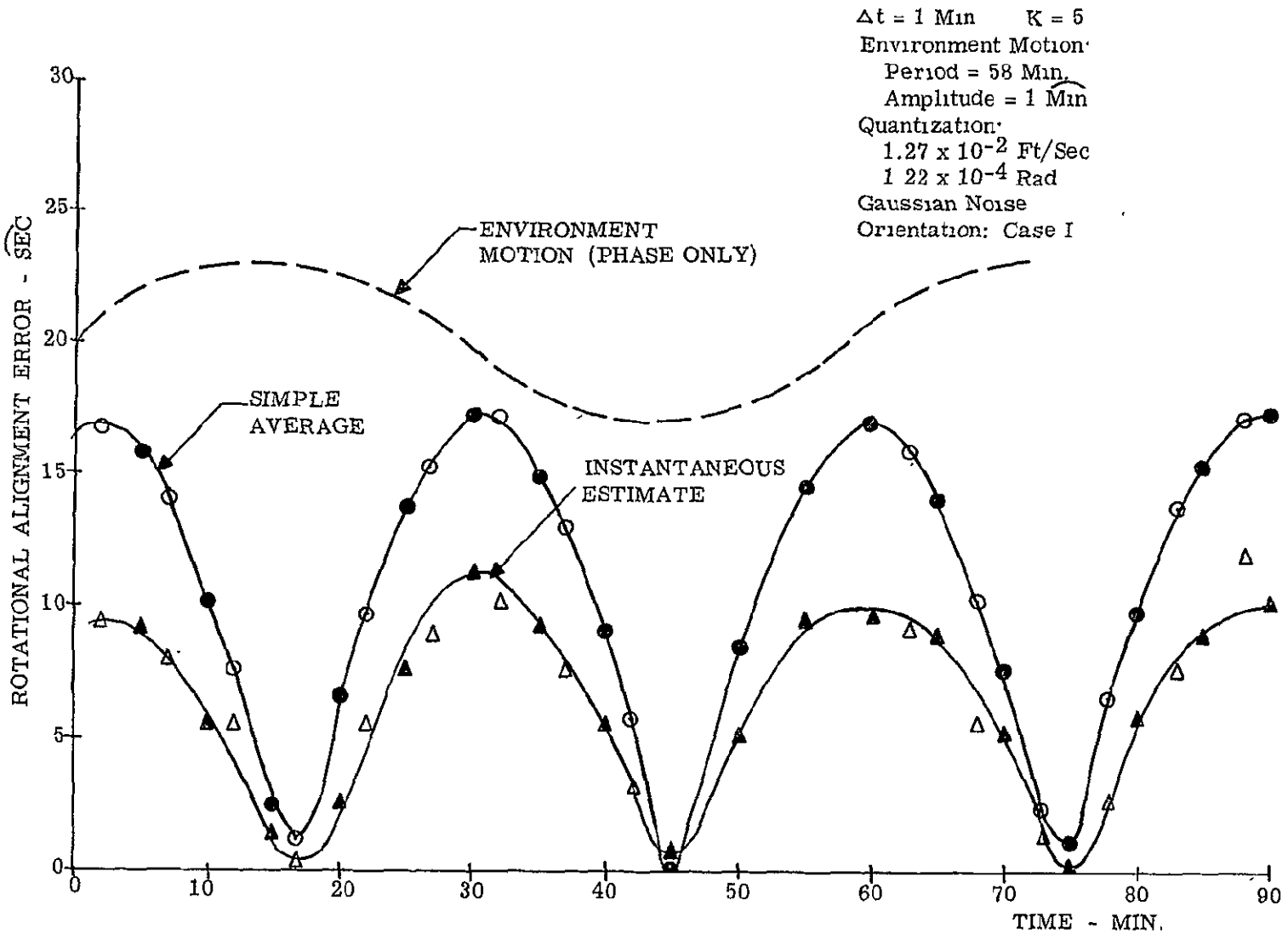

Figure 5-6. Alignment Error – Iterative Technique

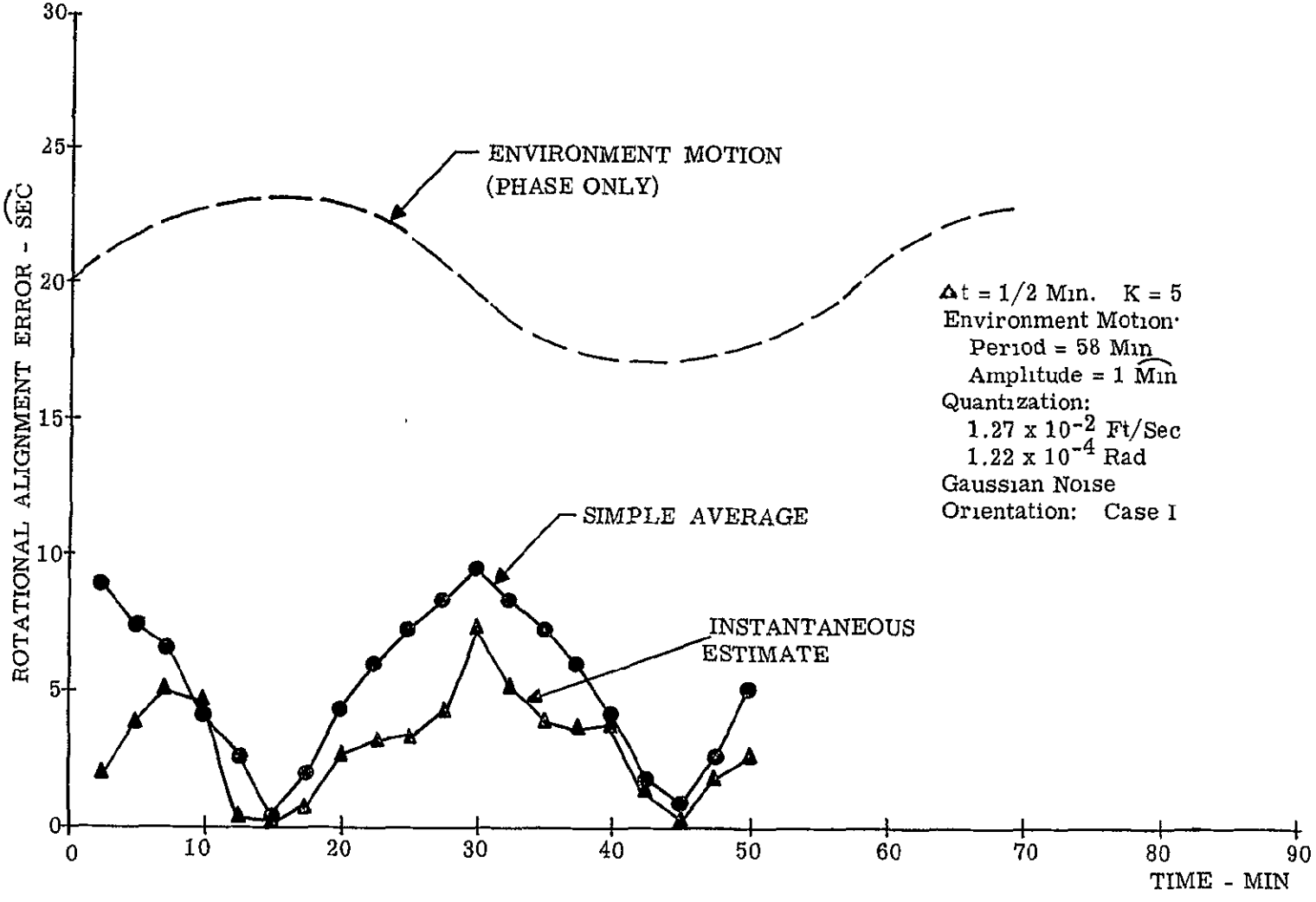

Figure 5-7. Alignment Error – Iterative Technique

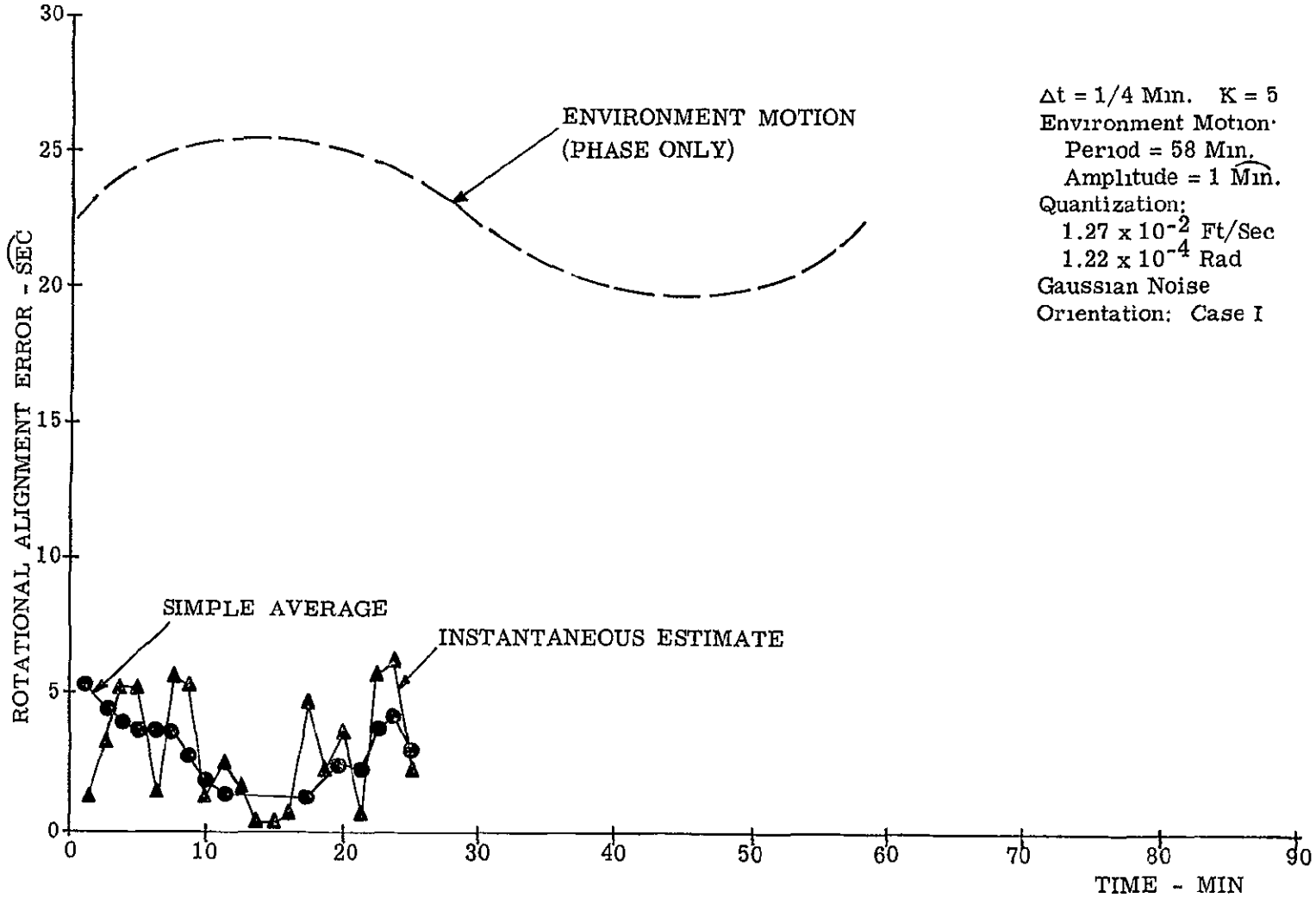

Figure 5-8. Alignment Error – Iterative Technique

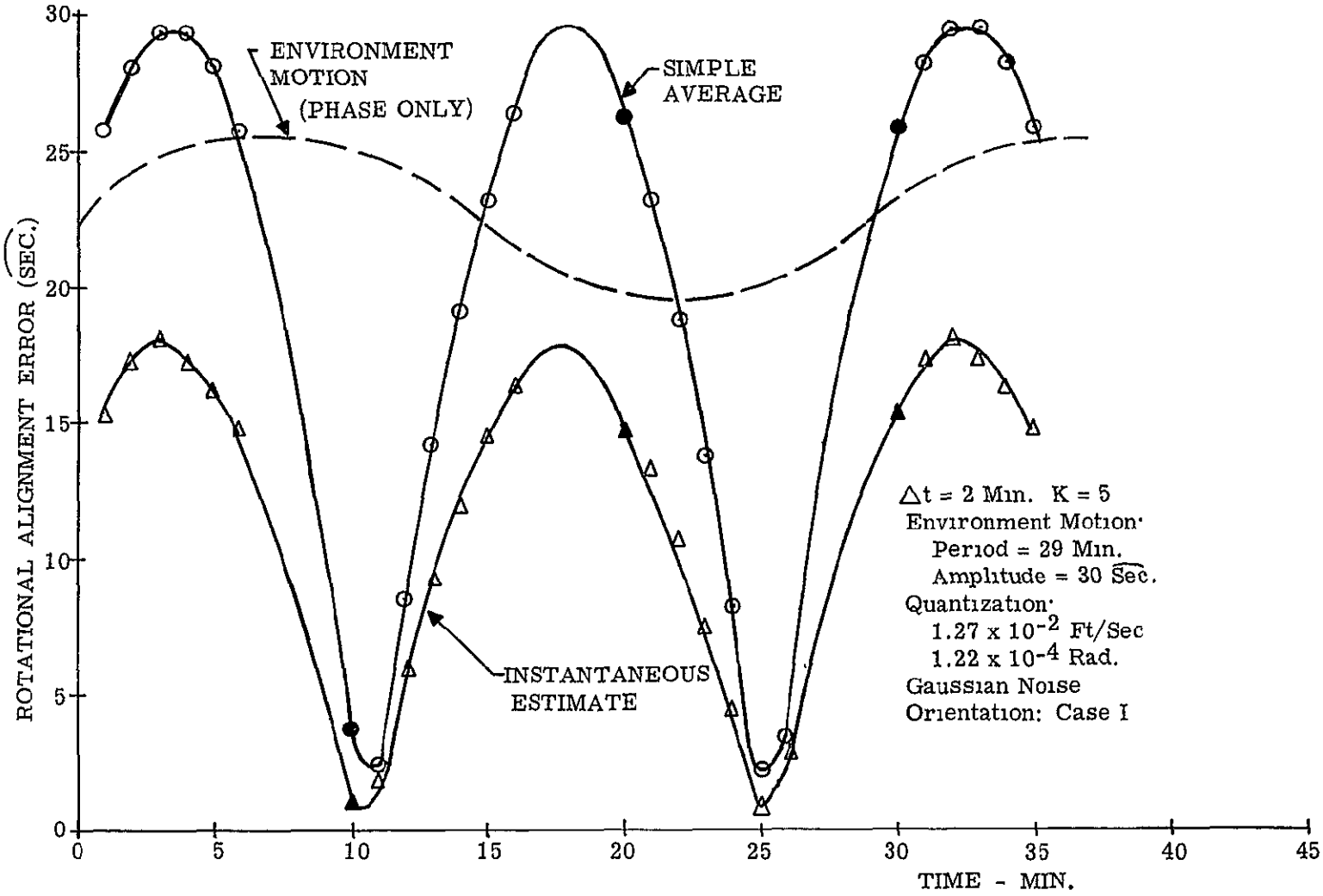

Figure 5-9. Alignment Error – Iterative Technique

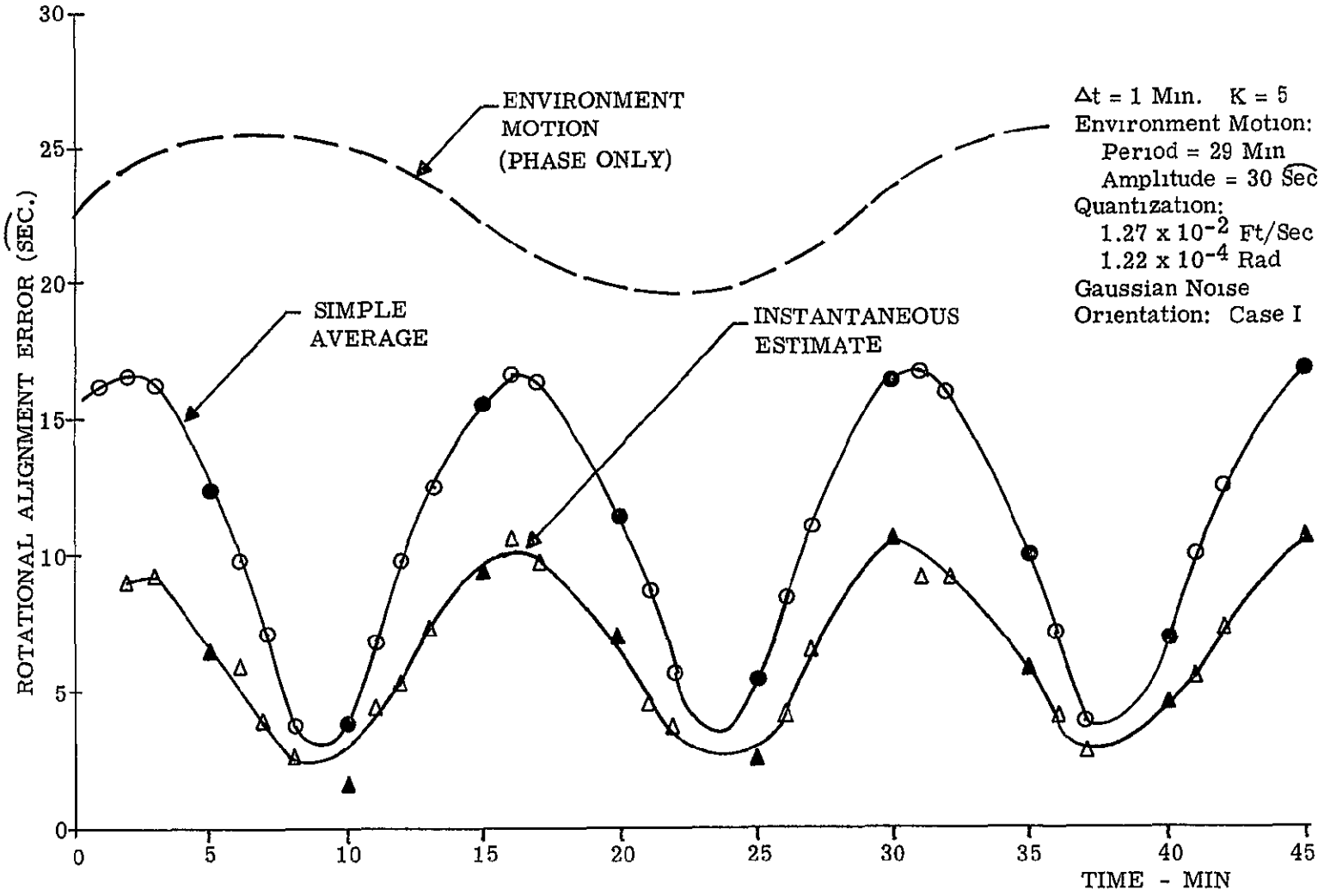

Figure 5-10. Alignment Error – Iterative Technique

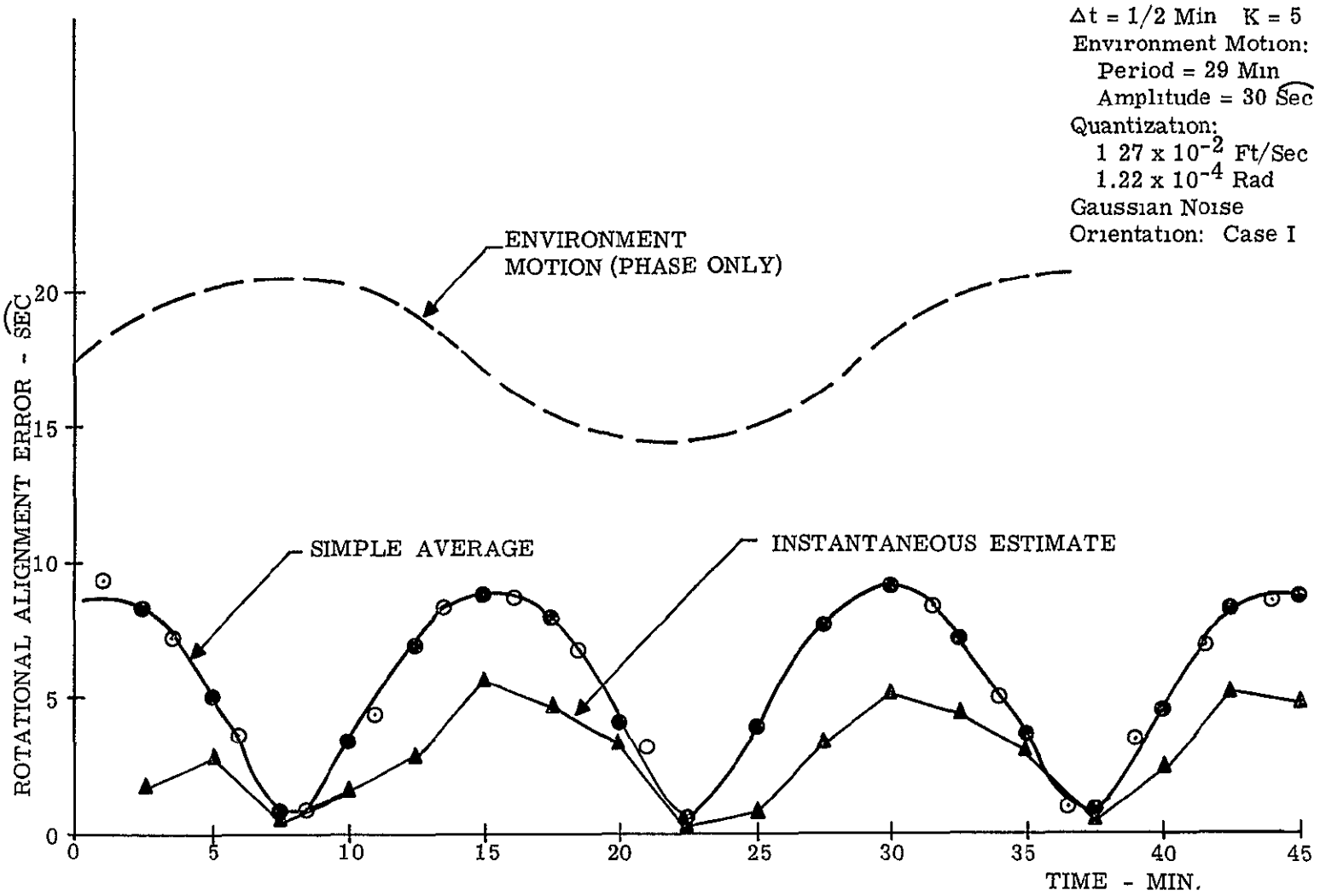

Figure 5-11. Alignment Error – Iterative Technique

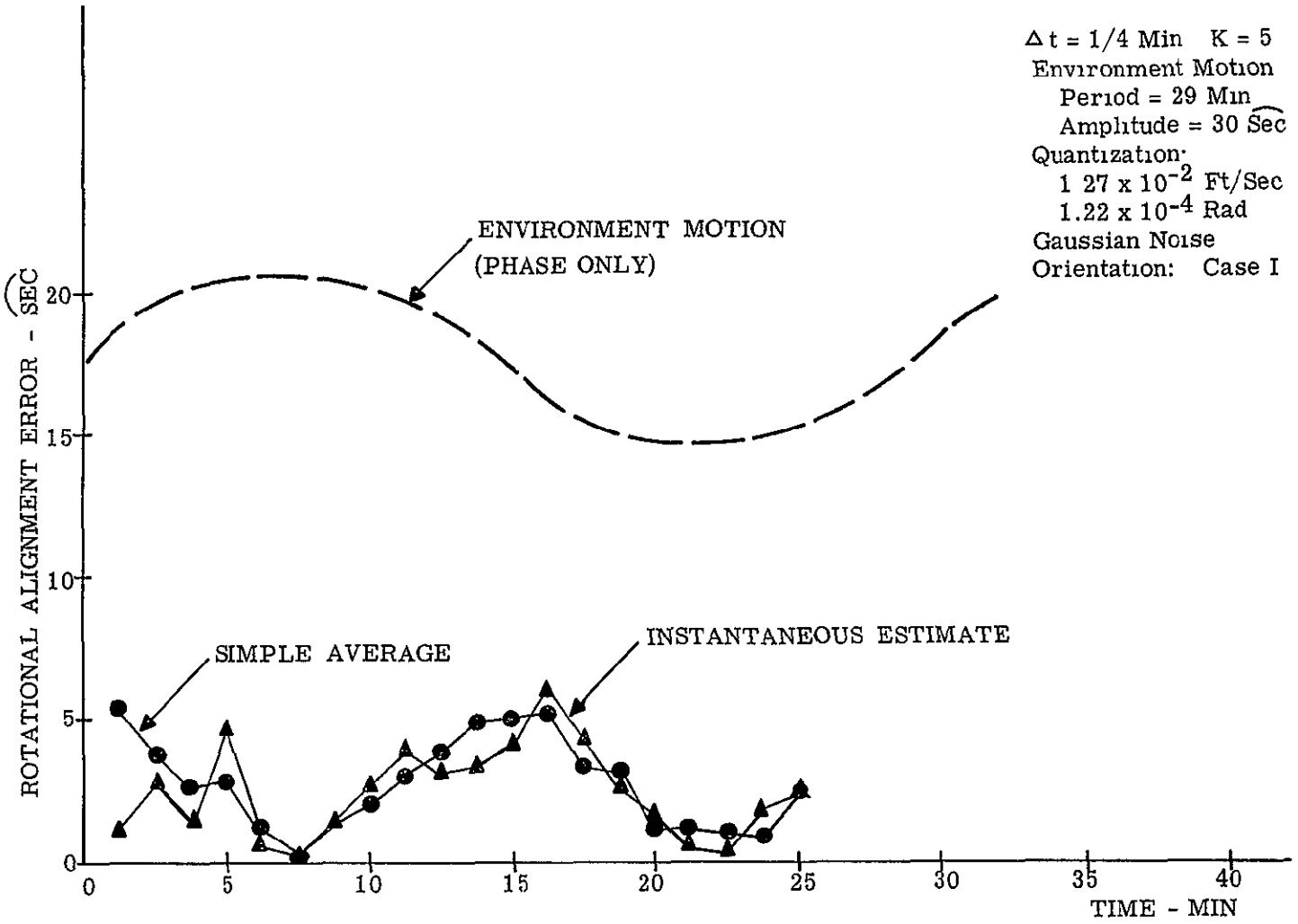

Figure 5-12. Alignment Error – Iterative Technique

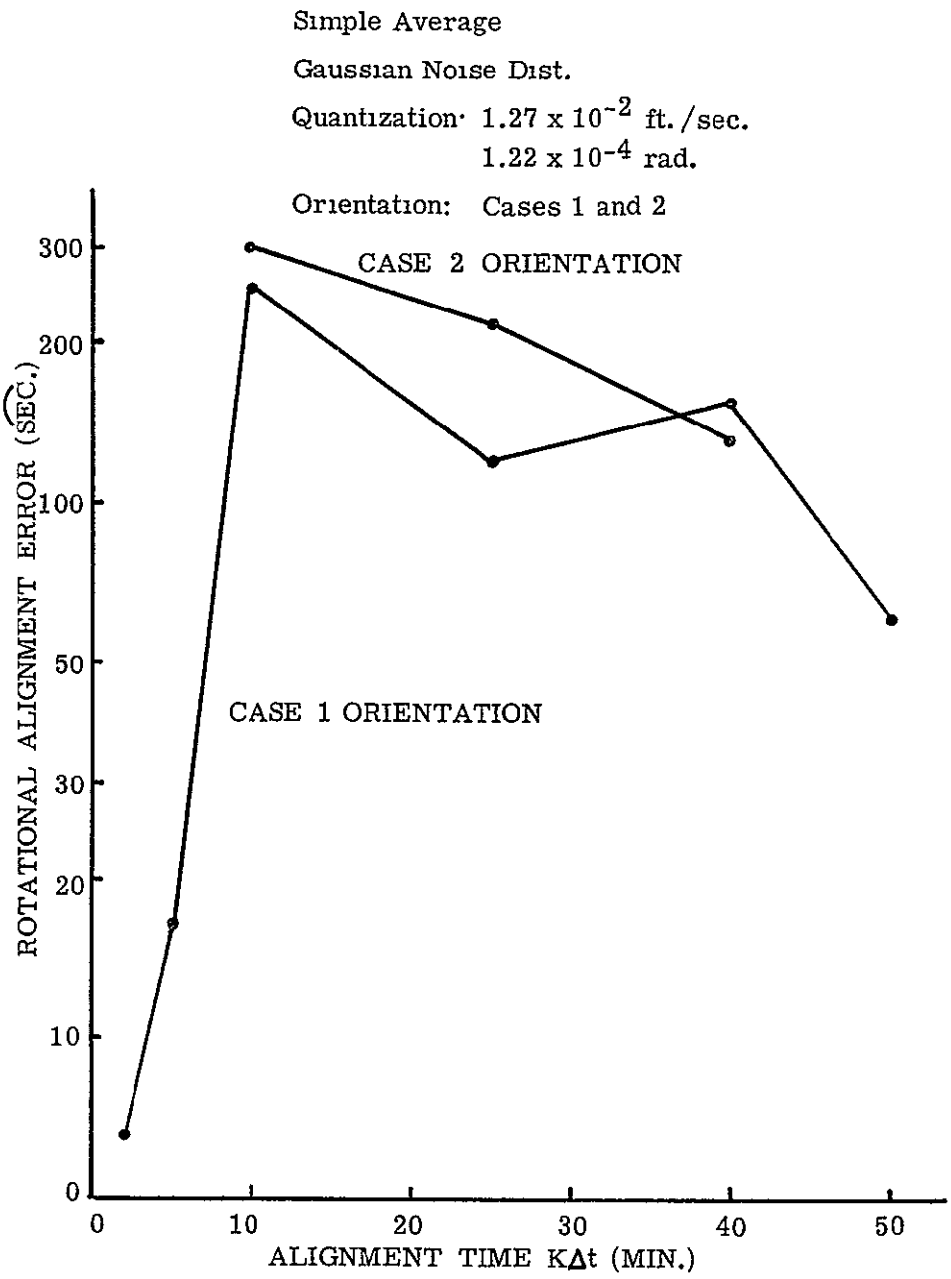

Figure 5-13. Gyrocompass Alignment Error vs Alignment Time For Simple Average

The absissa is time in minutes. The curves represent the alignment error based on data taken over the last $K\Delta t$ minutes. For example, in Figure 5-6, the alignment error at 25 minutes is eight seconds of arc based on data taken between 20 and 25 minutes. The phase of the low frequency motion is indicated with a sine-wave (dashed line). The open circles and triangles indicate data points from other phases shifted by a multiple of the basic period.

The covariance matrix converges in two or three iterations to an asymptotic value. Hence the error does not converge. The uncertainty of the motion during the measurement interval $K\Delta t$ is dominant over the other noise inputs.

The maximum error occurs when the rotational velocity is largest; the error is almost periodic with a period that is one-half the period of the motion. For $\Delta t \geq 30$ seconds the error is approximately proportional to $\left|\sin(\omega t + \phi_0)\right| + \epsilon$. The residual error ϵ is the consequence of other noise sources and quantization. These graphs illustrate that the rotational motion from the environment is the dominant source of error. For $\Delta t > 30$ seconds, the instantaneous estimate is uniformly better than the simple average. On the other hand, for $\Delta t < 30$ seconds, the instantaneous estimate has sporadic error spikes. Also for the $\Delta t < 30$ seconds, the effect of the LF motion is comparable to the effect of quantization and other noise sources. For the low frequency noise with a 29 minute period, the results are graphed in Figure 5-9, 5-10, 5-11, and 5-12. Note that the error is not reduced by one-half even though the motion is one-half the previous value. These curves have the same characteristics as the 58 minute curves.

The iterative alignment technique requires more computer computation and memory than the non-iterative techniques. In each application the increased computation requirements must be balanced with the gain in alignment accuracy to obtain an "optimum" alignment system. In some applications, the computer capability may prohibit using the iterative technique. The computation requirements can be reduced by using the asymptotic value of the covariance matrix.

5.3.1.3 Gyrocompass Alignment

The alignment error for the simple average technique is graphed in Figure 5-13 as a function of alignment time, $K\Delta t$. This error is the rms error based on ten trials. Since gyro quantization error is large, the alignment error is strongly dependent on the quantization error in the east gyro output. In the simulation output we confirmed that alignment error is directly correlated to the gyro quantization in the east direction.

If the instantaneous estimate of gravity is used, we will obtain an improved estimate of the gravity components, as indicated on Figure 5-13; compare graphs for K=1 and K=5. The Gyrocompass Alignment error will not be reduced as much as the level alignment error in Figure 5-13 since gyro quantization is dominant.

5.3.2 Sensor Quantization

Several tests were performed to determine the effect of sensor quantization. The results are in Table 5-3. The entries are the rms alignment errors based on ten trials. The following assumptions were made: the low-frequency rotational motion was one minute of arc with a one hour period; the first data input to the Estimation Routine was taken when the body frame was level. Orientation Case 1 was used; the word length was not restricted in the estimation routine. Also, K=5 for all tests and Δt = 30 seconds for one test and 5 minutes for the other. A gaussian HF rotational noise was used.

The results for level alignment are in columns A and C. Note that the posterior-mean estimate is sensitive to the quantization level for small values of Δt. Also, the accuracy is not improved when the quantization is reduced below 1.27×10^{-2} ft/sec. and 1.22×10^{-4} rad.

The results for Gyrocompass Alignment are in column D. The largest entries (116 for Δt = 30 seconds and 120 for Δt = 5 minutes) result from a single trial in which there is one quantum error in the east-west gyro output. Note that even with the lowest quantization level (and Δt = 30 seconds) the quantization error in the east gyro is very significant.

5.3.3 Computer Word Length

As a first cut in determining the efforts of computer word length on alignment accuracy, a word length truncation was placed in the estimation routine in the computer simulations performed. A complete study of this effect could not be accomplished because of time limitation. The simulations were based on the same assumptions used for sensor quantization (Section 5.3.2) with quantization of 1.27×10^{-2} ft/sec. and 1.22×10^{-4} rad. Simulations were performed for word lengths of 15, 24, and 27 bits. The results of these simulations are shown in Table 5.4. The entries are the rms rotational alignment errors based on ten trials. Accuracy of the Level Alignment techniques are presented in columns A and C. The accuracy of the gyrocompass technique is presented in column D.

TABLE 5-3

ALIGNMENT ACCURACY VS SENSOR QUANTIZATION

Rotational Alignment Error ($\overset{\frown}{sec}$)

for
- Gaussian Noise Distribution
- Orientation Case I
- K = 5

A - Simple Average, Level

C - Posterior-Mean Estimate of Instantaneous Components, Level

D - Simple Average, Gyrocompass

Δt = 30 sec

QUANTIZATION		TECHNIQUE		
FT/SEC	RADIANS	A	C	D
1.27×10^{-3}	1.22×10^{-5}	8.3	3.7	116.0
1.27×10^{-2}	1.22×10^{-4}	8.4	4.2	10.2
1.27×10^{-1}	4.88×10^{-4}	9.0	26.8	10.5

Δt = 5 min

QUANTIZATION		TECHNIQUE		
FT/SEC	RADIANS	A	C	D
1.27×10^{-3}	1.22×10^{-5}	59.8	33.3	87.2
1.27×10^{-2}	1.22×10^{-4}	60.0	34.0	120.0
1.27×10^{-1}	4.88×10^{-4}	59.7	35.5	60.0

TABLE 5-4

ALIGNMENT ACCURACY VS COMPUTER WORD LENGTH

Rotational Alignment Error ($\widehat{sec}$)

for
- Gaussian Noise Distribution
- Orientation Case I
- K = 5
- Δt = 30 sec

A - Simple Average, Level

C - Posterior-Mean Estimate of Instantaneous Components, Level

D - Simple Average, Gyrocompass

WORD LENGTH	TECHNIQUE		
	A	C	D
27 Bits	8.4	3.2	10.2
24 Bits	8.3	3.5	10.2
15 Bits	10.6	9.9	11.6

The reader should be aware that the data given in Table 5.4 is not conclusive for a determination of the effects of word length on alignment accuracy. Only the estimation portion of alignment was considered. The program does not simulate the pre-processing or the determination of the T matrix. Further, the truncation performed was a simple truncation rather than a roundoff. Many of the computers that may be used with the ISU have roundoff capability and will be able to achieve better results than is indicated by the data in Table 5-4.

SECTION 6
ALIGNMENT ACCURACY VERSUS CALIBRATION ACCURACY

In the previous sections we considered the alignment accuracy as a function of instrument noise, environment noise, instrument readout quantization, estimation technique and alignment matrix computation. Referring back to Section 3, this leaves the consideration of the effect of calibration accuracy on the alignment accuracy. This investigation is the subject of this section.

In Section 6.1, the generalized error equations which relate calibration errors to errors in alignment are developed. In Section 6.2, these equations are evaluated for the orientation cases, 1 to 4. In Section 6.3, worst-case alignment errors are developed from a worst-case combination of calibration errors for all four orientations. Finally in Section 6.4, the statistics of alignment errors are derived in terms of the statistics of the calibration errors.

6.1 GENERALIZED ERROR EQUATIONS

The generalized error equations are developed in Chart 6-2 for both level and gyrocompass alignment. The assumptions leading to these equations are also listed in the chart. The Pre-Processing Computations, from which the error equations evolve, are presented in Chart 6-1.

6.2 ERROR EQUATION FOR CLASS 1 TO 4

The generalized error equations of Chart 6-2 are evaluated for each of the four orientation cases in this subsection. The results are listed in Charts 6-3 through 6-6. Note that the errors have been normalized by $\underline{g}$ and $\underline{\omega}^{\epsilon}$ and that $\Delta(C_{I0})$ and $\Delta(Q_{IS})$ have been dropped since they have a negligible effect on the results.

6.3 WORST-CASE ALIGNMENT ERRORS

The results of Section 6.2 are evaluated in this subsection for the worst-case combination of calibration errors. These results are presented in Chart 6-7. The expressions in this chart are then substituted into the generalized error equations of Charts 4-5 and 4-6 to produce equivalent ΔT and ΔTT^T matrices, Charts 6-8 and 6-9. These latter results can then be evaluated, applying the results of Chart 4-3, Alignment Precision, to produce the basic measures of alignment errors, cone angles and total rotation angle.

PREPROCESSING COMPUTATIONS

Inputs $(\Sigma\gamma)_{k2}, (\Sigma\gamma)_{k1}, (\Sigma\delta)_k$, and $\left(\Sigma n_2^T\right)$ for k = 1, 2, 3

The outputs $\int_t^{t+\Delta t} (\underline{\omega}\cdot\underline{B}_k)dt$ and $\int_t^{t+\Delta t} (\underline{a}\cdot\underline{B}_k)dt$ (k = 1, 2, 3) are given by the following computations

Level GC

- $P_k^A \equiv [(\Sigma\gamma)_{k2} - (\Sigma\gamma)_{k1}]$
- $P_k^G \equiv (\Sigma\delta)_k$
- $\Delta t \equiv S_2^T\left(\Sigma n_2^T\right)$
- $[\overline{(\underline{\omega}\cdot\underline{G}_k)\Delta t}] \equiv P_k^G(\Delta\Phi)_k - (R)_k\Delta t$
- $[\overline{(\underline{a}\cdot\underline{A}_k)\Delta t}] \equiv P_k^A/(D_1)_k - (D_O)_k\Delta t$
- $(\overline{\underline{\omega}\cdot\underline{G}_k}) \equiv [\overline{(\underline{\omega}\cdot\underline{G}_k)\Delta t}]/\Delta t$
- $(\overline{\underline{a}\cdot\underline{A}_k}) \equiv [\overline{(\underline{a}\cdot\underline{A}_k)\Delta t}]/\Delta t$
- $(\overline{\underline{a}\cdot\underline{G}_k}) \equiv (\overline{\underline{a}\cdot\underline{A}_k})$
- $$(\overline{\underline{a}\cdot\underline{O}_k}) = \begin{bmatrix} 0 & 0 & 1 \\ 1 & 0 & 0 \\ 1 & 0 & 0 \end{bmatrix} \begin{bmatrix} (\overline{\underline{a}\cdot\underline{A}_1}) \\ (\overline{\underline{a}\cdot\underline{A}_2}) \\ (\overline{\underline{a}\cdot\underline{A}_3}) \end{bmatrix}$$
- $$(\overline{\underline{a}\cdot\underline{S}_k}) = \begin{bmatrix} 0 & -1 & 0 \\ 0 & 0 & -1 \\ 0 & 1 & 0 \end{bmatrix} \begin{bmatrix} (\overline{\underline{a}\cdot\underline{A}_1}) \\ (\overline{\underline{a}\cdot\underline{A}_2}) \\ (\overline{\underline{a}\cdot\underline{A}_3}) \end{bmatrix}$$
- $\int_t^{t+\Delta t}(\underline{\omega}\cdot\underline{G}_k)dt = [\overline{(\underline{\omega}\cdot\underline{G}_k)\Delta t}] - [(B_I)_k(\overline{\underline{a}\cdot\underline{G}_k}) + (B_O)_k(\overline{\underline{a}\cdot\underline{O}_k}) + (B_S)_k(\overline{\underline{a}\cdot\underline{S}_k})]\Delta t$
  $- [(C_{II})_k(\overline{\underline{a}\cdot\underline{G}_k})^2 + (C_{SS})_k(\overline{\underline{a}\cdot\underline{S}_k})^2]\Delta t$
  $- [(C_{IS})_k(\overline{\underline{a}\cdot\underline{G}_k})(\overline{\underline{a}\cdot\underline{S}_k}) + (C_{OS})_k(\overline{\underline{a}\cdot\underline{O}_k})(\overline{\underline{a}\cdot\underline{S}_k}) + (C_{IO})_k(\overline{\underline{a}\cdot\underline{G}_k})(\overline{\underline{a}\cdot\underline{O}_k})]\Delta t$
  $- [(Q_{II})_k(\overline{\underline{\omega}\cdot\underline{G}_k})^2 + (Q_{IS})_k(\overline{\underline{\omega}\cdot\underline{G}_k})(\overline{\underline{\omega}\cdot\underline{S}_k})]\Delta t$
- $\int_t^{t+\Delta t}(\underline{a}\cdot\underline{A}_k)dt = [\overline{(\underline{a}\cdot\underline{A}_k)\Delta t}] - (D_2)_k(\overline{\underline{a}\cdot\underline{A}_k})^2\Delta t - (D_3)_k(\overline{\underline{a}\cdot\underline{A}_k})^3\Delta t$
- $\int_t^{t+\Delta t}(\underline{\omega}\cdot\underline{B}_k)dt = \sum_\ell Q_{k\ell}^G \int_t^{t+\Delta t}(\underline{\omega}\cdot\underline{G}_\ell)dt$
- $\int_t^{t+\Delta t}(\underline{a}\cdot\underline{B}_k)dt = \sum_\ell Q_{k\ell}^A \int_t^{t+\Delta t}(\underline{a}\cdot\underline{A}_\ell)dt$

where

- $$Q^G = \begin{bmatrix} 1 & -(\underline{G}_1\cdot\underline{B}_2) & -(\underline{G}_1\cdot\underline{B}_3) \\ -(\underline{G}_2\cdot\underline{B}_1) & 1 & -(\underline{G}_2\cdot\underline{B}_3) \\ -(\underline{G}_3\cdot\underline{B}_1) & -(\underline{G}_3\cdot\underline{B}_2) & 1 \end{bmatrix}$$
- $$Q^A = \begin{bmatrix} 1 & -(\underline{A}_1\cdot\underline{B}_2) & -(\underline{A}_1\cdot\underline{B}_3) \\ -(\underline{A}_2\cdot\underline{B}_1) & 1 & -(\underline{A}_2\cdot\underline{B}_3) \\ -(\underline{A}_3\cdot\underline{B}_1) & -(\underline{A}_3\cdot\underline{B}_2) & 1 \end{bmatrix}$$

GENERALIZED ERROR EQUATIONS

With the assumptions

- All calibration constants are in error
- The Q matrix errors are deviations from an identity matrix.
- No noise.
- No quantization errors.
- $\underline{a} = \underline{g}$ = constant, $\underline{\omega} = \underline{\omega}^E$ = constant
- As error coefficients $\overline{(\underline{\omega}^E \cdot \underline{G}_k)} = (\underline{\omega}^E \cdot \underline{B}_k)$ and $\overline{(\underline{g} \cdot \underline{A}_k)} = (\underline{g} \cdot \underline{B}_k)$

These assumptions lead to the following error equations

Level GC

- $\Delta(\underline{\omega}^E \cdot \underline{B}_k) = \Delta(\underline{\omega}^E \cdot \underline{G}_k) + \sum_\ell \Delta Q^G_{k\ell} \, (\underline{\omega}^E \cdot \underline{B}_\ell)$
- $\Delta(\underline{g} \cdot \underline{B}_k) = \Delta(\underline{g} \cdot \underline{A}_k) + \sum_\ell \Delta Q^A_{k\ell} \, (\underline{g} \cdot \underline{A}_\ell)$

where

- $\Delta(\underline{\omega}^E \cdot \underline{G}_k) = \Delta(\Delta\Phi)_k/(\Delta\Phi)_k (\underline{\omega}^E \cdot \underline{B}_k) - \Delta R_k - \Delta(B_I)_k (\underline{g} \cdot \underline{B}_k)$

$$- \Delta(B_O)_k (\underline{g} \cdot \underline{O}_k) - \Delta(B_S)_k (\underline{g} \cdot \underline{S}_k) - \Delta(C_{II})_k (\underline{g} \cdot \underline{B}_k)^2$$

$$- \Delta(C_{SS})_k (\underline{g} \cdot \underline{S}_k)^2 - \Delta(C_{IS})_k (\underline{g} \cdot \underline{B}_k)(\underline{g} \cdot \underline{S}_k)$$

$$- \Delta(C_{OS})_k (\underline{g} \cdot \underline{O}_k)(\underline{g} \cdot \underline{S}_k) - \Delta(C_{IO})_k (\underline{g} \cdot \underline{B}_k)(\underline{g} \cdot \underline{O}_k)$$

$$- \Delta(Q_{II})_k (\underline{\omega}^E \cdot \underline{B}_k)^2 - \Delta(Q_{IS})_k (\underline{\omega}^E \cdot \underline{B}_k)(\underline{\omega}^E \cdot \underline{S}_k)$$

- $\Delta(\underline{g} \cdot \underline{A}_k) = -[(\underline{g} \cdot \underline{B}_k) - (D_0)_k] \, \Delta(D_1)_k/(D_1)_k - \Delta(D_0)_k$

$$- \Delta(D_2)_k (\underline{g} \cdot \underline{B}_k)^2 - \Delta(D_3)_k (\underline{g} \cdot \underline{B}_k)^3$$

- $\Delta Q^A = \begin{bmatrix} 0 & -\Delta(\underline{A}_1 \cdot \underline{B}_2) & -\Delta(\underline{A}_1 \cdot \underline{B}_3) \\ -\Delta(\underline{A}_2 \cdot \underline{B}_1) & 0 & -\Delta(\underline{A}_2 \cdot \underline{B}_3) \\ -\Delta(\underline{A}_3 \cdot \underline{B}_1) & -\Delta(\underline{A}_3 \cdot \underline{B}_2) & 0 \end{bmatrix}$
- $\Delta Q^G = \begin{bmatrix} 0 & -\Delta(\underline{G}_1 \, \underline{B}_2) & -\Delta(\underline{G}_1 \cdot \underline{B}_3) \\ -\Delta(\underline{G}_2 \cdot \underline{B}_1) & 0 & -\Delta(\underline{G}_2 \cdot \underline{B}_3) \\ -\Delta(\underline{G}_3 \cdot \underline{B}_1) & -\Delta(\underline{G}_3 \cdot \underline{B}_2) & 0 \end{bmatrix}$
- $(\underline{g} \cdot \underline{O}_k) = \begin{bmatrix} 0 & 0 & 1 \\ 1 & 0 & 0 \\ 1 & 0 & 0 \end{bmatrix} \begin{bmatrix} (\underline{g} \cdot \underline{B}_1) \\ (\underline{g} \cdot \underline{B}_2) \\ (\underline{g} \cdot \underline{B}_3) \end{bmatrix}$
- $(\underline{g} \cdot \underline{S}_k) = \begin{bmatrix} 0 & -1 & 0 \\ 0 & 0 & -1 \\ 0 & 1 & 0 \end{bmatrix} \begin{bmatrix} (\underline{g} \cdot \underline{B}_1) \\ (\underline{g} \cdot \underline{B}_2) \\ (\underline{g} \, \underline{B}_3) \end{bmatrix}$

CASE 1 ERROR EQUATIONS

The nominal alignment is given by:

$$[T] = \begin{bmatrix} 0 & 0 & 1 \\ 1 & 0 & 0 \\ 0 & 1 & 0 \end{bmatrix} \quad \text{latitude} = 45^{o}$$

The error equations are:

Level GC

- $$\left(\frac{\Delta(\underline{\omega}^{E} \cdot \underline{B}_1)}{\omega^{E}}\right) = -\left(\frac{\Delta R_1}{\omega^{E}}\right) - \left(\frac{\Delta(B_O)g}{\omega^{E}}\right) - 0.707(\Delta(\underline{G}_1 \cdot \underline{B}_2)) - 0.707(\Delta(\underline{G}_1 \cdot \underline{B}_3))$$

- $$\left(\frac{\Delta(\underline{\omega}^{E} \cdot \underline{B}_2)}{\omega^{E}}\right) = 0.707\left(\frac{\Delta(\Delta\Phi)_2}{(\Delta\Phi)_2}\right) - \left(\frac{\Delta R_2}{\omega^{E}}\right) - \left(\frac{\Delta(B_S)_2 g}{\omega^{E}}\right) - \left(\frac{\Delta(C_{SS})_2 g^2}{\omega^{E}}\right)$$

$$-0.500\left(\Delta(Q_{II})_2 \omega^{E}\right) - 0.707(\Delta(\underline{G}_1 \cdot \underline{B}_3))$$

- $$\left(\frac{\Delta(\underline{\omega}^{E} \cdot \underline{B}_3)}{\omega^{E}}\right) = 0.707\left(\frac{\Delta(\Delta\Phi)_3}{(\Delta\Phi)_3}\right) - \left(\frac{\Delta R_3}{\omega^{E}}\right) - \left(\frac{\Delta(B_I)_3 g}{\omega^{E}}\right) - \left(\frac{\Delta(C_{II})_3 g^2}{\omega^{E}}\right)$$

$$-0.500\left(\Delta(Q_{II})_3 \omega^{E}\right) - 0.707(\Delta(\underline{G}_3 \cdot \underline{B}_2))$$

- $$\left(\frac{\Delta(\underline{g} \cdot \underline{B}_1)}{g}\right) = -0.100\left(\frac{\Delta(D_1)_1}{(D_1)_1}\right) - \left(\frac{\Delta(D_0)_1}{g}\right) - (\Delta(\underline{A}_1 \cdot \underline{B}_3))$$

- $$\left(\frac{\Delta(\underline{g} \cdot \underline{B}_2)}{g}\right) = -0.100\left(\frac{\Delta(D_1)_2}{(D_1)_2}\right) - \left(\frac{\Delta(D_0)_2}{g}\right) - (\Delta(\underline{A}_2 \cdot \underline{B}_3))$$

- $$\left(\frac{\Delta(\underline{g} \cdot \underline{B}_3)}{g}\right) = -1.000\left(\frac{\Delta(D_1)_3}{(D_1)_3}\right) - \left(\frac{\Delta(D_0)_3}{g}\right) - (\Delta(D_2)_3 g) - \left(\Delta(D_3)_3 g^2\right)$$

CASE 2 ERROR EQUATIONS

The nominal alignment is given by

$$[T] = \begin{bmatrix} 0.577 & 0.577 & 0.577 \\ 0.815 & -0.407 & -0.407 \\ 0 & 0.707 & -0.707 \end{bmatrix} \qquad \text{latitude} = 45^{\circ}$$

The error equations are

Level GC

$$\bullet \left(\frac{\Delta(\underline{\omega}^E \cdot \underline{B}_1)}{\omega^E}\right) = 0.407\left(\frac{\Delta(\Delta\Phi)_1}{(\Delta\Phi)_1}\right) - 0.577\left(\frac{\Delta(B_I)_1 g}{\omega^E}\right) - 0.577\left(\frac{\Delta(B_O)_1 g}{\omega^E}\right) + 0.577\left(\frac{\Delta(B_S)_1 g}{\omega^E}\right)$$

$$- 0.333\left(\frac{\Delta(C_{II})_1 g^2}{\omega^E}\right) - 0.333\left(\frac{\Delta(C_{SS})_1 g^2}{\omega^E}\right) + 0.333\left(\frac{\Delta(C_{OS})_1 g^2}{\omega^E}\right) - 0.333\left(\frac{\Delta(C_{IS})_1 g^2}{\omega^E}\right)$$

$$- 0.166(\Delta(Q_{II})\omega^E) - 0.907(\Delta(\underline{G}_1 \cdot \underline{B}_2)) + 0.093(\Delta(\underline{G}_1 \cdot \underline{B}_3)) - \frac{\Delta R_1}{\omega^E}$$

$$\bullet \left(\frac{\Delta(\underline{\omega}^E \cdot \underline{B}_2)}{\omega^E}\right) = 0.907\left(\frac{\Delta(\Delta\Phi)_2}{(\Delta\Phi)_2}\right) - 0.577\left(\frac{\Delta(B_I)_2 g}{\omega^E}\right) - 0.577\left(\frac{\Delta(B_O)_2 g}{\omega^E}\right) + 0.577\left(\frac{\Delta(B_S)_2 g}{\omega^E}\right)$$

$$- 0.333\left(\frac{\Delta(C_{II})_2 g^2}{\omega^E}\right) - 0.333\left(\frac{\Delta(C_{SS})_2 g^2}{\omega^E}\right) - 0.333\left(\frac{\Delta(C_{IS})_2 g^2}{\omega^E}\right) - 0.333\left(\frac{\Delta(C_{OS})_2 g^2}{\omega^E}\right)$$

$$- 0.824(\Delta(Q_{II})_2\omega^E) - 0.407(\Delta(\underline{G}_2 \cdot \underline{B}_1)) - 0.093(\Delta(\underline{G}_2 \cdot \underline{B}_3)) - \frac{\Delta R_2}{\omega^E}$$

$$\bullet \left(\frac{\Delta(\underline{\omega}^E \cdot \underline{B}_3)}{\omega^E}\right) = 0.093\left(\frac{\Delta(\Delta\Phi)_3}{(\Delta\Phi)_3}\right) - 0.577\left(\frac{\Delta(B_I)_3 g}{\omega^E}\right) - 0.577\left(\frac{\Delta(B_O)_3 g}{\omega^E}\right) - 0.577\left(\frac{\Delta(B_S)_3 g}{\omega^E}\right)$$

$$- 0.333\left(\frac{\Delta(C_{II})_3 g^2}{\omega^E}\right) - 0.333\left(\frac{\Delta(C_{SS})_3 g^2}{\omega^E}\right) - 0.333\left(\frac{\Delta(C_{IS})_3 g^2}{\omega^E}\right) - 0.333\left(\frac{\Delta(C_{OS})_3 g^2}{\omega^E}\right)$$

$$- 0.008(\Delta(Q_{II})_3\omega^E) - 0.407(\Delta(\underline{G}_3 \cdot \underline{B}_1)) - 0.907(\Delta(\underline{G}_3 \cdot \underline{B}_2)) - \frac{\Delta R_3}{\omega^E}$$

$$\bullet\bullet \left(\frac{\Delta(\underline{g} \cdot \underline{B}_1)}{g}\right) = -0.677\left(\frac{\Delta(D_I)_1}{(D_I)_1}\right) - \left(\frac{\Delta(D_0)_1}{g}\right) - 0.333(\Delta(D_2)_1 g) - 0.192(\Delta(D_3)_1 g^2)$$

$$- 0.577(\Delta(\underline{A}_1 \cdot \underline{B}_2)) - 0.577(\Delta(\underline{A}_1 \cdot \underline{B}_3))$$

$$\bullet\bullet \left(\frac{\Delta(\underline{g} \cdot \underline{B}_2)}{g}\right) = -0.677\left(\frac{\Delta(D_I)_2}{(D_I)_2}\right) - \left(\frac{\Delta(D_0)_2}{g}\right) - 0.333(\Delta(D_2)_2 g) - 0.192(\Delta(D_3)_2 g^2)$$

$$- 0.577(\Delta(\underline{A}_2 \cdot \underline{B}_1)) - 0.577(\Delta(\underline{A}_2 \cdot \underline{B}_3))$$

$$\bullet\bullet \left(\frac{\Delta(\underline{g} \cdot \underline{B}_3)}{g}\right) = -0.677\left(\frac{\Delta(D_I)_3}{(D_I)_3}\right) - \left(\frac{\Delta(D_0)_3}{g}\right) - 0.333(\Delta(D_2)_3 g) - 0.192(\Delta(D_3)_3 g^2)$$

$$- 0.577(\Delta(\underline{A}_3 \cdot \underline{B}_1)) - 0.577(\Delta(\underline{A}_3 \cdot \underline{B}_2))$$

CASE 3 ERROR EQUATIONS

The nominal alignment is given by

$$[T] = \begin{bmatrix} 0 & -0.707 & -0.707 \\ 1 & 0 & 0 \\ 0 & 0.707 & 0.707 \end{bmatrix} \quad \text{latitude} = 45^{\circ}$$

The error equations are

Level GC

$$\bullet \quad \left(\frac{\Delta(\underline{\omega}^E \cdot \underline{B}_1)}{\omega^E}\right) = -\left(\frac{\Delta R_1}{\omega^E}\right) - 0.707\left(\frac{\Delta(B_O)_1 g}{\omega^E}\right) - 0.707\left(\frac{\Delta(B_S)_1 g}{\omega^E}\right)$$

$$-0.500\left(\frac{\Delta(C_{SS})_1 g^2}{\omega^E}\right) - 0.500\left(\frac{\Delta(C_{OS})_1 g^2}{\omega^E}\right) - (\Delta(\underline{G}_1 \cdot \underline{B}_3))$$

$$\bullet \quad \left(\frac{\Delta(\underline{\omega}^E \cdot \underline{B}_2)}{\omega^E}\right) = -\left(\frac{\Delta R_2}{\omega^E}\right) + 0.707\left(\frac{\Delta(B_I)_2 g}{\omega^E}\right) - 0.707\left(\frac{\Delta(B_O)_2 g}{\omega^E}\right) - 0.500\left(\frac{\Delta(C_{II})_2 g^2}{\omega^E}\right)$$

$$-0.500\left(\frac{\Delta(C_{SS})_2 g^2}{\omega^E}\right) - 0.500\left(\frac{\Delta(C_{IS})_2 g^2}{\omega^E}\right) - (\Delta(\underline{G}_2 \cdot \underline{B}_3))$$

$$\bullet \quad \left(\frac{\Delta(\underline{\omega}^E \cdot \underline{B}_3)}{\omega^E}\right) = \left(\frac{\Delta(\Delta\Phi)_3}{(\Delta\Phi)_3}\right) - \left(\frac{\Delta R_3}{\omega^E}\right) - 0.707\left(\frac{\Delta(B_I)_3 g}{\omega^E}\right) - 0.707\left(\frac{\Delta(B_S)_3 g}{\omega^E}\right)$$

$$-0.500\left(\frac{\Delta(C_{II})_3 g^2}{\omega^E}\right) - 0.500\left(\frac{\Delta(C_{SS})_3 g^2}{\omega^E}\right) + 0.500\left(\frac{\Delta(C_{IS})_3 g^2}{\omega^E}\right) - (\Delta(Q_{II})_3 \omega^E)$$

$$\bullet \bullet \quad \left(\frac{\Delta(\underline{g} \cdot \underline{B}_1)}{g}\right) = -0\ 100\left(\frac{\Delta(D_1)_1}{(D_1)_1}\right) - \left(\frac{\Delta(D_0)_1}{g}\right) + 0.707(\Delta(\underline{A}_1 \cdot \underline{B}_2)) - 0.707(\Delta(\underline{A}_1\ \underline{B}_3))$$

$$\bullet \bullet \quad \left(\frac{\Delta(\underline{g} \cdot \underline{B}_2)}{g}\right) = 0.607\left(\frac{\Delta(D_1)_2}{(D_1)_2}\right) - \left(\frac{\Delta(D_0)_2}{g}\right) - 0.500(\Delta(D_2)_2 g) + 0\ 354(\Delta(D_3)_2 g^2)$$

$$-0.707(\Delta(\underline{A}_2 \cdot \underline{B}_3))$$

$$\bullet \bullet \quad \left(\frac{\Delta(\underline{g} \cdot \underline{B}_3)}{g}\right) = -0.807\left(\frac{\Delta(D_1)_3}{(D_1)_3}\right) - \left(\frac{\Delta(D_0)_3}{g}\right) - 0.500(\Delta(D_2)_3 g) - 0.354(\Delta(D_3)_3 g^2)$$

$$+0.707(\Delta(\underline{A}_3 \cdot \underline{B}_2))$$

CASE 4 ERROR EQUATIONS

The nominal alignment is given by

$$T = \begin{bmatrix} 0.407 & -0.093 & 0.907 \\ 0.815 & -0.407 & -0.407 \\ 0.407 & 0.907 & -0.093 \end{bmatrix} \qquad \text{latitude} = 45$$

The error equations are

Level GC

$$\bullet \left(\frac{\Delta(\underline{\omega}^E \underline{B}_1)}{\omega^E}\right) = 0.577\left(\frac{\Delta(\Delta\Phi)_1}{(\Delta\Phi)_1}\right) - \left(\frac{\Delta R_1}{\omega^E}\right) - 0.407\left(\frac{\Delta(B_I)_1 g}{\omega^E}\right) - 0.907\left(\frac{\Delta(B_O)_1 g}{\omega^E}\right) - 0.093\left(\frac{\Delta(B_S)_1 g}{\omega^E}\right)$$

$$- 0.166\left(\frac{\Delta(C_{II})g^2}{\omega^E}\right) - 0.009\left(\frac{\Delta(C_{SS})_1 g^2}{\omega^E}\right) - 0.038\left(\frac{\Delta(C_{IS})_1 g^2}{\omega^E}\right) - 0.084\left(\frac{\Delta(C_{OS})_1 g^2}{\omega^E}\right)$$

$$- 0.333(\Delta(Q_{II})\omega^E) - 0.577(\Delta(\underline{G}_1\ \underline{B}_2)) - 0.577(\Delta(\underline{G}_1\ \underline{B}_3))$$

$$\bullet \left(\frac{\Delta(\underline{\omega}^E \underline{B}_2)}{\omega^E}\right) = 0.577\left(\frac{\Delta(\Delta\Phi)_2}{(\Delta\Phi)_2}\right) - \left(\frac{\Delta R_2}{\omega^E}\right) + 0.093\left(\frac{\Delta(B_I)_2 g}{\omega^E}\right) - 0.407\left(\frac{\Delta(B_O)_2 g}{\omega^E}\right) + 0.907\left(\frac{\Delta(B_S)_2 g}{\omega^E}\right)$$

$$- 0.009\left(\frac{\Delta(C_{II})g^2}{\omega^E}\right) - 0.820\left(\frac{\Delta(C_{SS})_2 g^2}{\omega^E}\right) - 0.084\left(\frac{\Delta(C_{IS})_2 g^2}{\omega^E}\right) - 0.368\left(\frac{\Delta(C_{OS})_2 g^2}{\omega^E}\right)$$

$$- 0.333(\Delta(Q_{II})_2\omega^E) - 0.577(\Delta(\underline{G}_2\ \underline{B}_1)) - 0.577(\Delta(\underline{G}_2\ \underline{B}_3))$$

$$\bullet \left(\frac{\Delta(\underline{\omega}^E \underline{B}_3)}{\omega^E}\right) = 0.577\left(\frac{\Delta(\Delta\Phi)_3}{(\Delta\Phi)_3}\right) - \left(\frac{\Delta R_3}{\omega^E}\right) - 0.907\left(\frac{\Delta(B_I)_3 g}{\omega^E}\right) - 0.407\left(\frac{\Delta(B_O)_3 g}{\omega^E}\right) - 0.093\left(\frac{\Delta(B_S)_3 g}{\omega^E}\right)$$

$$- 0.820\left(\frac{\Delta(C_{II})_3 g^2}{\omega^E}\right) - 0.009\left(\frac{\Delta(C_{SS})_3 g^2}{\omega^E}\right) - 0.084\left(\frac{\Delta(C_{IS})_3 g^2}{\omega^E}\right) - 0.038\left(\frac{\Delta(C_{OS})_3 g^2}{\omega^E}\right)$$

$$- 0.577(\Delta(Q_{II})_3\omega^E) - 0.577(\Delta(\underline{G}_3\ \underline{B}_1)) - 0.577(\Delta(\underline{G}_3\ \underline{B}_2))$$

$$\bullet\ \bullet \left(\frac{\Delta(\underline{g}\cdot\underline{B}_1)}{g}\right) = -0.507\left(\frac{\Delta(D_I)_1}{(D_I)_1}\right) - \left(\frac{\Delta(D_O)_1}{g}\right) - 0.166(\Delta(D_2)_1 g) - 0.068(\Delta(D_3)_1 g^2)$$

$$+ 0.093(\Delta(\underline{A}_1\cdot\underline{B}_2)) - 0.907(\Delta(\underline{A}_1\ \underline{B}_3))$$

$$\bullet\ \bullet \left(\frac{\Delta(\underline{g}\cdot\underline{B}_2)}{g}\right) = -0.007\left(\frac{\Delta(D_I)_2}{(D_I)_2}\right) - \left(\frac{\Delta(D_O)_2}{g}\right) - 0.009(\Delta(D_2)_2 g)$$

$$- 0.407(\Delta(\underline{A}_2\ \underline{B}_1)) - 0.907(\Delta(\underline{A}_2\ \underline{B}_3))$$

$$\bullet\ \bullet \left(\frac{\Delta(\underline{g}\ \underline{B}_3)}{g}\right) = -\left(\frac{\Delta(D_I)_3}{(D_I)_3}\right) - \left(\frac{\Delta(D_O)_3}{g}\right) - 0.820(\Delta(D_2)_3 g) - 0.741(\Delta(D_3)_3 g^2)$$

$$- 0.407(\Delta(\underline{A}_3\cdot\underline{B}_1)) - 0.407(\Delta(\underline{A}_3\ \underline{B}_2))$$

WORST CASE CALIBRATION ERRORS

	Case 1	Case 2	Case 3	Case 4
$\left(\frac{\Delta(\underline{\omega}^E \cdot \underline{B}_1)}{\omega^E}\right)$	$2E_1 + 1.41E_2$	$4.06E_1 + 1.57E_2$	$3.41E_1 + E_2$	$2.70E_1 + 2.07E_2$
$\left(\frac{\Delta(\underline{\omega}^E \cdot \underline{B}_2)}{\omega^E}\right)$	$3E_1 + 1.66E_2$	$4.06E_1 + 2.23E_2$	$3.91E_1 + E_2$	$3.69E_1 + 2.07E_2$
$\left(\frac{\Delta(\underline{\omega}^E \cdot \underline{B}_3)}{\omega^E}\right)$	$3E_1 + 1.66E_2$	$4.06E_1 + 1.42E_2$	$3.91E_1 + 2E_2$	$3.36E_1 + 2.06E_2$
$\left(\frac{\Delta(\underline{g} \cdot \underline{B}_1)}{g}\right)$	$1.1E_3 + E_4$	$2.36E_3 + E_4$	$1.51E_3 + E_4$	$1.74E_3 + E_4$
$\left(\frac{\Delta(\underline{g} \cdot \underline{B}_2)}{g}\right)$	$1.1E_3 + E_4$	$2.36E_3 + E_4$	$2.17E_3 + E_4$	$1.52E_3 + E_4$
$\left(\frac{\Delta(\underline{g} \cdot \underline{B}_3)}{g}\right)$	$3.1E_3 + E_4$	$2.36E_3 + E_4$	$2.37E_3 + E_4$	$3.39E_3 + E_4$

Gyro errors: $E_1 = \left|\frac{\Delta R}{\omega^E}\right| = \left|\frac{\Delta B g}{\omega^E}\right| = \left|\frac{\Delta C g^2}{\omega^E}\right|$; $E_2 = \left|\frac{\Delta(\Delta\Phi)}{(\Delta\Phi)}\right| = \left|\Delta(\underline{G} \cdot \underline{B})\right| = \left|\Delta Q\, \omega^E\right|$

Accelerometer errors. $E_3 = \left|\frac{\Delta(D_1)}{(D_1)}\right| = \left|\Delta(\underline{A} \cdot \underline{B})\right| = \left|\Delta D_2 g\right| = \left|\Delta D_3 g^2\right|$, $E_4 = \left|\frac{\Delta D_0}{g}\right|$

CHART 6-7

WORST CASE LEVEL ALIGNMENT FROM CALIBRATION ERRORS

	Case 1	Case 2	Case 3	Case 4
ΔT_{11}	$1.1E_3 + E_4$	$3.14E_3 + 1.33E_4$	$1.51E_3 + E_4$	$2.77E_3 + 1.24E_4$
ΔT_{12}	$1.1E_3 + E_4$	$3.14E_3 + 1.33E_4$	$2.27E_3 + E_4$	$1.85E_3 + 1.11E_4$
ΔT_{13}	0	$3.14E_3 + 1.33E_4$	$2.27E_3 + E_4$	$1.37E_3 + 0.63E_4$
ΔT_{21}	0	$2.22E_3 + 0.94E_4$	0	$1.10E_3 + 0.50E_4$
ΔT_{22}	0	$5.55E_3 + 2.36E_4$	$1.07E_3 + 0.71E_4$	$1.07E_3 + 0.59E_4$
ΔT_{23}	$1.1E_3 + E_4$	$5.55E_3 + 2.36E_4$	$1.07E_3 + 0.71E_4$	$3.19E_3 + 1.53E_4$
ΔT_{31}	0	0	0	$0.55E_3 + 0.25E_4$
ΔT_{32}	0	$5.78E_3 + 2.45E_4$	$2.27E_3 + E_4$	$0.31E_3 + 0.16E_4$
ΔT_{33}	$1.1E_3 + E_4$	$5.78E_3 + 2.45E_4$	$2.27E_3 + E_4$	$2.50E_3 + 1.44E_4$
$(\Delta TT^T)_{12}$	$1.1E_3 + E_4$	$3.85E_3 + 1.63E_4$	$1.51E_3 + E_4$	$2.84E_3 + 1.63E_4$
$(\Delta TT^T)_{13}$	$1.1E_3 + E_4$	$7.70E_3 + 3.27E_4$	$2.14E_3 + 1.4. E_4$	$2.13E_3 + 1.41E_4$
$(\Delta TT^T)_{23}$	0	$3.14E_3 + 1.33E_4$	0	$1.66E_3 + 0.49E_4$

CHART 6-8

WORST CASE GYROCOMPASS FROM CALIBRATION ERRORS

	Case 1	Case 2	Case 3	Case 4
ΔT_{11}	$1.1E_3 + E_4$	$3.13E_3 + 1.33E_4$	$1.51E_3 + E_4$	$2.73E_3 + 1.24E_4$
ΔT_{12}	$1.1E_3 + E_4$	$3.13E_3 + 1.33E_4$	$2.27E_3 + E_4$	$1.85E_3 + 1.11E_4$
ΔT_{13}	0	$3.13E_3 + 1.33E_4$	$2.27E_3 + E_4$	$1.37E_3 + 0.63E_4$
ΔT_{21}	0	$2.22E_3 + 0.94E_4$	0	$2.94E_1 + 1.95E_2$
ΔT_{22}	$1.41E_1 + E_2$ $+ 1.1E_3 + E_4$	$6.64E_1 + 2.77E_2$ $+ 0.50E_3 + 0.21E_4$	$3.41E_1 + E_2$ $+ 2.14E_3 + 1.41E_4$	$6.53E_1 + 4.33E_2$ $+ 3.42E_3 + 1.63E_4$
ΔT_{23}	$1.1E_3 + E_4$	$6.64E_1 + 2.77E_2$ $+ 4.93E_3 + 2.10E_4$	$3.41E_1 + E_2$	$0.66E_1 + 0.44E_2$ $+ 3.42E_3 + 1.63E_4$
ΔT_{31}	$1.41E_1 + E_2$ $+ 1.1E_3 + E_4$	$7.65E_1 + 3.20E_2$ $+ 3.49E_3 + 1.48E_4$	$4.83E_1 + 1.41E_2$ $+ 1.51E_3 + E_4$	$5.87E_1 + 3.89E_2$ $+ 2.77E_3 + 1.24E_4$
ΔT_{32}	0	$3.83E_1 + 1.60E_2$ $+ 2.71E_3 + 1.15E_4$	$6.80E_3 + 3E_4$	$2.94E_1 + 1.95E_2$ $+ 1.37E_3 + 0.63E_4$
ΔT_{33}	$1.1E_3 + E_4$	$3.83E_1 + 1.60E_2$ $+ 2.71E_3 + 1.15E_4$	$2.27E_3 + E_4$	$2.94E_1 + 1.95E_2$ $+ 1.85E_3 + 1.11E_4$
$(\Delta T T^T)_{12}$	$1.1E_3 + E_4$	$3.84E_3 + 1.63E_4$	$1.51E_3 + E_4$	$3.42E_3 + 1.63E_4$
$(\Delta T T^T)_{13}$	$1.1E_3 + E_4$	$3.33E_3 + 1.41E_4$	$3.21E_3 + 1.41E_4$	$2.40E_3 + 1.41E_4$
$(\Delta T T^T)_{23}$	$1.41E_1 + E_2$ $+ 1.1E_3 + E_4$	$9.38E_1 + 3.92E_2$ $+ 3.84E_3 + 1.63E_4$	$4.83E_1 + 1.41E_2$ $+ 1.51E_3 + E_4$	$7.20E_1 + 4.78E_2$ $+ 3.42E_3 + 1.63E_4$

CHART 6-9

6.4 STATISTICAL ERRORS

A set of one-sigma values of the calibration coefficients was provided by ERC and are listed on Chart 6-10. These values were used to derive the one-sigma values of

$$\frac{\Delta(\underline{g} \cdot \underline{B}_k)}{g}$$

and

$$\frac{\Delta(\underline{\omega}^E \circ \underline{B}_k)}{\omega^E}$$

by applying the results of Charts 6-3 through 6-6 of Section 6.2. The one-sigma values of these quantities, defined as σ_{gk} and $\sigma_{\omega k}$ respectively, are listed in Chart 6-10 for all four orientation cases. Finally, these latter values along with the results of Section 4.3 were used to derive the one-sigma values of the elements of the ΔT and $\Delta T T^T$ matrices for both level and gyrocompass alignment and for all four orientations. These values are presented in Charts 6-11 and 6-12.

An analysis of the statistical calibration errors listed in Chart 6-10 showed a strong dependence of the results on the particular one-sigma value selected for gyro bias. Additional statistical analysis of this coefficient is indicated. The development in this section has been presented in enough detail to permit a calculation by the reader of statistical alignment errors for a different set of coefficient one-sigma values, should this be desirable in the future.

STATISTICAL CALIBRATION ERRORS

	Case 1	Case 2	Case 3	Case 4
$\sigma_{\omega 1}$	12.0×10^{-3}	12.1×10^{-3}	12.2×10^{-3}	12.0×10^{-3}
$\sigma_{\omega 2}$	12.3×10^{-3}	12.1×10^{-3}	12.2×10^{-3}	12.3×10^{-3}
$\sigma_{\omega 3}$	12.3×10^{-3}	12.1×10^{-3}	12.2×10^{-3}	12.2×10^{-3}
σ_{g1}	12.1×10^{-6}	12.5×10^{-6}	12.1×10^{-6}	12.4×10^{-6}
σ_{g2}	12.1×10^{-6}	12.5×10^{-6}	11.5×10^{-6}	11.8×10^{-6}
σ_{g3}	12.9×10^{-6}	12.5×10^{-6}	12.7×10^{-6}	13.4×10^{-6}

Coefficient One-Sigma Values

Gyro Bias	0.1 deg/hr	Accelerometer Bias	6.7×10^{-6} g
Scale Factor	10^{-4}	Scale Factor	10^{-5}
Unbalance	0.15 deg/hr/g	Second Order	0.9×10^{-6} g/g^2
Compliance	0.04 deg/hr/g^2	Third Order	0.1×10^{-6} g/g^3
Misalignment	3×10^{-5}	Misalignment	10^{-5}

CHART 6-10

STATISTICAL LEVEL ALIGNMENT FROM CALIBRATION ERRORS

	Case 1	Case 2	Case 3	Case 4
$\sigma_{\Delta T11}$	12.1×10^{-6}	10.2×10^{-6}	12.1×10^{-6}	11.5×10^{-6}
$\sigma_{\Delta T12}$	12.1×10^{-6}	10.2×10^{-6}	8.6×10^{-6}	11.8×10^{-6}
$\sigma_{\Delta T13}$	0	10.2×10^{-6}	8.6×10^{-6}	5.3×10^{-6}
$\sigma_{\Delta T21}$	0	7.2×10^{-6}	0	4.6×10^{-6}
$\sigma_{\Delta T22}$	0	9.5×10^{-6}	8.6×10^{-6}	5.4×10^{-6}
$\sigma_{\Delta T23}$	12.1×10^{-6}	9.5×10^{-6}	8.6×10^{-6}	11.5×10^{-6}
$\sigma_{\Delta T31}$	0	0	0	2.3×10^{-6}
$\sigma_{\Delta T32}$	0	10.8×10^{-6}	8.6×10^{-6}	1.3×10^{-6}
$\sigma_{\Delta T33}$	12.1×10^{-6}	10.8×10^{-6}	8.6×10^{-6}	12.8×10^{-6}
$\sigma_{\Delta TT^T12}$	12.1×10^{-6}	12.5×10^{-6}	12.1×10^{-6}	12.5×10^{-6}
$\sigma_{\Delta TT^T13}$	12.1×10^{-6}	12.5×10^{-6}	12.1×10^{-6}	11.9×10^{-6}
$\sigma_{\Delta TT^T23}$	0	8.8×10^{-6}	0	5.3×10^{-6}

CHART 6-11

STATISTICAL GYROCOMPASS FROM CALIBRATION ERRORS

	Case 1	Case 2	Case 3	Case 4
$\sigma_{\Delta T11}$	12.1×10^{-6}	10.2×10^{-6}	12.1×10^{-6}	11.5×10^{-6}
$\sigma_{\Delta T12}$	12.1×10^{-6}	10.2×10^{-6}	8.6×10^{-6}	11.8×10^{-6}
$\sigma_{\Delta T13}$	0	10.2×10^{-6}	8.6×10^{-6}	5.3×10^{-6}
$\sigma_{\Delta T21}$	0	7.2×10^{-6}	0	7.0×10^{-3}
$\sigma_{\Delta T22}$	17.0×10^{-3}	12.1×10^{-3}	12.2×10^{-3}	15.5×10^{-3}
$\sigma_{\Delta T23}$	12.1×10^{-6}	12.1×10^{-3}	12.2×10^{-3}	1.6×10^{-3}
$\sigma_{\Delta T31}$	17.0×10^{-3}	14.0×10^{-3}	17.3×10^{-3}	14.0×10^{-3}
$\sigma_{\Delta T32}$	0	7.0×10^{-3}	8.6×10^{-6}	7.0×10^{-3}
$\sigma_{\Delta T33}$	12.1×10^{-6}	7.0×10^{-3}	8.6×10^{-6}	7.0×10^{-3}
$\sigma_{\Delta TTT12}$	12.1×10^{-6}	12.5×10^{-6}	12.1×10^{-6}	12.5×10^{-6}
$\sigma_{\Delta TTT13}$	12.1×10^{-6}	12.5×10^{-6}	12.1×10^{-6}	11.9×10^{-6}
$\sigma_{\Delta TTT23}$	17.0×10^{-3}	17.1×10^{-3}	17.3×10^{-3}	17.1×10^{-3}

CHART 6-12

APPENDIX A
SUPPORTING CALIBRATION NOISE ANALYSIS

Section 2.2 develops the equations relating coefficient errors to sensor output error, ΔP, for both gyros and accelerometers. Charts 2-3 and 2-4 list these equations together with equations which describe $(\Delta P)_{rms}$ in terms of the statistics of the noise environment. The curves in Figures 2-1 through 2-4 show how these coefficient errors vary with the time interval, Δt, over which the sensor output is averaged.

In this Appendix we show the development of the noise equations in more detail than was given in Section 2.2. Section A.1 outlines the approach to the problem and relates the statistics of the output to those of the input to the process. The stochastic process considered includes the geometry of the problem and the averaging as well as the sensor itself, for the ΔP of Section 2.2 is the sensor output after it has been averaged over the time interval, Δt. In fact, sensor characteristics play a relatively minor role in the noise analysis.

Sections A.2 and A.3 discuss the geometrical effects and the statistics of the sensor input for gyro and accelerometer respectively. Finally, Section A.4 gives some of the mathematical details and approximations employed in the calculations for Figures 2-1 through 2-6 in Section 2.2.

A.1 APPROACH TO THE PROBLEM

The data, P, used in calibration is the sensor output summed over a time interval, Δt. The noise-induced error is ΔP and it is our aim here to relate ΔP to the input noise. The sensor, together with the subsequent summation of the pulses, is considered a stochastic process. The input to this process is a stochastic variable (the environment noise) plus, in the case of the gyro, an input equivalent to the internally-generated noise. The process model adopted for both gyros and accelerometers is

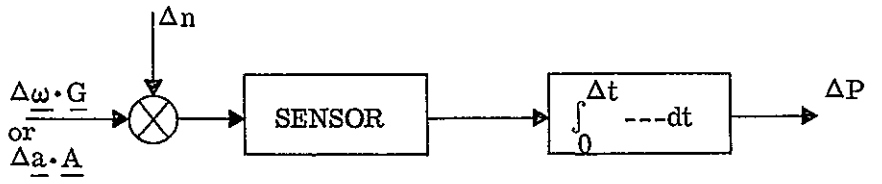

where Δn is the input equivalent sensor noise (gyro only), and $\Delta\underline{\omega}\cdot\underline{G}$ and $\Delta\underline{a}\cdot\underline{A}$ represent environment noise inputs to gyro and accelerometer, respectively. The summation has been replaced with an integration which means we are neglecting the sampling process and replacing it with a continuous process. This has little effect on the results since the sample interval is small compared with Δt.

Then the power spectral densities* of input and output are related by:

$$P_p(f) = \left|T_S(j\omega)\right|^2 \left|T_I(j\omega)\right|^2 P_{in}(f) \qquad \text{(A-1)}$$

where $P_p(f)$ = power spectral density of output error, ΔP

$P_{in}(f)$ = power spectral density of the input

$T_S(j\omega)$ = transfer function of the sensor

$T_I(j\omega)$ = transfer function of the integration.

The variance of the output error is related to the output power spectral density by (assuming stationary noise):

$$\text{var}\,[\Delta P] = \int_{-\infty}^{\infty} P_p(f)df \qquad \text{(A-2)}$$

Finally, the rms error is the square root of the variance.

The following sections discuss the gyro and accelerometer separately. As will be shown, the effect of environment vibrations upon both types of sensor depends on the sensor's orientation wrt** environment noise and also wrt $\underline{\omega}^E$ and $\underline{g}$, respectively. For this reason two sensor orientations are investigated (vertical and horizontal) and simplifying assumptions are made concerning the orientation of environment noise wrt these directions.

It is appropriate to discuss the integration transfer function $T_I(j\omega)$ at this point since it is common to both types of sensor.

---

*Other approaches might be taken to the problem. This approach is dictated by the nature of the available noise data.

**wrt = with respect to.

Let $\Delta P(t)$ be expressed as

$$\Delta P = \int_{-\infty}^{\infty} x(\tau)w(\tau)d\tau$$

where $x(\tau)$ is the input to the integration and $w(\tau)$ is a boxcar weighting function defined as one in the interval $t-\Delta t \leq \tau \leq t$ and zero outside this interval. Then the transfer function is:

$$T_I(j\omega) = L[w(t)] = \int_0^{\Delta t} e^{-j\omega t}dt$$

$$= \frac{e^{-j\omega\Delta t}-1}{j\omega}, \quad \omega = 2\pi f$$

and the square is:

$$\left|T_I(j\omega)\right|^2 = \frac{(e^{-j\omega\Delta t}-1)\,(e^{j\omega\Delta t}-1)}{(-j\omega)\qquad(j\omega)}$$

$$= \frac{2(1-\cos\ \omega\Delta t)}{\omega^2}$$

A.2 GYRO

The input sensed by the gyro is $\underline{\omega}\cdot\underline{G}$

where $\underline{G}$ = a unit vector along the gyro input axis
$\underline{\omega}$ = the total angular velocity of the gyro with respect to inertial space.

Now the gyro is on a turntable rotating with a constant angular velocity $\underline{\omega}^T$ with respect to the laboratory. The laboratory (the "environment") is subject to vibrations due to traffic, earth tremors, wind, etc. This is represented by saying the laboratory oscillates with an angular velocity $\underline{\omega}^e$ with respect to inertial space. Hence

$$\underline{\omega} = \underline{\omega}^T + \underline{\omega}^e + \underline{\omega}^E$$

and

$$\underline{\omega}\cdot\underline{G} = \underline{\omega}^T\cdot\underline{G} + \underline{\omega}^e\cdot\underline{G} + \underline{\omega}^E\cdot\underline{G}$$

Then the error in $\underline{\omega} \cdot \underline{G}$ is

$$\Delta(\underline{\omega} \cdot \underline{G}) = \Delta(\underline{\omega}^T \cdot \underline{G}) + \Delta(\underline{\omega}^e \cdot \underline{G}) + \Delta(\underline{\omega}^E \cdot \underline{G})$$

This can be simplified by observing that the first term on the right is zero if the gyro is firmly attached to the turntable.

Let $\underline{\omega}^e = \underline{\omega}_o^e + \Delta\underline{\omega}^e$ in the second term where $\underline{\omega}_o^e$ is the mean of $\underline{\omega}^e$. The mean has been assumed zero, so that we need only be concerned with $\Delta\underline{\omega}^e$, the distribution about the mean. Then the second term becomes $\Delta\underline{\omega}^e \cdot \underline{G}$. To simplify the problem and to get a "maximum rms" error, we will neglect the $\underline{\omega}^T$ modulation of $\Delta\underline{\omega}^e \cdot \underline{G}$ and compute the errors due to environment angular displacement noise for the two cases: gyro vertical and gyro horizontal.

For the $\Delta(\underline{\omega}^E \cdot \underline{G})$ term we have to consider in what coordinate system these omegas are defined. The dot product is invariant with respect to a linear coordinate transformation, but to be meaningful both vectors must be expressed in the same coordinate system. For our purposes here it is a matterof indifference whether $\underline{G}$ is fixed or $\underline{\omega}^E$ is fixed. We want to focus attention on the angle between them, which varies due to the vibration of the laboratory environment. (The angular velocity noise $\Delta\underline{\omega}^e$ is the time derivative of this angle.) Let $\theta = \theta_o + \Delta\theta$ be this angle. Then

$$\underline{\omega}^E \cdot \underline{G} = \omega^E \cos\theta$$

and

$$\Delta(\underline{\omega}^E \cdot \underline{G}) = \omega^E \Delta \cos\theta$$

$$\doteq (-\omega^E \sin\theta_o)\Delta\theta$$

where $\Delta\theta$ can be termed the angular displacement noise. Thus an important part of the input noise error arises from the gyro sensing a variable component of earth rate, the variation being due to vibration of the surrounding environment.

Putting all together we find that the input error is

$$\Delta(\underline{\omega} \cdot \underline{G}) = \Delta\underline{\omega}^e \cdot \underline{G} + (-\omega^E \sin\theta_o)\Delta\theta$$

Finally, the input power density spectrum is

$$P_{in}(f) = \left\{ \begin{array}{c} \text{input spectrum equivalent} \\ \text{of sensor noise} \end{array} \right\} + \left\{ \begin{array}{c} \text{Power spectrum} \\ \text{of } \Delta(\underline{\omega} \cdot \underline{G}) \end{array} \right\}$$

$$P_{in}(f) = P_n(f) + \cos^2\phi_o P_{\omega e}(f) + (\omega^E \sin\theta_o)^2 P_\theta(f) \qquad \text{(A-3)}$$

where $P_n(f)$ = power spectral density of gyro internal noise

$P_{\omega e}(f)$ = power spectral density of angular velocity noise $\Delta\omega^e$

$P_\theta(f)$ = power spectral density of angular displacement noise, $\Delta\theta$

ϕ_o = angle between $\underline{G}$ and the horizontal plane.

The angle ϕ_o enters via the dot product $\Delta\underline{\omega}^e \cdot \underline{G}$. For completeness, there should be an azimuth angle here too, but this dot product is independent of azimuth since we assume the angular velocity noise is isotropic in the horizontal plane and zero in the vertical. If it were completely isotropic we could drop the $\cos\phi_o$ factor also.

The variance of the gyro output noise is found by substituting (A-1) and (A-3) into (A-2) and performing the indicated integration, after functional expressions are found for the transfer functions and power spectra. It turns out the resulting integrand is not integrable in general, so the integration is performed numerically.

The angular displacement noise spectrum $P_\theta(f)$ is that given in Figure 3-4, Section 3.2.2, of the Development Document. This must be converted to $(\text{radians})^2$ rms/cps before being used in the computations. The angular velocity noise spectrum, $P_{\omega e}(f)$, is derived from the same figure by multiplying by $(2\pi f)^2 = (j\omega)(-j\omega)$. This corresponds to differentiation in the time domain. Since the angular displacement (and hence the angular velocity) is assumed isotropic in the horizontal plane and zero in the vertical, $\cos\phi_o$ in Equation (A-3) is equal to zero for a vertical position of the gyro-sensitive axis and equal to one for a horizontal position. Furthermore, $\sin\theta_o = 1/\sqrt{2}$ for both orientations, since θ_o is assumed equal to 45^o.

To summarize, we have for the variance of the gyro noise error

$$\text{var } [\Delta P] = \int_{-\infty}^{\infty} P_p(f)\, df$$

where $P_p(f) = |T_S(j\omega)|^2 |T_I(j\omega)|^2 \left[P_n(f) + \left(\frac{\omega_E}{2} \right)^2 P_\theta(f) \right]$, for gyro vertical

$= |T_S(j\omega)|^2 |T_I(j\omega)|^2 \left[P_n(f) + \left(\frac{\omega_E}{\sqrt{2}} \right)^2 P_\theta(f) + P_{\omega e}(f) \right]$, for gyro horizontal

Sensor dynamics for the gyro was approximated by a 20 Hz first order loop. Consequently,

$$|T_S(j\omega)|^2 \doteq \frac{1}{1 + (f/20)^2}$$

is adopted for the squared transfer function.

A.3 ACCELEROMETER

The description of accelerometer input is similar to that of the gyro. The input sensed by the accelerometer is $\underline{a} \cdot \underline{A}$, where

$\underline{A}$ = a unit vector along the input axis of the accelerometer

$\underline{a}$ = total acceleration

$= \underline{a}^e + \underline{g}$

$\underline{a}^e$ = environment acceleration (noise)

$\underline{g}$ = acceleration of gravity

The unwanted input, or noise, is

$$\Delta(\underline{a} \cdot \underline{A}) = \Delta(\underline{a}^e \cdot \underline{A}) + \Delta(\underline{g} \cdot \underline{A})$$

Assume: $\Delta \underline{g} = 0$

$\underline{a}^e = \underline{a}^e_o + \Delta \underline{a}^e$, with the mean, $\underline{a}^e_o$, equal to zero.

Then $$\Delta(\underline{a} \cdot \underline{A}) = \Delta \underline{a}^e \cdot \underline{A} + \Delta(\underline{g} \cdot \underline{A})$$

The first term on the right is the component of environment noise along $\underline{A}$ and the second term is the variation in the component of $\underline{g}$ sensed by the accelerometer; the variation being due to the angular vibration of $\underline{A}$ with respect to $\underline{g}$. If $\theta = \theta_o + \Delta\theta$ is the angle between $\underline{A}$ and $\underline{g}$, then:

$$\Delta(\underline{g} \cdot \underline{A}) \doteq (-g \sin\theta_o)\Delta\theta$$

Then the input power spectral density is

$$P_{in}(f) = \cos^2\phi_o P_{ae}(f) + (g \sin\theta_o)^2 P_\theta(f) \qquad \text{(A-4)}$$

where $P_{ae}(f)$ = power spectral density of the environment acceleration noise

$P_\theta(f)$ = power spectral density of the angular displacement noise, $\Delta\theta$

ϕ_o = angle between $\underline{a}^e$ and $\underline{A}$

θ_o = nominal angle between $\underline{g}$ and $\underline{A}$

g = magnitude of $\underline{g}$

The variance of the accelerometer output noise is found by substituting (A-1) and (A-4) into (A-2) and integrating numerically.

The noise spectra $P_{ae}(f)$ and $P_\theta(f)$ are those given in Figure 3-3 and 3-4 in Section 3.2.2 of the Development Document. Figure 3-4 gives $P_\theta(f)$ in $\widehat{\text{sec.}}^2$ rms per cps.

Since the random acceleration inputs are assumed isotropic, $\cos\phi_o$ is equal to 1 in equation A-4, for all orientations of the accelerometer. But since the random rotational inputs are assumed isotropic only in the horizontal plane (and zero about a vertical axis), $\sin\theta_o$ in equation A-4 is one for a horizontal accelerometer and zero for a vertical accelerometer.

To summarize then, we have

$$\text{var}\,[\Delta P] = \int_{-\infty}^{\infty} P_p(f)df$$

and

$$P_p(f) = |T_s(j\omega)|^2 |T_I(j\omega)|^2 P_{ae}(f) \quad \text{, for acc. vertical}$$

$$= |T_s(j\omega)|^2 |T_I(j\omega)|^2 [P_{ae}(f) + g^2 P_\theta(f)] \quad \text{, for acc. horizontal}$$

Sensor dynamics for the accelerometer was approximated by a 1000 Hz first order loop. Then the squared transfer function is

$$\left|T_S(j\omega)\right|^2 \doteq \frac{1}{1 + (f/1000)^2}$$

A.4 COMPUTATIONAL DETAILS

This subsection gives the computational details and approximations used in the computations for the noise curves in Section 2.2, Figures 2-1 through 2-6. Some of the approximations are rather rough, but this is not unreasonable in view of the approximate character of the power spectra and the fact that these spectra may not be representative of the actual noise environment at the Laboratory site. The results should be interpreted with suitable reservations. We first discuss the gyros, then the accelerometers.

Gyro

For the gyro we have

$$\text{var}\,[\Delta P] = \int_0^\infty \left|T_S(j\omega)\right|^2 \left|T_I(j\omega)\right|^2 \left[P_n(f) + \cos^2\phi_o\, P_{\omega e}(f) + (\omega^E \sin\theta_o)^2\, P_\theta(f)\right] df \quad \text{(A-5)}$$

where $\left|T_S(j\omega)\right|^2 \doteq \dfrac{1}{1 + (f/20)^2}$

$$\left|T_I(j\omega)\right|^2 = \frac{2(1 - \cos 2\pi f \Delta t)}{(2\pi f)^2}$$

and where $\cos\phi_o = 1$ for the gyro in a horizontal position

$= 0$ for the gyro in a vertical position

and $\sin\theta_o = 1/\sqrt{2}$ in both positions.

For the input equivalent to the internal noise, we adopted a spectrum which is flat up to a frequency of $(100 \text{ hours})^{-1}$ and which yields an rms noise of 5×10^{-3} degree/hour when integrated from $(14 \text{ hours})^{-1}$ to ∞, and having a peak at 16 cps. For computation, this spectrum was approximated piecewise as given in the following table:

Table A-1

f(cps)	$P_n(f)$ $((deg/hr)^2/cps)$
0 to $(100\ hrs)^{-1}$	3.02×10^{-2}
$(100\ hrs)^{-1}$ to 10^{-3}	$2.33 \times 10^{-13} f^{-2}$
10^{-3} to 8	2.33×10^{-7}
8 to 24	1×10^{-6}
Above 24	$6 \times 10^{-4} f^{-2}$

For the angular displacement noise spectrum, $P_\theta(f)$, Figure 3-4 of subsection 3.2.2 of the Development Document was used. This figure gives the spectrum in $(deg/hr)^2$ per cps. When this is converted to $(radians)^2$ per cps and multiplied by $(\omega^E/\sqrt{2})^2$ with ω^E = 15 deg/hr, it is approximated piecewise as in the following table:

Table A-2

f(cps)	$(\omega^E \sin\theta_0)^2 P_\theta(f)$ $((deg/hr)^2/cps)$
0 to 5×10^{-6}	0.106
5×10^{-6} to 0.317	$2.64 \times 10^{-2} f^{-2}$
0.317 to 3.17	2.64×10^{-4}
3.17 to 15.7	$2.64 \times 10^{-10} f^{-2}$
Above 15.7	$1.15 \times 10^{-6} f^{-5}$

The angular velocity spectrum, which is needed only for the horizontal position, was derived from Table A-2 by multiplication by

$$(j\omega)(-j\omega) = (2\pi f)^2$$

which corresponds to differentiation in the time domain.

The integrand in equation (A-2) is not integrable due to the $\left| T_I(j\omega) \right|^2$ factor, so this factor was also approximated piecewise. This factor is one at f=0 and descends to zero at $f = 1/\Delta t$ with a shape similar to $\cos^2(2\pi f \Delta t)$. Beyond this frequency it proceeds in arcs of rapidly diminishing amplitude with zeros at $1/k\Delta t$, $k = 3, 5, 7, \ldots$. For the numerical work, this was approximated by a constant 0.7 from 0 to $1/\Delta t$ and by the

envelope of the peaks, $1/(\pi f \Delta t)^2$, thereafter. Since the breakpoint depends on the calibration time, Δt, a new approximation is made for each value of Δt plotted. For the curves of Section 2.2, the noise errors were computed for calibration times of 2, 5, 10, 15, 20, 30, 40, and 50 minutes.

As mentioned earlier, the sensor transfer function $\left|T_S(j\omega)\right|^2$ does not change the results significantly.

It may be of interest to compare the separate contributions of the noise sources. In terms of contributions to the variance, and using the above approximation, we have, in $(\text{deg/hr})^2$:

$$\text{Contribution of sensor noise} \doteq 1.7 \times 10^{-7} + \frac{2.6 \times 10^{-7}}{\Delta t} + \frac{5.5 \times 10^{-9}}{(\Delta t)^2}$$

$$\text{Contribution of } \Delta\theta \text{ noise} \doteq 1.8 \times 10^{-7} - 2.4 \times 10^{-12}\Delta t - \frac{8.5 \times 10^{-12}}{(\Delta t)^2}$$

$$\text{Contribution of } \omega^e \text{ noise} \doteq \frac{4.35 \times 10^{-2}}{\Delta t} + \frac{2.11 \times 10^{-1}}{(\Delta t)^2}$$

Accelerometer

For the accelerometer, we have:

$$\text{var}\,[\Delta P] = \int_0^\infty \left|T_S(j\omega)\right|^2 \left|T_I(j\omega)\right|^2 \{P_{ae}(f) + \sin^2\theta_o P_\theta(f)\}\,df \qquad \text{(A-6)}$$

where $\left|T_S(j\omega)\right|^2 \doteq \dfrac{1}{1 + (f/1000)^2}$

$$\left|T_I(j\omega)\right|^2 = \frac{2(1 - \cos 2\pi f \Delta t)}{(2\pi f)^2}$$

as given previously. The factor g^2 multiplying the $P_\theta(f)$ term has been omitted because we want the variance in units of g^2. Then the standard deviation will be in units of g. As with the gyro, $P_\theta(f)$ from Figure 3-4 of Section 3.2.2 (Development Document) must

be converted to $(\text{radians})^2/\text{cps}$. The environment acceleration noise spectrum $P_{ae}(f)$ from Figure 3-3 of the same section is already in units of g^2/cps.

The sensor transfer function is effectively set equal to one for the same reasons discussed above for the gyro case. The numerical approximations for the angular displacement spectrum, $P_\theta(f)$, and for the integration transfer function, $\left|T_I(j\omega)\right|^2$, have also been given in the discussion of the gyro.

The environment acceleration spectrum, $P_{ae}(f)$, is from Figure 3-3 of the Development Document. For numerical work, this was approximated stepwise as follows:

Table A-3

f (cps)	$P_{ae}(f)$ (g^2rms/cps)
0 to 10^{-2}	10^{-15}
10^{-2} to 10^{-1}	10^{-11}
10^{-1} to 1	10^{-9}
1 to 10^3	10^{-8}
10^2 to 10^3	10^{-11}
Above 10^3	0

For the accelerometer in a horizontal position, the major source of error is the angular displacement noise which causes the accelerometer to sense a varying component of the gravity vector. The separate contributions to the variance of ΔP are (in units of g^2):

$$\left.\begin{array}{l}\text{Contribution of environment}\\ \text{acceleration}\end{array}\right\} \doteq \frac{1.1 \times 10^{-15}}{\Delta t} + \frac{1.92 \times 10^{-8}}{(\Delta t)^2}$$

$$\left.\begin{array}{l}\text{Contribution of g-pickup}\\ \text{due to } \Delta\theta \text{ noise}\end{array}\right\} \doteq 9.4 \times 10^{-9} - 2.3 \times 10^{-14}\Delta t + \frac{6.7 \times 10^{-15}}{(\Delta t)^2}$$

If a bubble is used to correct for the low frequency portion of the angular displacement noise, either mechanically or mathematically, the contribution of this error source is (in units of g^2):

$$\left.\begin{array}{l}\text{Contribution of } \Delta\theta \text{ noise} \\ \text{based on Model 1}\end{array}\right\} = 7.1 \times 10^{-11} - 2.3 \times 10^{-14}\Delta t + \frac{6.7 \times 10^{-15}}{(\Delta t)^2}$$

$$\left.\begin{array}{l}\text{Contribution of } \Delta\theta \text{ noise} \\ \text{based on Model 2}\end{array}\right\} = \frac{1.5 \times 10^{-8}}{\Delta t} - \frac{2.4 \times 10^{-7}}{(\Delta t)^2}$$

for the two modifications of angular displacement noise spectrum that were investigated. These two cases represent two models for the angular displacement spectrum after correction by the bubble level. In Model 1 the spectrum is simply assumed to be zero for frequencies below $(50 \text{ min})^{-1}$. In Model 2 the spectrum is assumed to be:

$$P_\theta(f) = \frac{K}{1 + (\omega/\omega_o)^2}$$

In this case the contribution to the variance of ΔP is:

$$\text{var}\left[\int_0^{\Delta t} \theta(t)\,dt\right] = \frac{2C_1}{C_2^2}\left[e^{-C_2 \Delta t} - 1 + C_2 \Delta t\right]$$

where $C_1 = \omega_o K\pi/2$

$C_2 = \omega_o$

For the computations we took

$C_1 = (4.5 \text{ sec})^2$ (converted to radians^2)

$C_2 = 2\pi \times 10^{-2}/\text{sec}$